Shocks in the laboratory

A focus on collisionless shocks generated by high power lasers

Emmanuel d'Humières
Université de Bordeaux-CNRS-CEA, CELIA, Talence, France

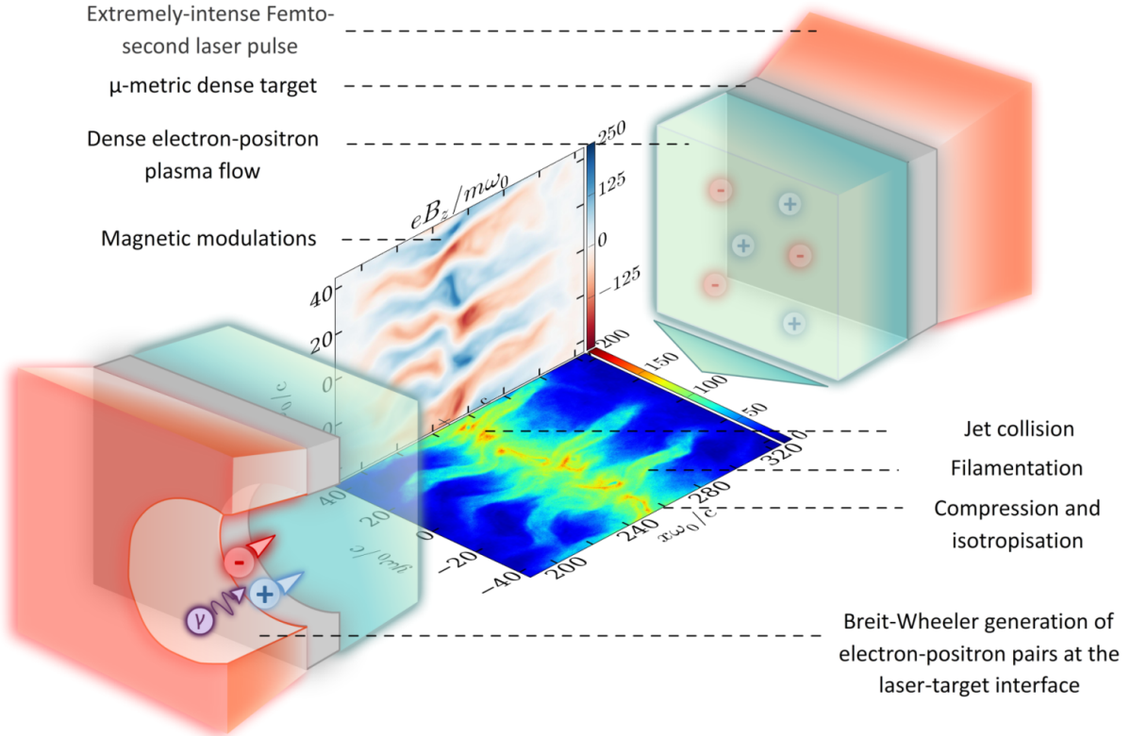

emmanuel.dhumieres@u-bordeaux.fr

Outline

- High power laser systems and applications
- Collisionless shocks for laser particle acceleration
- Importance of collisionless shocks in astrophysics
- Experimental and numerical studies of collisionless shocks of interest for astrophysics
- Collision of plasmas in an external magnetic field as a platform to study magnetized collisionless shocks
- Collisionless shocks in electron-positron plasmas using extreme-light laser pulses
- Conclusions and perspectives

A brief history of lasers for controlled fusion
From 1962 to the present day

- **1960s:** first proposals and first experiments (USA, France, Russia)
- **1970s:** de-classification in 1971 and first steps of systematic research, multibeam lasers (Janus, Shivas, Kalmar), neutrons (1968, 10^{13} in 1988), compression (20 g/cc in 1979, 600 g/cc in 1991). Understanding of physical and technical problems (instabilities, transport)
- **1980s:** progress in power and energy: transition from CO_2 (Helios) to 3ω Nd (Nova, Phébus, Vulcan, Gekko), excimer lasers, CPA lasers
- **1990s:** instability control, smoothing, large NIF and LMJ projects, Omega laser, first PW laser, Centurion program (indirect attack), acceleration of particles
- **2000s:** NIF and LMJ lasers, new ignition schemes, applications outside the FCI (accelerators, radiography, medicine, astrophysics), new projects (ELI, HiPER)
- **2009:** construction of NIF is completed
- **After 2010:** multiplication of PW systems (Berkeley, GIST, CLPU, HZDR, INRS…)
- **2014:** construction of LMJ is completed
- **2017:** ARC and PETAL will operate
- **2018:** Apollon and ELI first experiments

High power laser facilities in the world

- USA: Livermore (LLNL), Los Alamos (LANL), Rochester (LLE), Berkeley, UT, Michigan
- UK: Didcot (Rutherford lab), Aldermaston (AWE)
- France: CEA (CESTA, Saclay), Ecole Polytechnique (LULI, LOA), CELIA
- Germany: Garching, Jena, Munich, Dresden, Dusseldorf
- Czech Republic: PALS
- Japon: Osaka (ILE), Kyoto (JAERI)
- South Korea: GIST
- Russia: Moscou (Lebedev, MEPHI), Arsamas
- China: Pekin, Shanghai

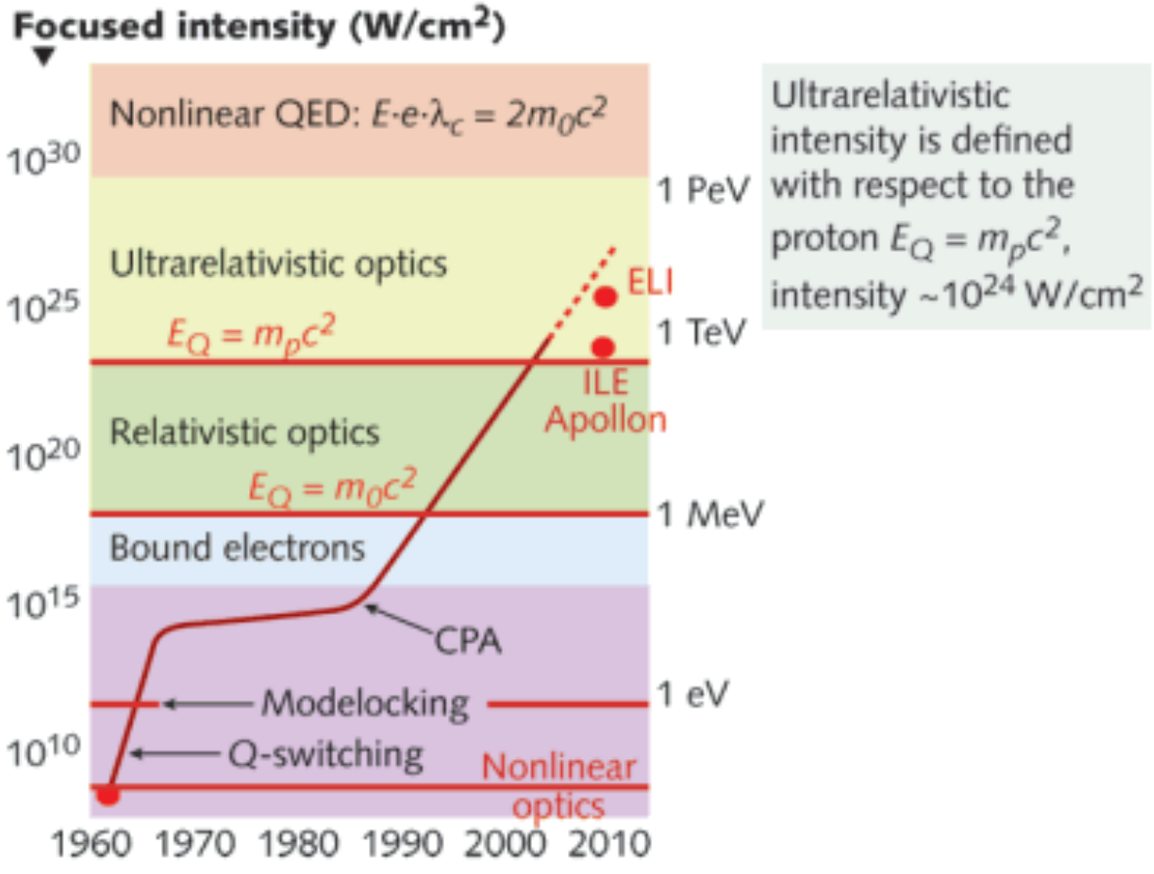

From 1974 to 1984 LLNL built a series of laser systems of ever-increasing power and energy for fusion research

The National Ignition Facility

Janus (1974) – 100 J 1ω

Nova (1984) – 100 kJ 1ω

The National Ignition Facility concentrates all the energy in a football stadium-sized facility into a mm^3

The National Ignition Facility

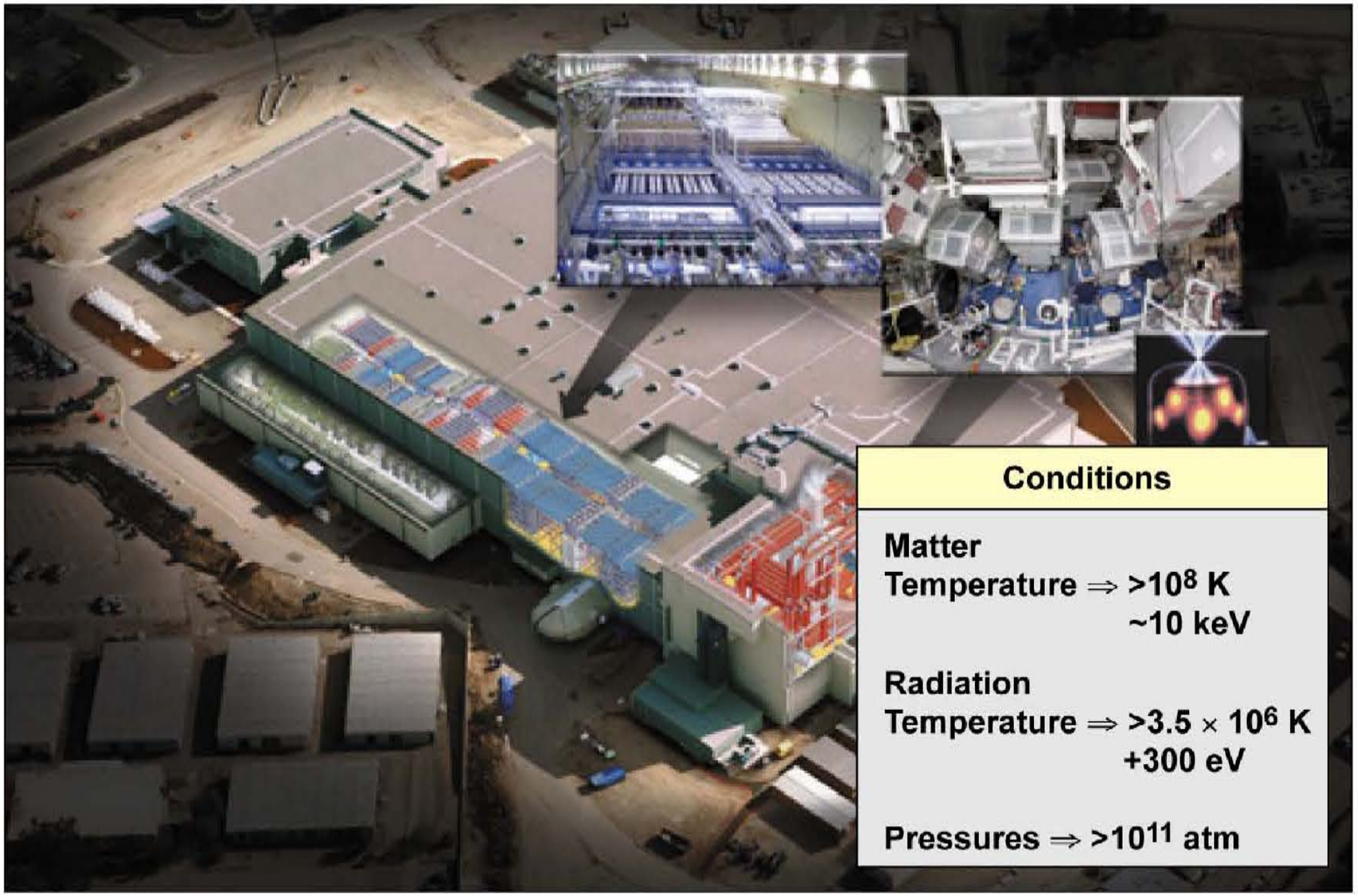

March 2009 : 192 beams delivered 1.1 MJ in 3w

Photos from NIF: interaction chamber

https://lasers.llnl.gov/multimedia/photo_gallery

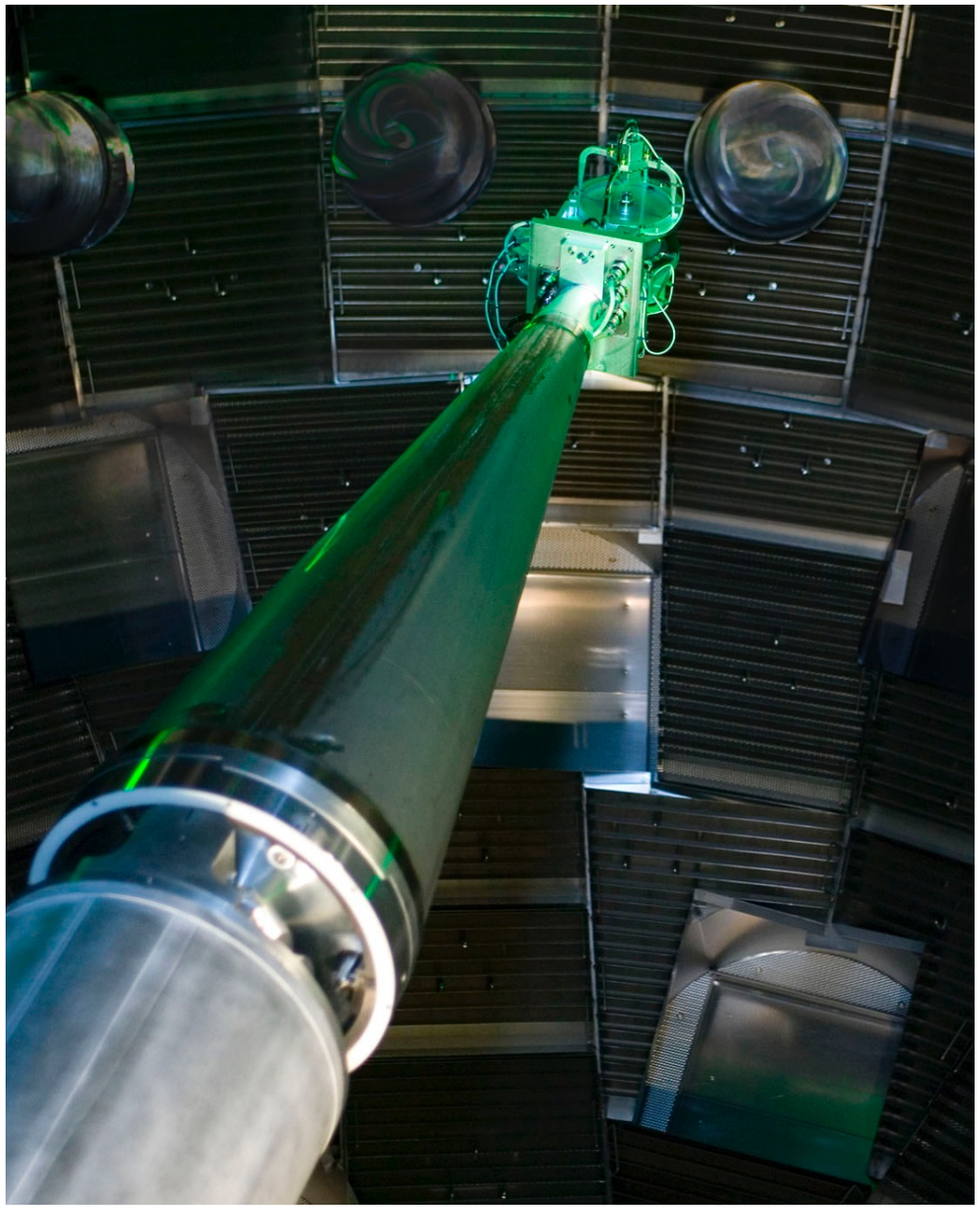

Construction photos from LMJ: closing the roof

Laser facilities of power above 100 terawatts (TW) in the world as a function of their power and energy

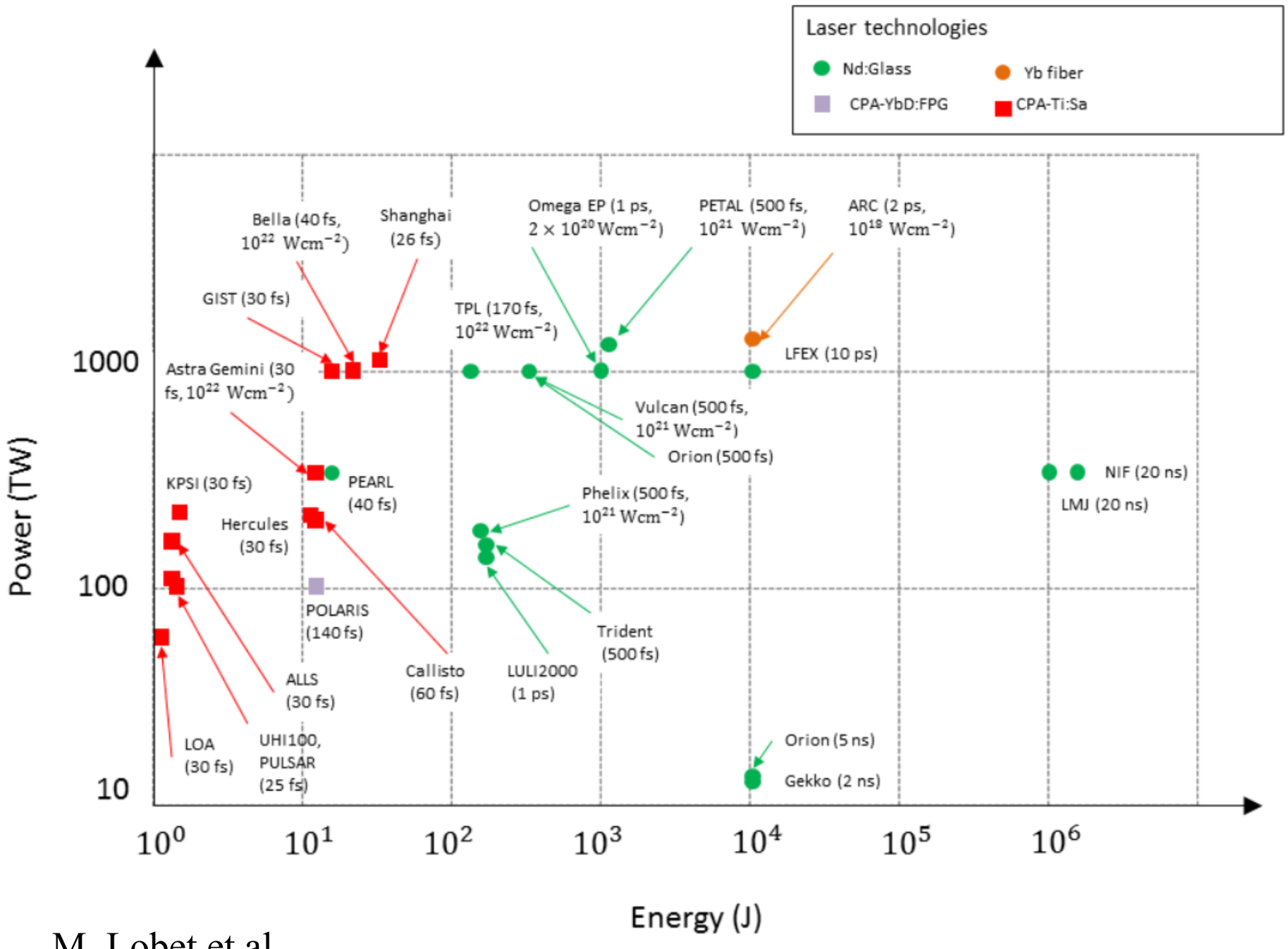

M. Lobet et al.

ICF and the High Energy Density Physics

New generation of high power lasers gives access to macroscopic volumes of hot and dense matter

$E/V > 10^{11}$ J/m^3
$P > 1$ Mbar

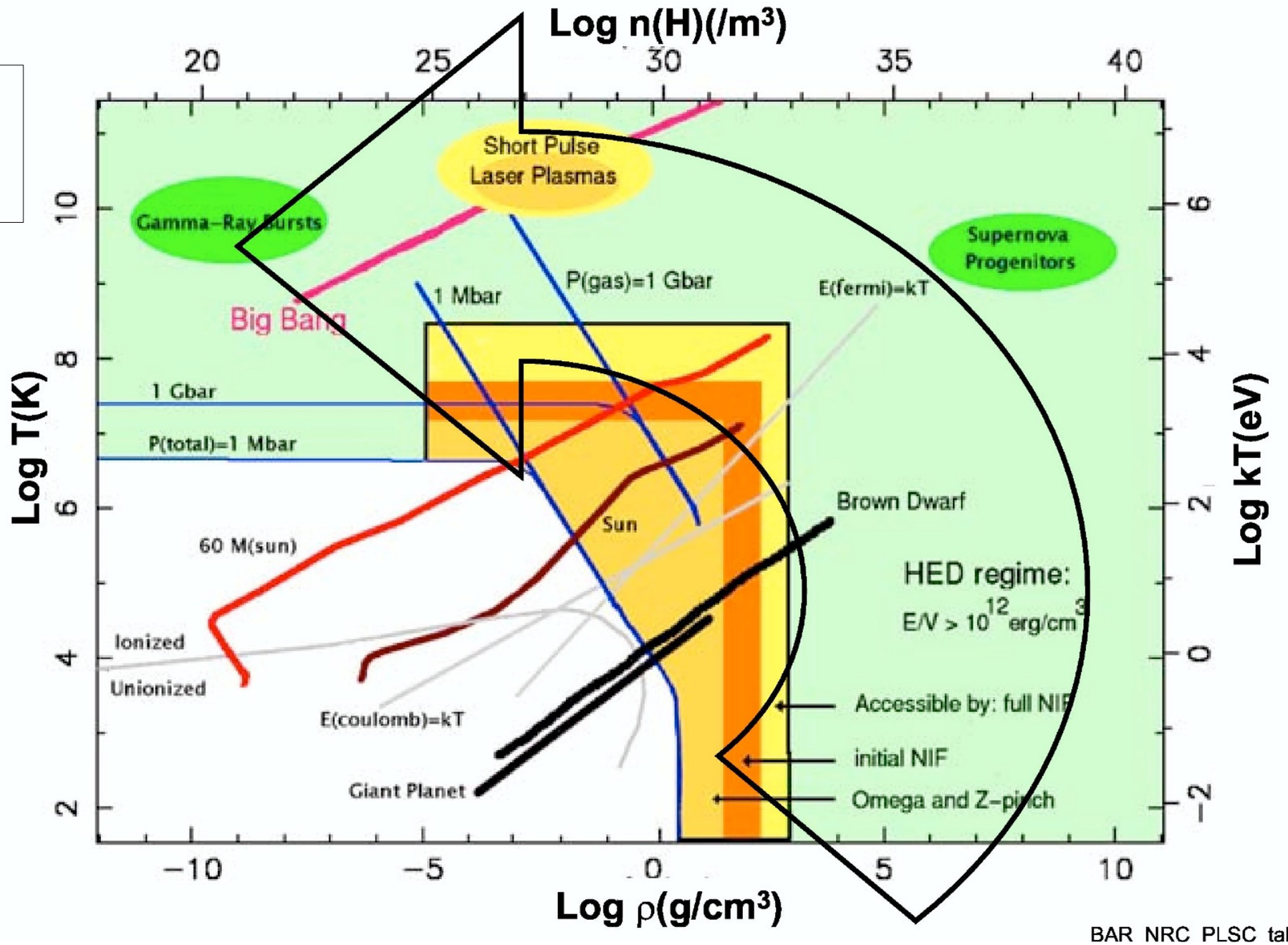

BAR NRC PLSC tal

Jets and shocks in nature

Cas-A SNR from core-collapse SN1680

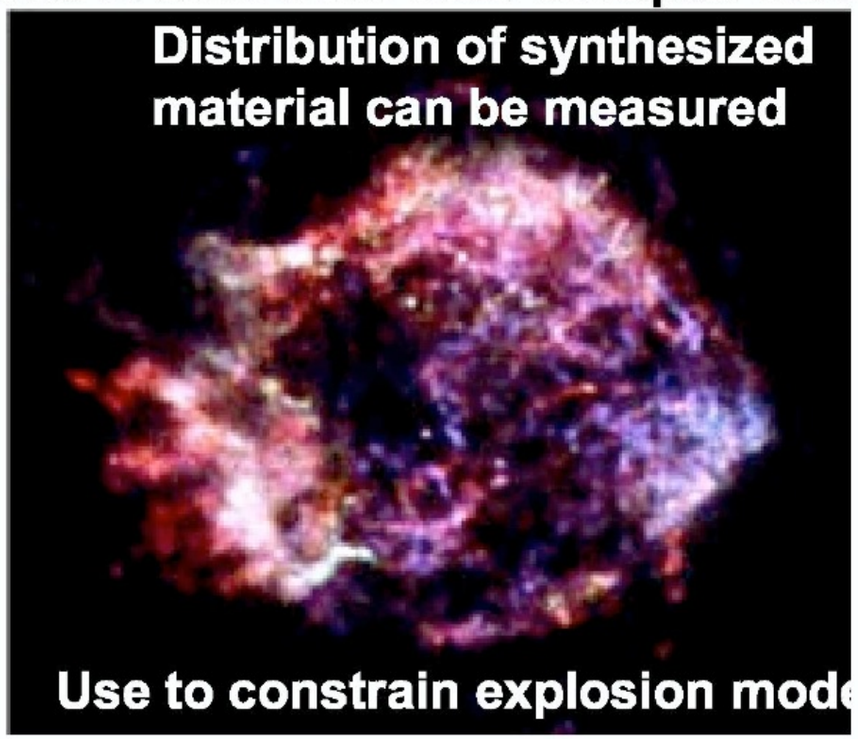

J.P. Hughes *et al.*
Ap. J. 528, L109

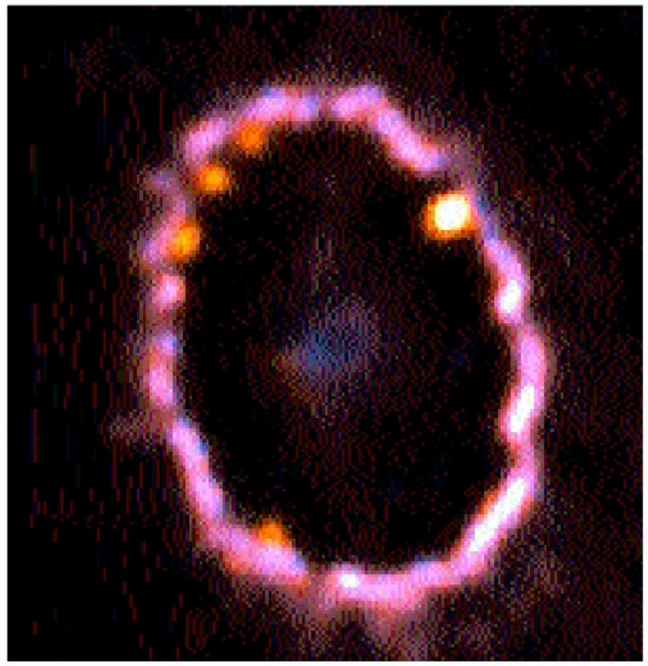

Diameter = 1 light year,
t = 12 years

Supernova 1987A remnant in the Large Magellanic Cloud,taken with HST WFPC2.

NASA, P. Challis and R. Kirshner (CfA),
P. Garnavich (Univ. of Notre Dame),
and The SINS Collaboration, STScI - PRC00-11

Radiative jets in laser experiments

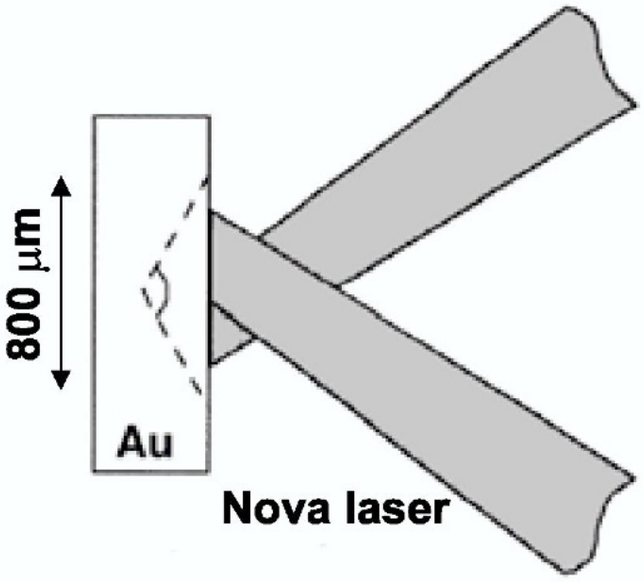

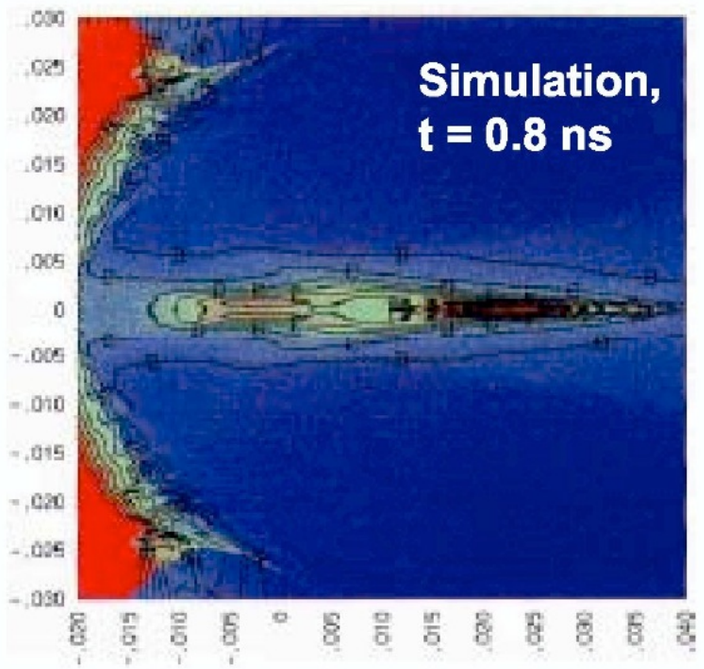

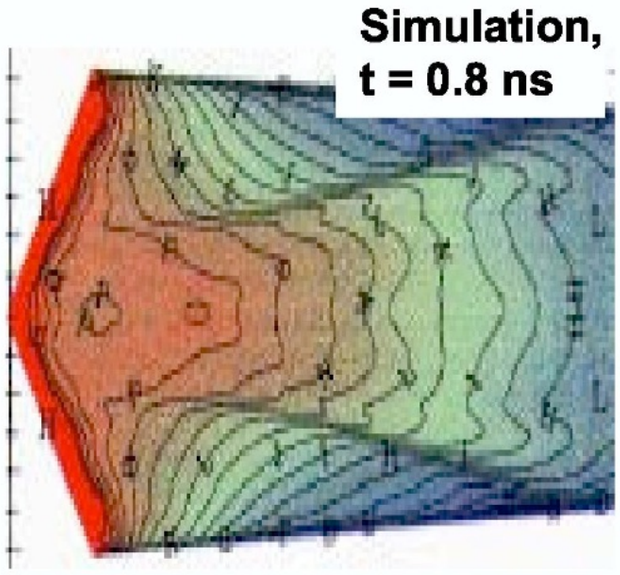

Emission images

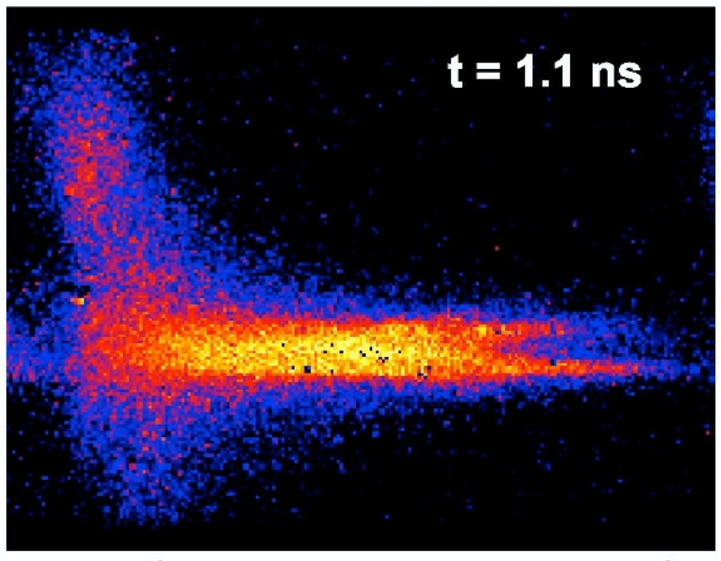

Farley et al., PRL 83, 1982 (1999)

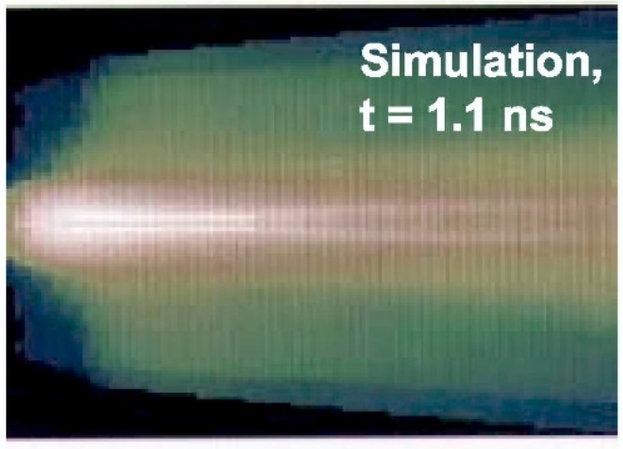

X-ray radiographs

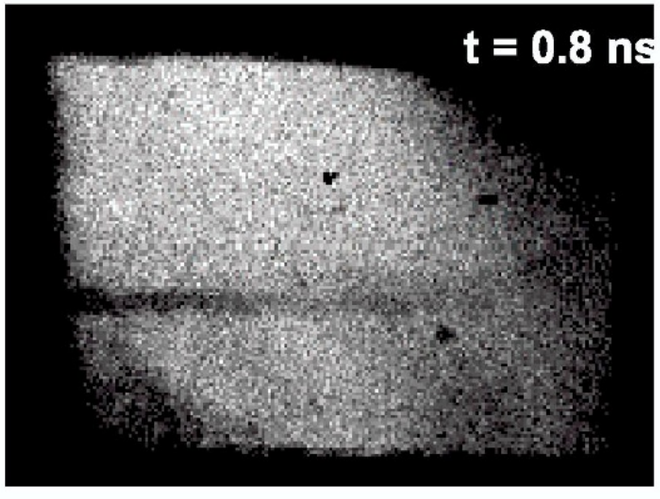

Radiative shocks

Topology/geometry

Are really the shocks 1D ?

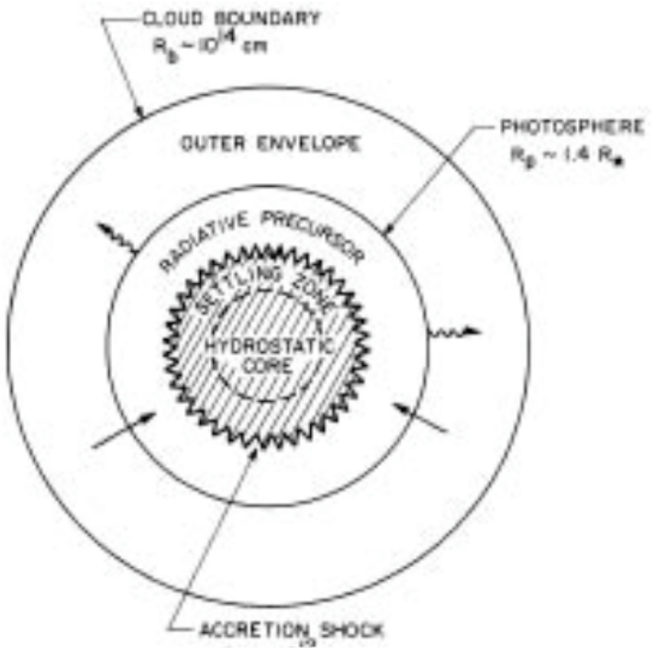

Spherical accretion shock of protostellar formation

(from Stahler et al ApJ 1986)

(location at $\rho \sim 10^{-10} g/cm^3$, T ~ several 10^3 K, several 100 km/s for $1M_\odot$, Stahler et al ApJ 1986, Winkler et al. ApJ 1980)

CO shell around carbon star TT Cygni, IRAM

(from *Olofsson et al AA 2000)*

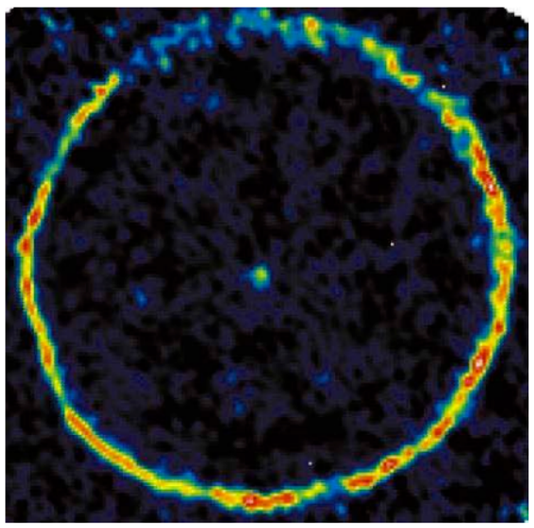

CO shell :
0.007 $M_\odot$, clumps, v ~ 20 km/s, width 1.9 10^{16} cm, $n_H = 250\ cm^{-3}$

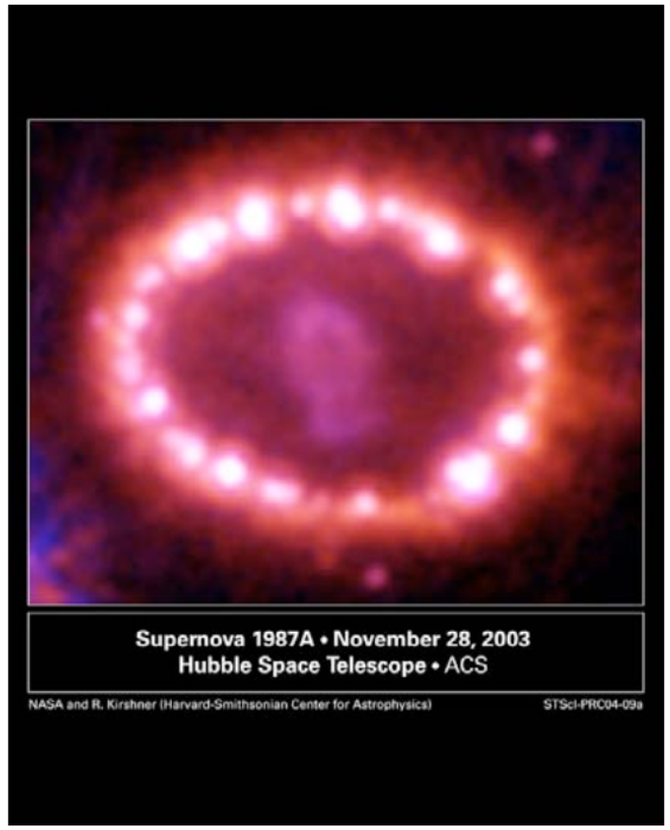

interaction of SNR 1987A with ISM in nov 2003, HST (*credit NASA)*

Present expansion v ~ 4000 km/s, glowing mass ~0.1 $M_\odot$,width of the equatorial ring ~ 10^{17} cm, $n_H = 3\ 10^3$ - $3\ 10^4\ cm^{-3}$, velocity of the shock in the ring several 100 km/s

Radiative shocks in the lab

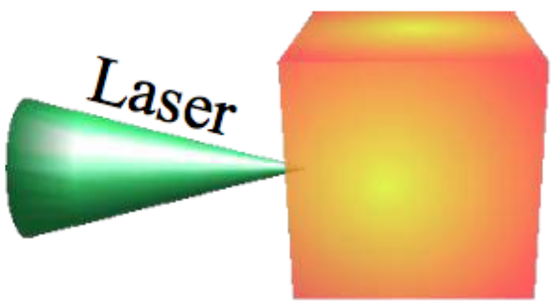

Irradiation par laser

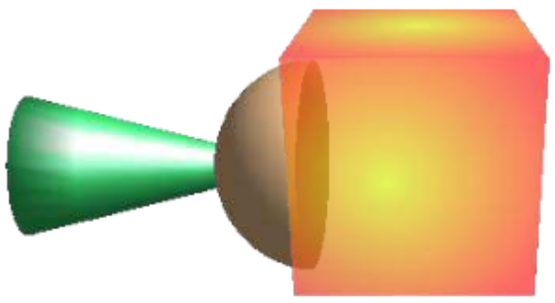

Ablation

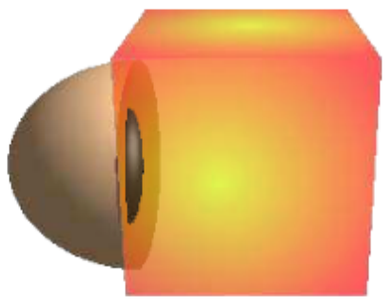

Choc dans le pousseur

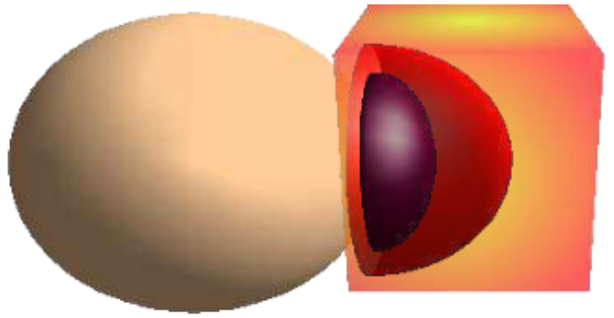

Choc + Précurseur radiatif

Gated Optical Imager diagnostic

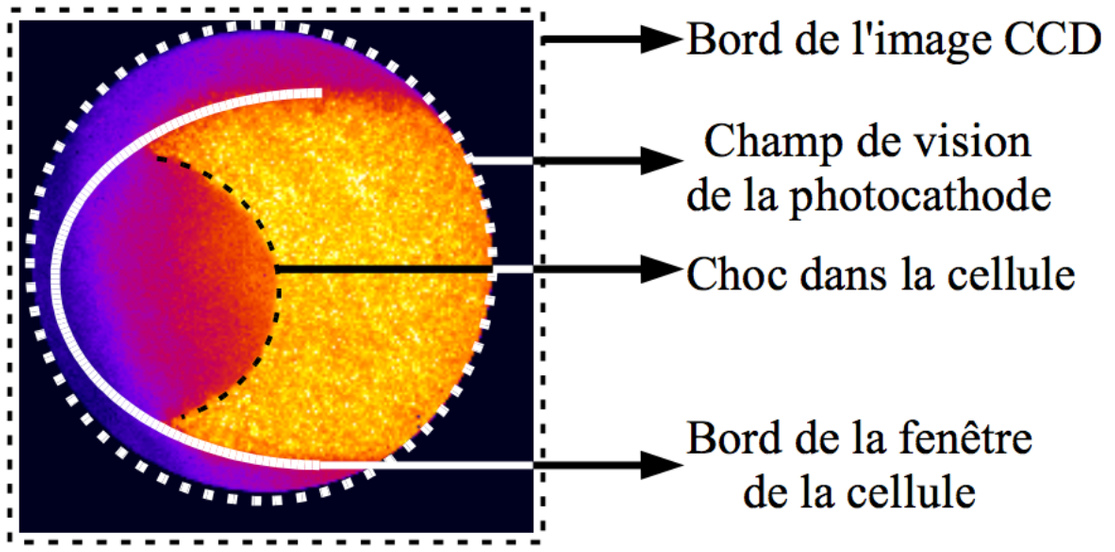

Compactness of Laser Plasma Accelerators

RF Cavity

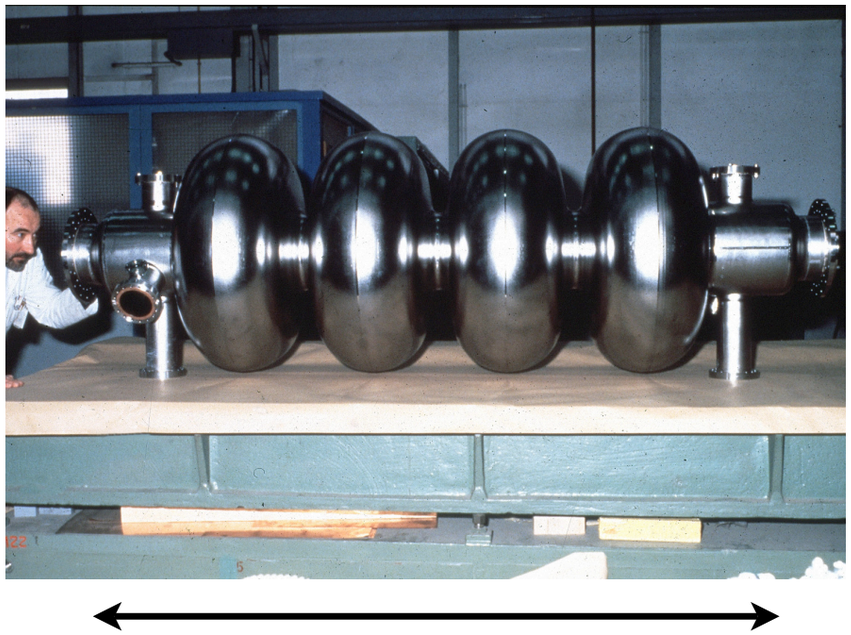

1 m => 50 MeV Gain

Electric field < 100 MV/m

Plasma Cavity

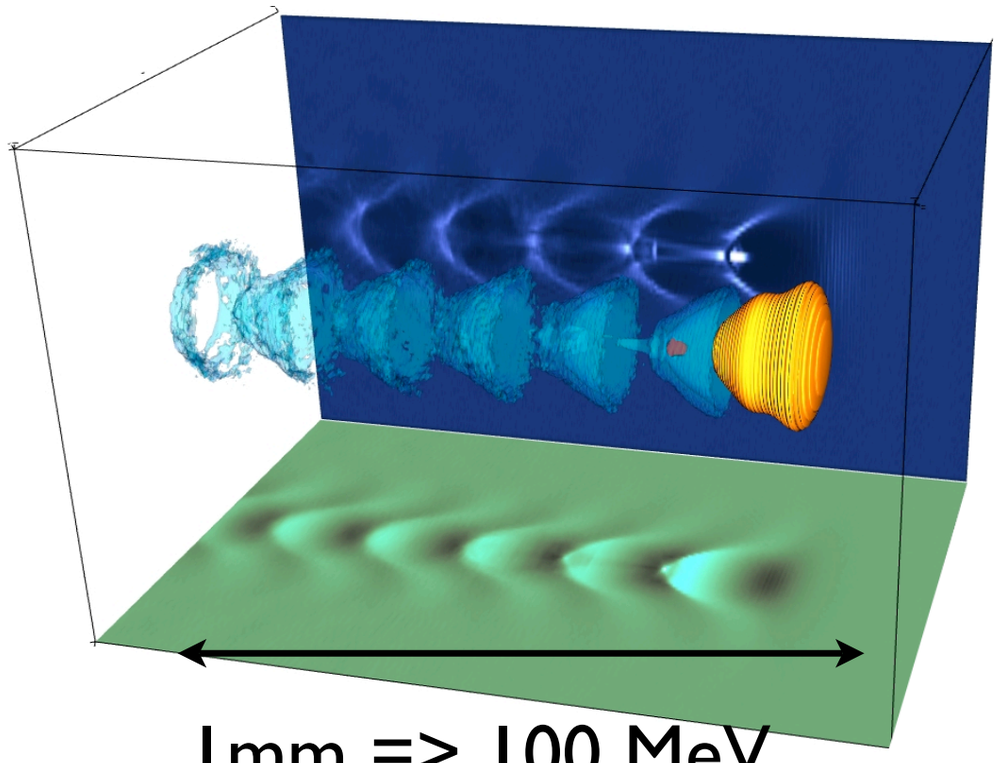

1mm => 100 MeV

Electric field > 100 GV/m

V. Malka *et al.*, Science **298**, 1596 (2002)

Basics of laser ion acceleration

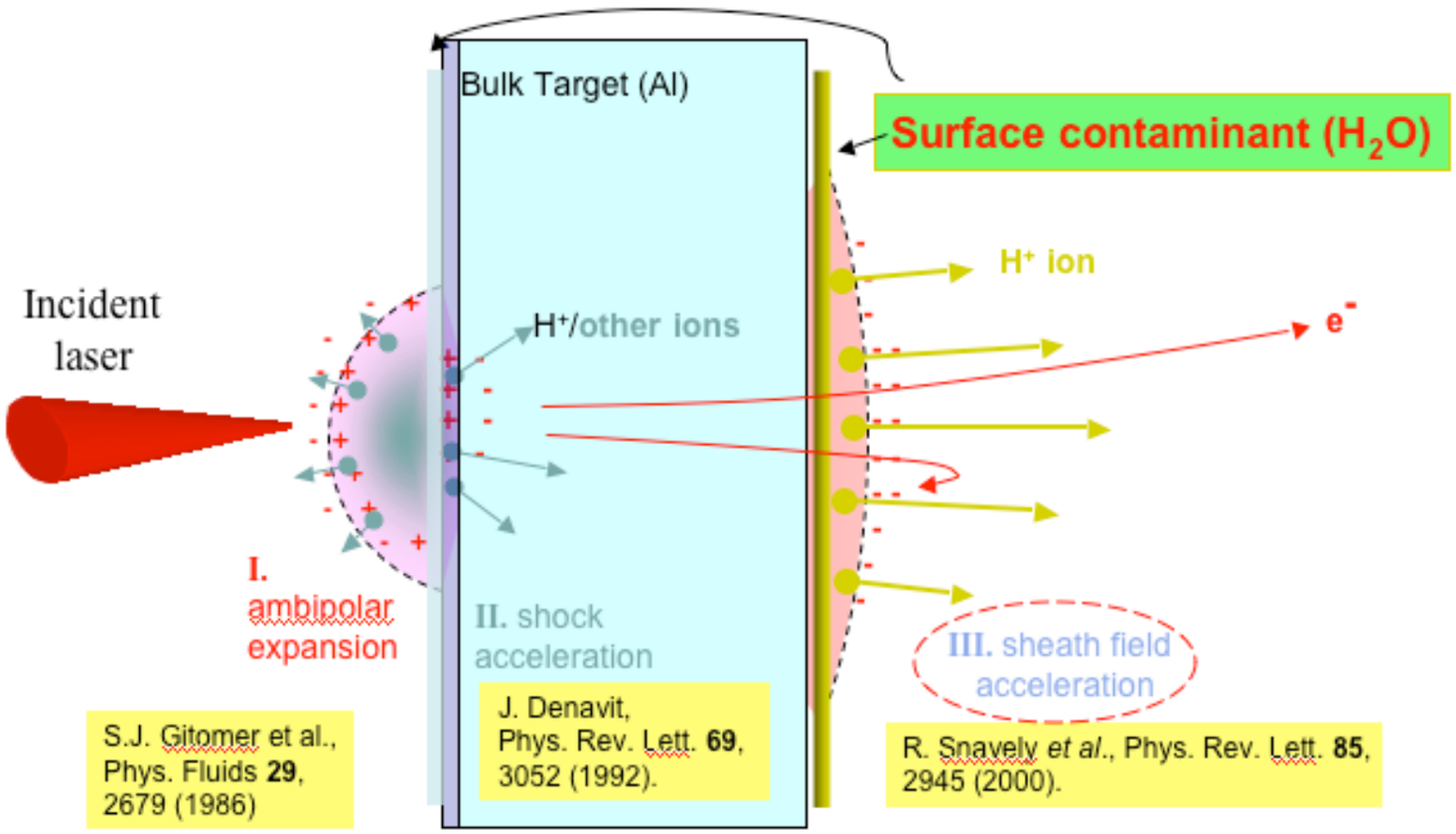

M. Allen et al., Phys. Rev. Lett. **93**, 265004 (2004); J. Fuchs et al., Phys. Rev. Lett. **94**, 045004 (2005).

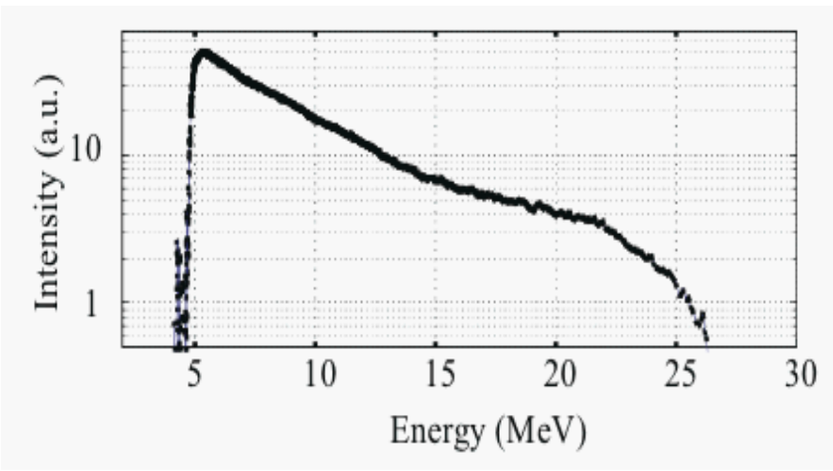

Typical proton spectrum obtained at LULI.

- **Low emittance** (<0.004 mm-mrad for the transverse emittance and $<10^{-4}$ eV-s for the longitudinal emittance)
- **Compact and short duration** (tens of microns and ps at the source).
- **High spectral cut-off**
- **TNSA:** Maximum proton energy depends on hot electrons temperature and density.
- **Main application for now**: proton radiography of dense plasmas (through electromagnetic fields).
- **Potential applications:** medicine, high energy physics, nuclear physics…

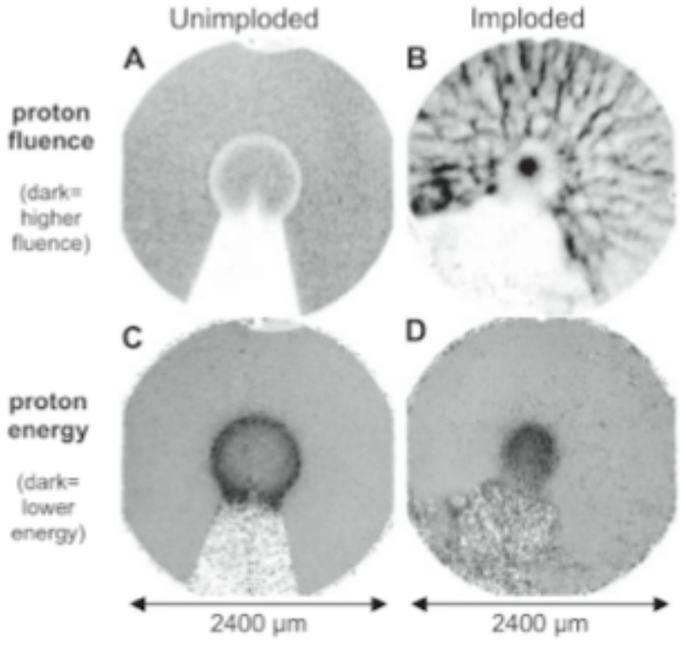

J. R. Rygg et al.
Science **319**, 1223 (2008)

Outline

- High power laser systems and applications
- **Collisionless shocks for laser particle acceleration**
- Importance of collisionless shocks in astrophysics
- Experimental and numerical studies of collisionless shocks of interest for astrophysics
- Collision of plasmas in an external magnetic field as a platform to study magnetized collisionless shocks
- Collisionless shocks in electron-positron plasmas using extreme-light laser pulses
- Conclusions and perspectives

Collisionless shocks acceleration of ions in tuned density gradients → relaxed constraints on laser

Experimental observations:

- Shock acceleration with CO2 lasers [Palmer et al. PRL 106:014801, Haberberger et al. Nat. Phys. 8:95]
- Exploration of the near critical regime for various gradient conditions [M. Gauthier et al. PoP 21, 013102 (2014)]

Theoretical works:

- High density targets: L. Silva et al. PRL 2004
- Low density targets: E.d'Humières et al. JPCS 2010, F. Fiuza et al. PRL 2012, E. d'Humières et al. PPCF 2013

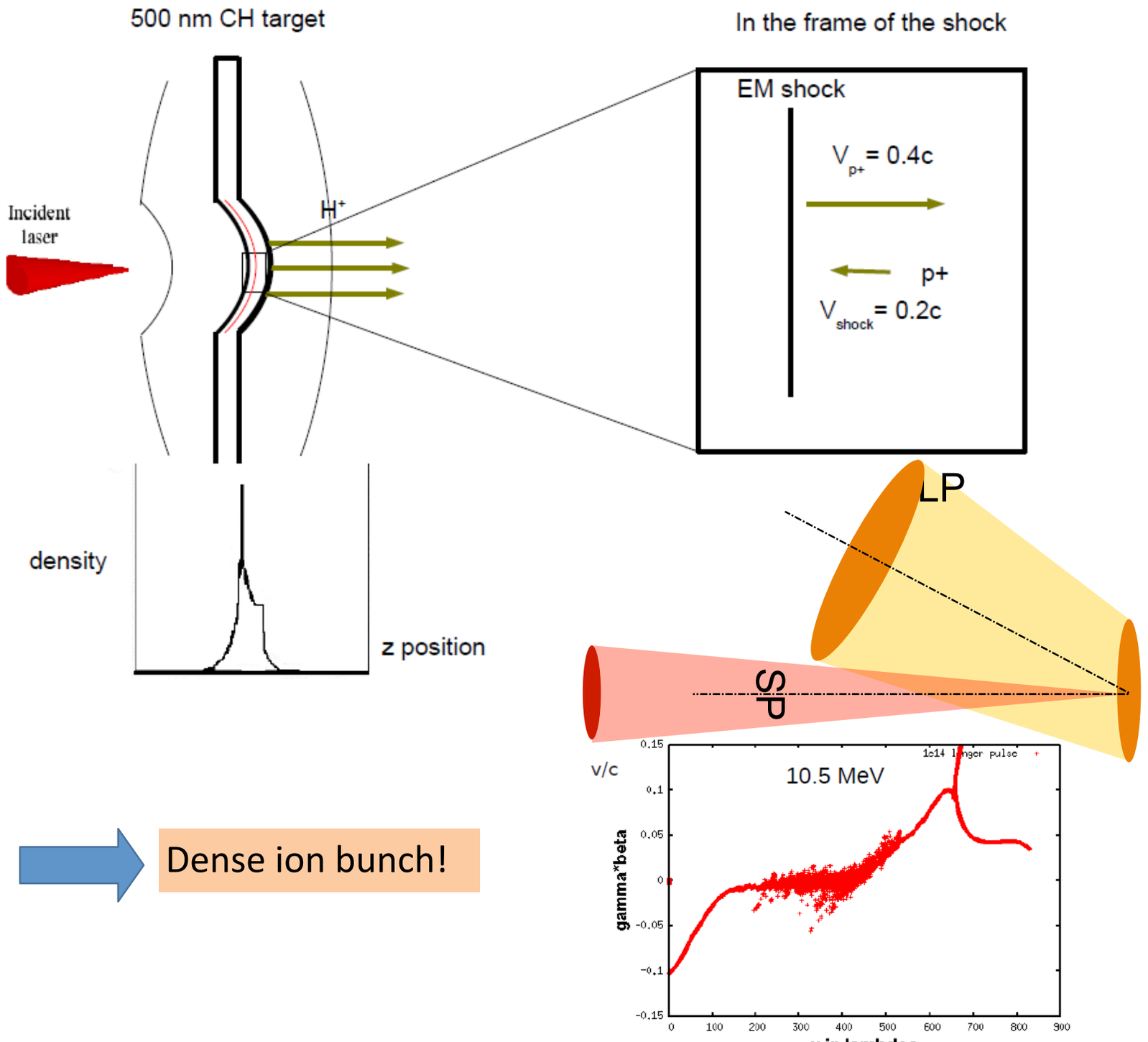

Dense ion bunch!

Two step process. First step: expansion due to hot electrons in a plasma gradient. Second step: electrostatic shock and ion reflection.

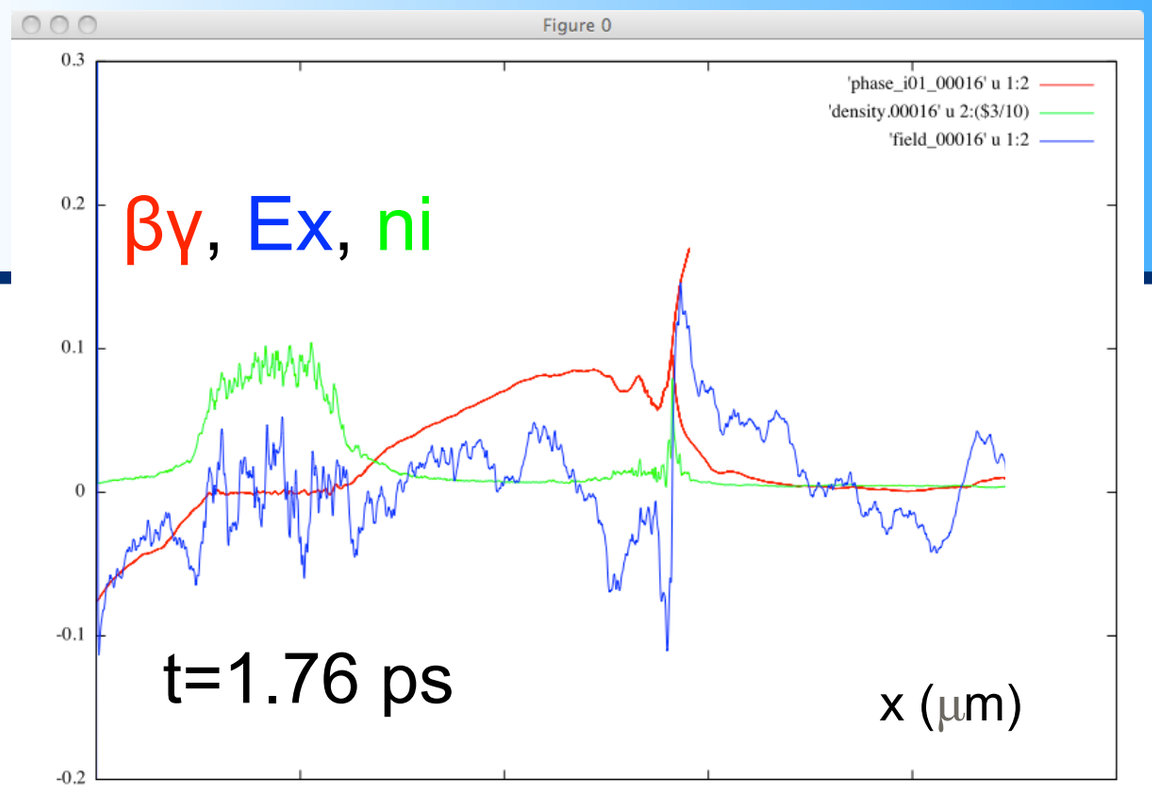

1D simulations, 4 MeV localized electron temperature, 0.08 n_c plasma with 40 μm FWHM $\cos^2$ profile, 0.004 n_c postplasma.

E. d'Humières et al., PAC11 proceedings (2011), EPS11 proceedings (2011)

The two-step mechanism can therefore be modeled using a **Boltzmann-Vlasov-Poisson model** [V. Yu. Bychenkov et al., Phys. Plasmas 11, 3242 (2004)]. Considering a hot initial electron population in a gradient with a postplasma. The model is isothermal.

BVP scaling

$$E_p = 2aT_h \ln\left(b\,\omega_{ph}t + \sqrt{1 + b^2\,t^2\omega_{ph}^2}\right)^2$$

Initial density profile in BVP simulation

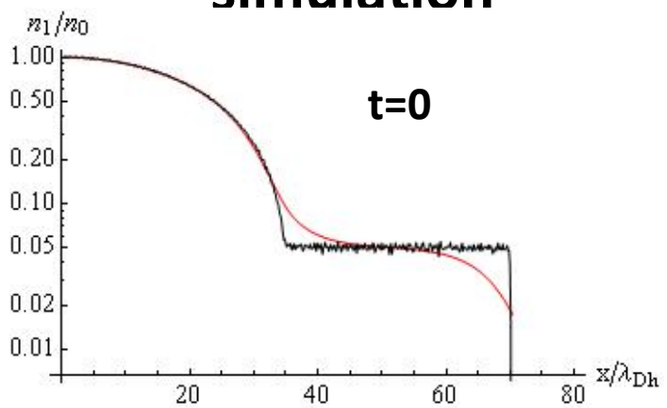

Black line– proton density profile, red line – electron density profile

n_0=0.08 n_{cr}, T_h=5 MeV, n_e=n_h, L=50μm

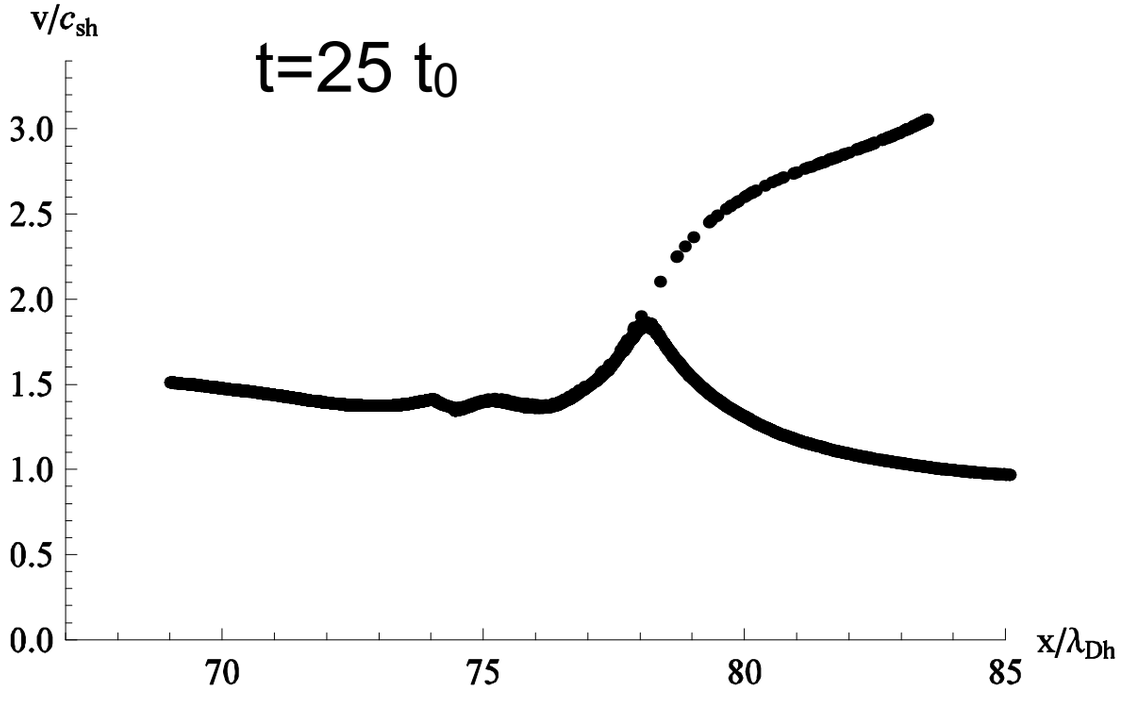

Strong magnetic field in the acceleration region when the ion wave is launched but not when the shock is launched, complex proton structures.

Laser

B_z

Ex

Proton phase space

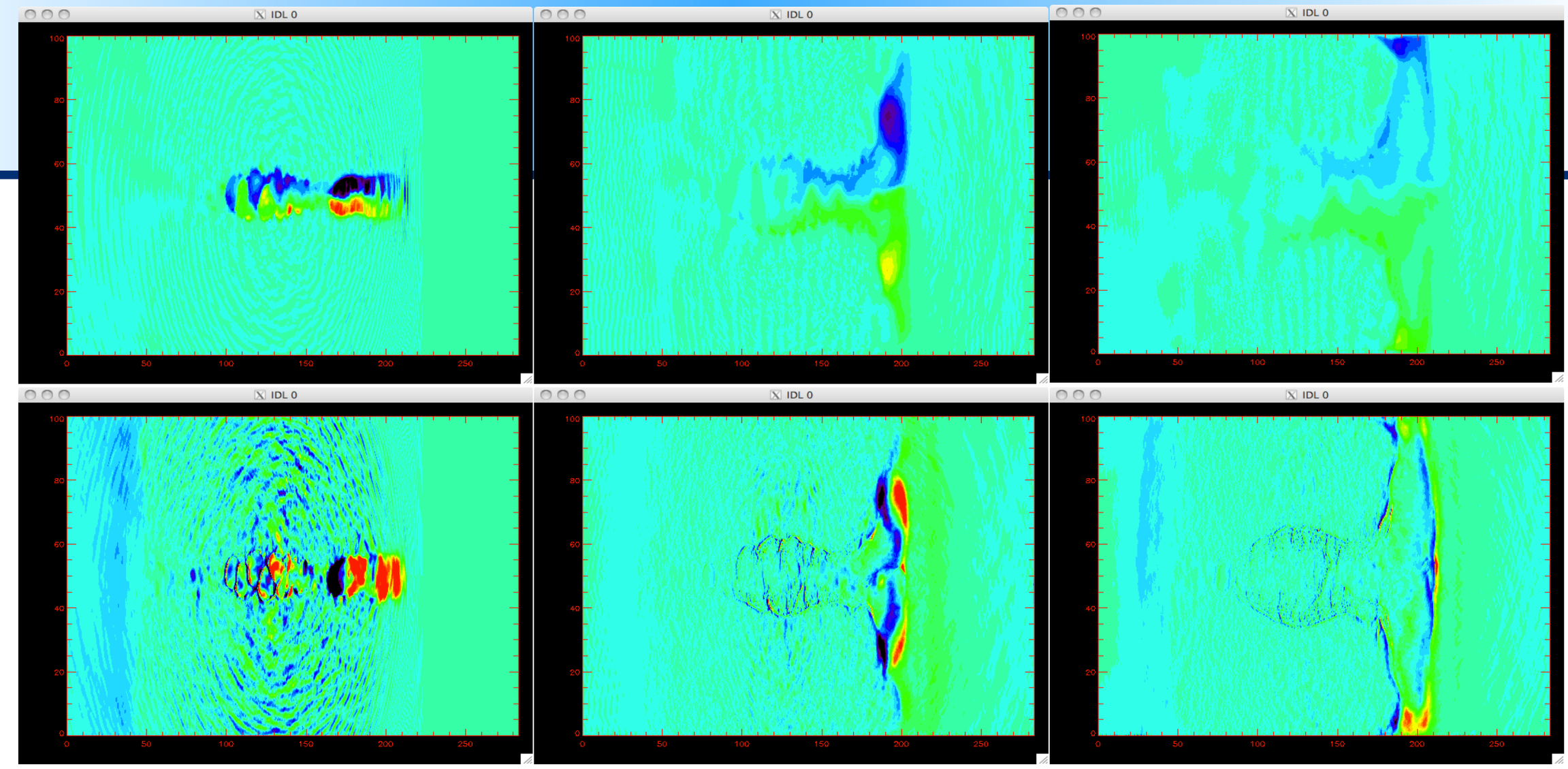

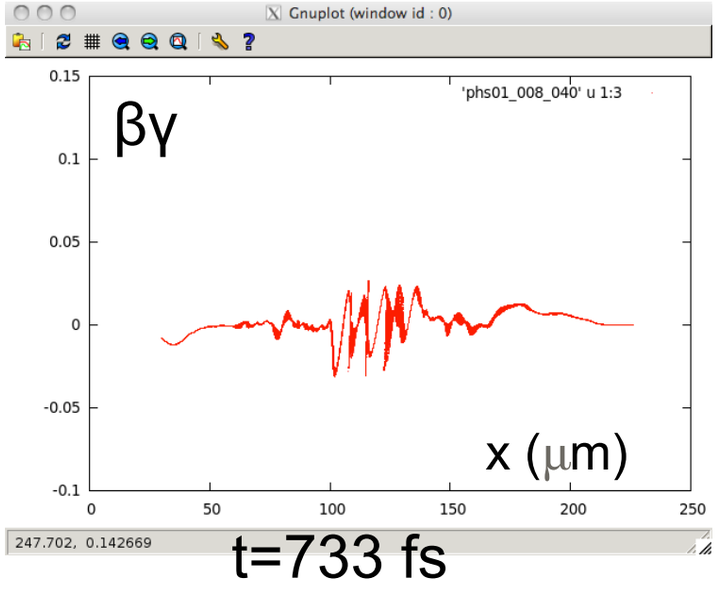

t=733 fs

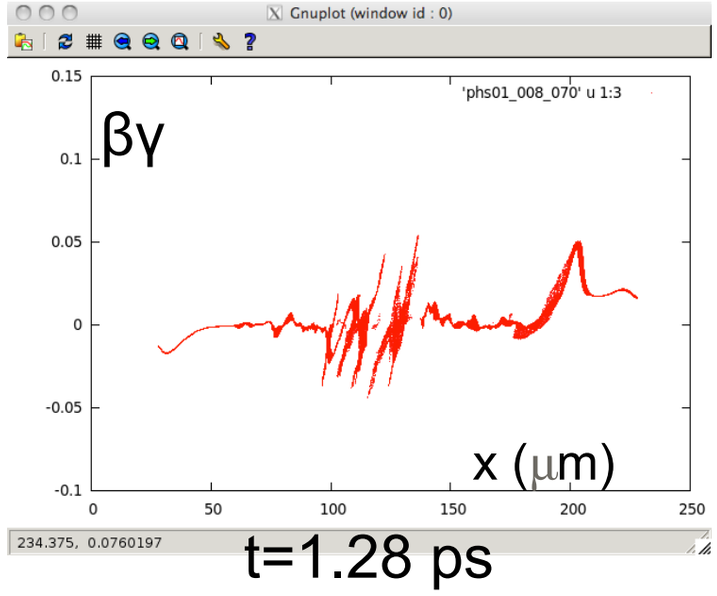

t=1.28 ps

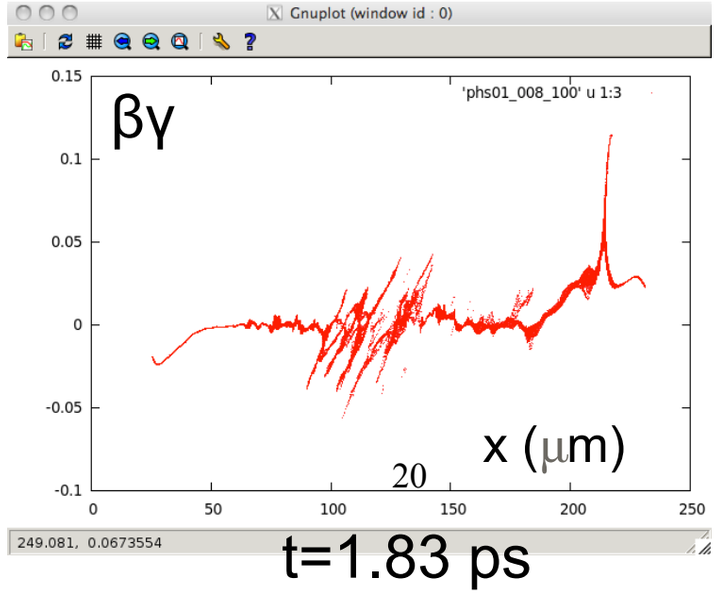

t=1.83 ps

Experiments on Titan (LLNL) using exploded foils

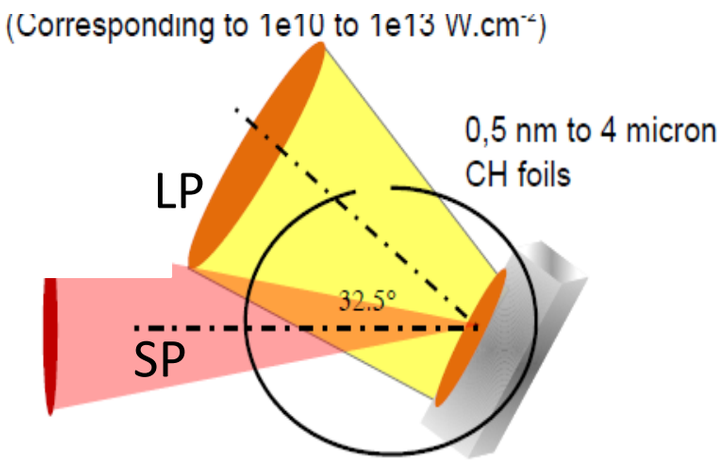

JLF-Titan

E.d'Humières et al.
PPCF 2013

P. Antici et al.

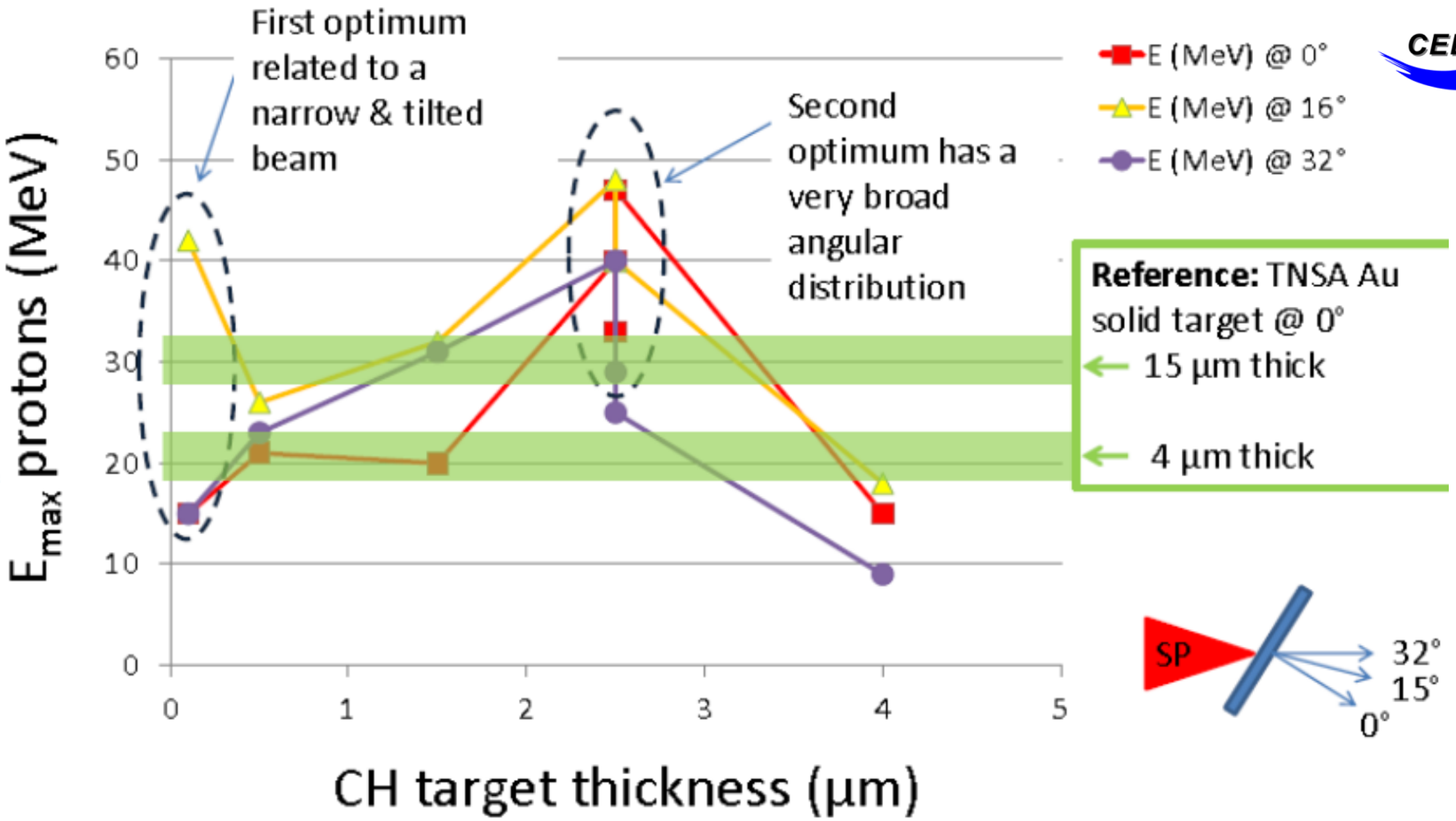

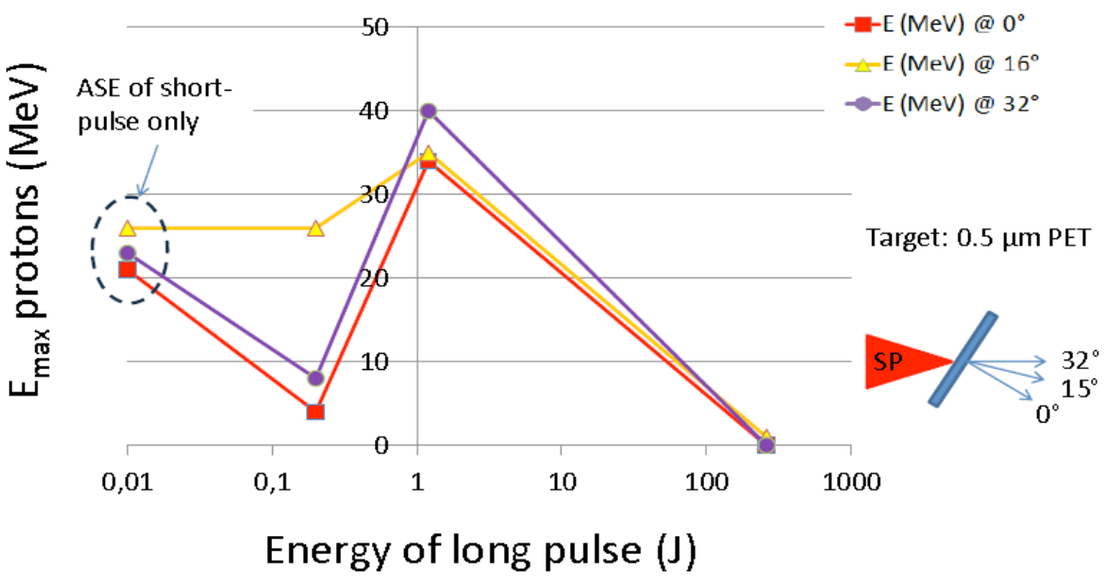

We can tune the proton energy by varying the level of the long-pulse energy prior to the short-pulse

First experiments with 300 microns thick gas jets produced a pure H+ beam peaked in energy and angle, but at low energy

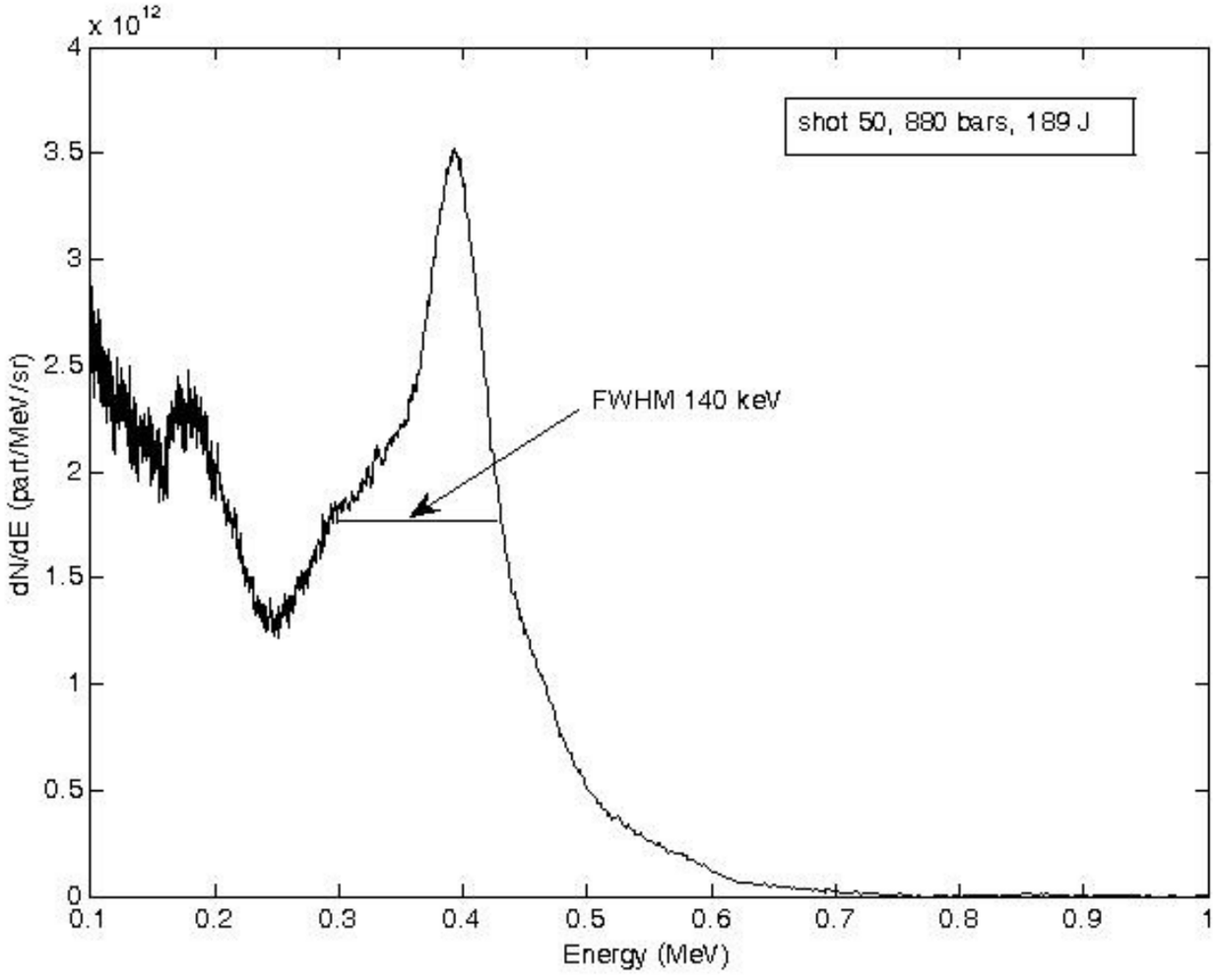

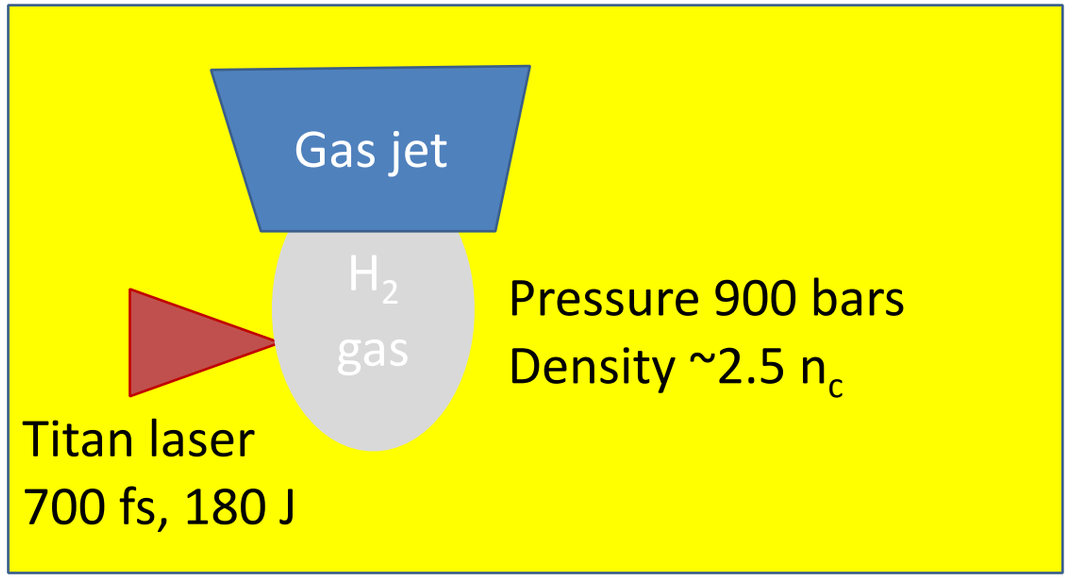

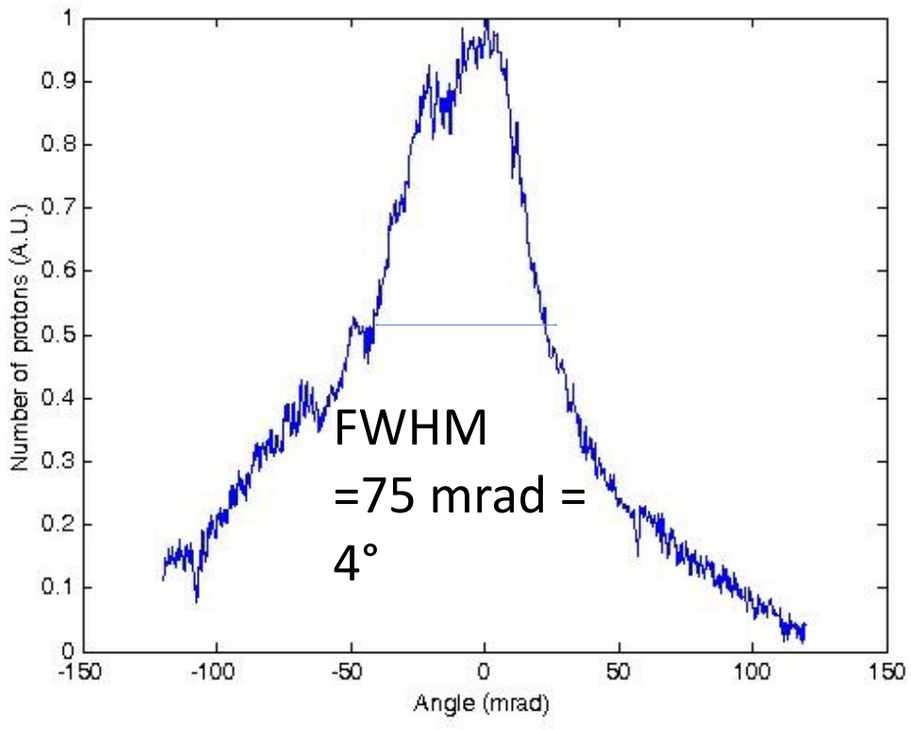

S. Chen et al.

Experiments of proton acceleration by electrostatic shocks

Experiment:

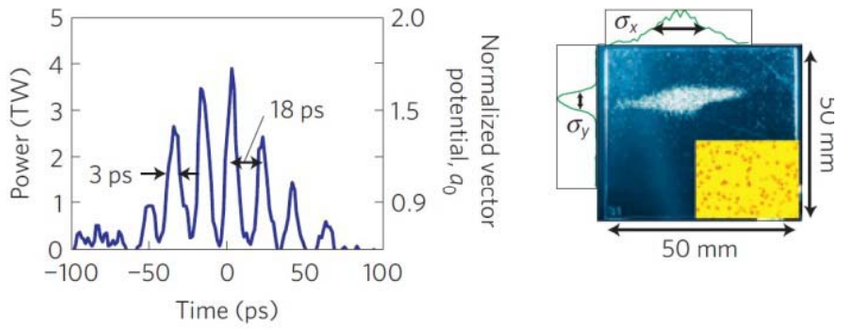

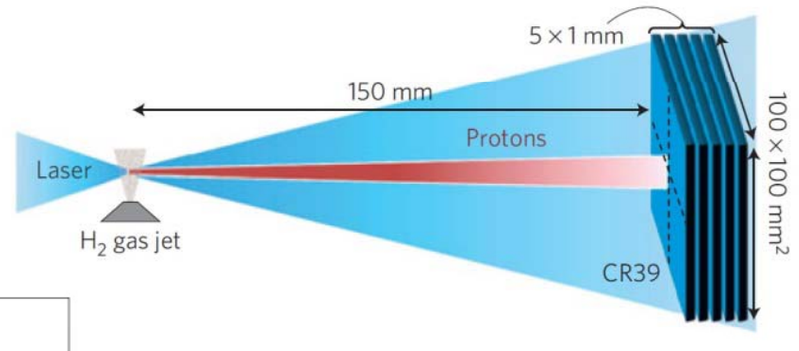

Fig. a.

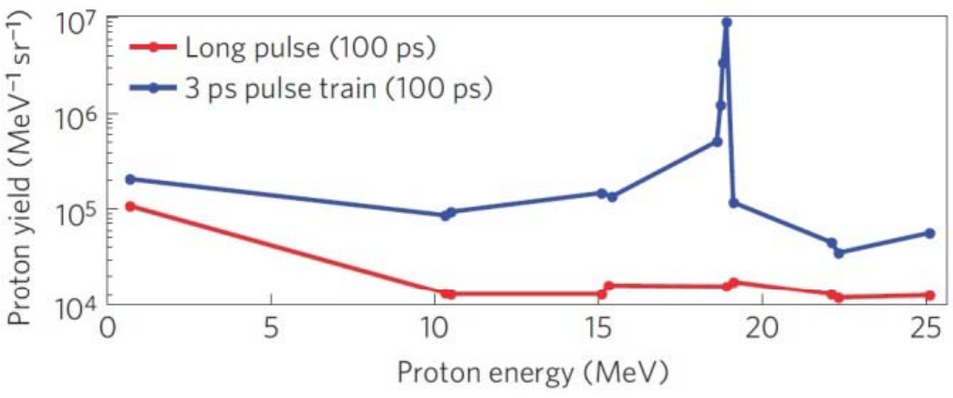

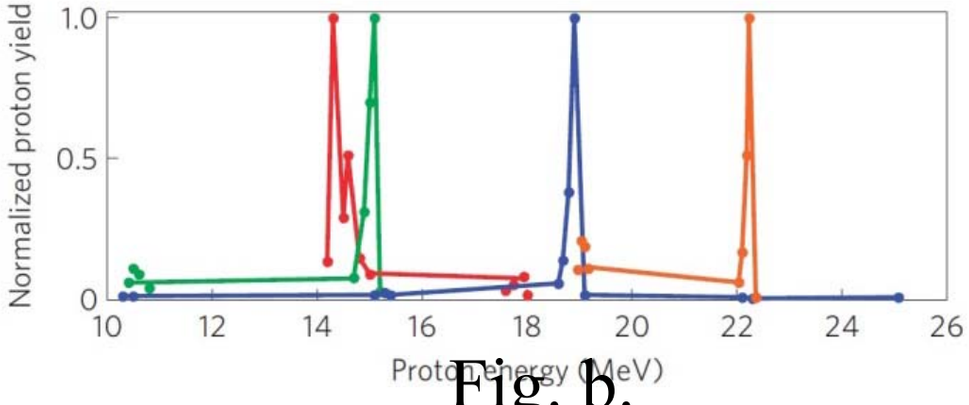

Fig. b.

Haberberger,
Nat. Phys. **8**, 95 (2012)

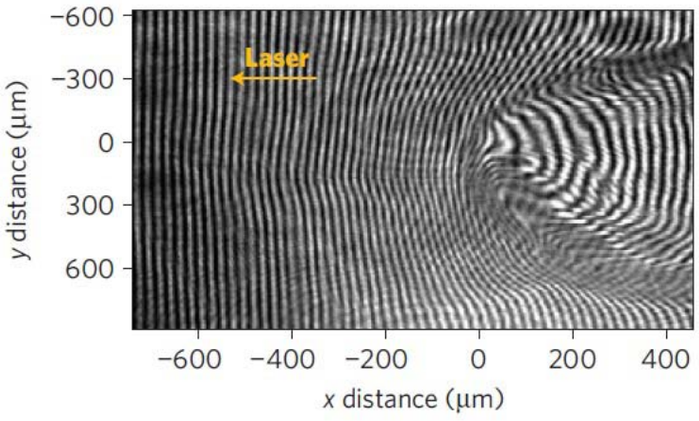

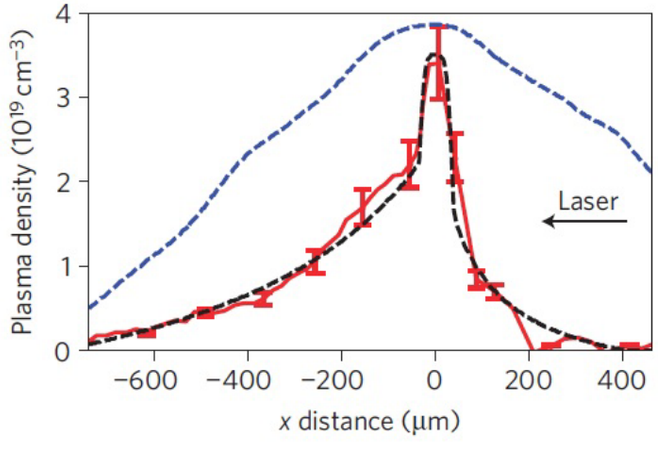

Fig. c.

Simulations of proton acceleration by electrostatic shocks

Simulation results:

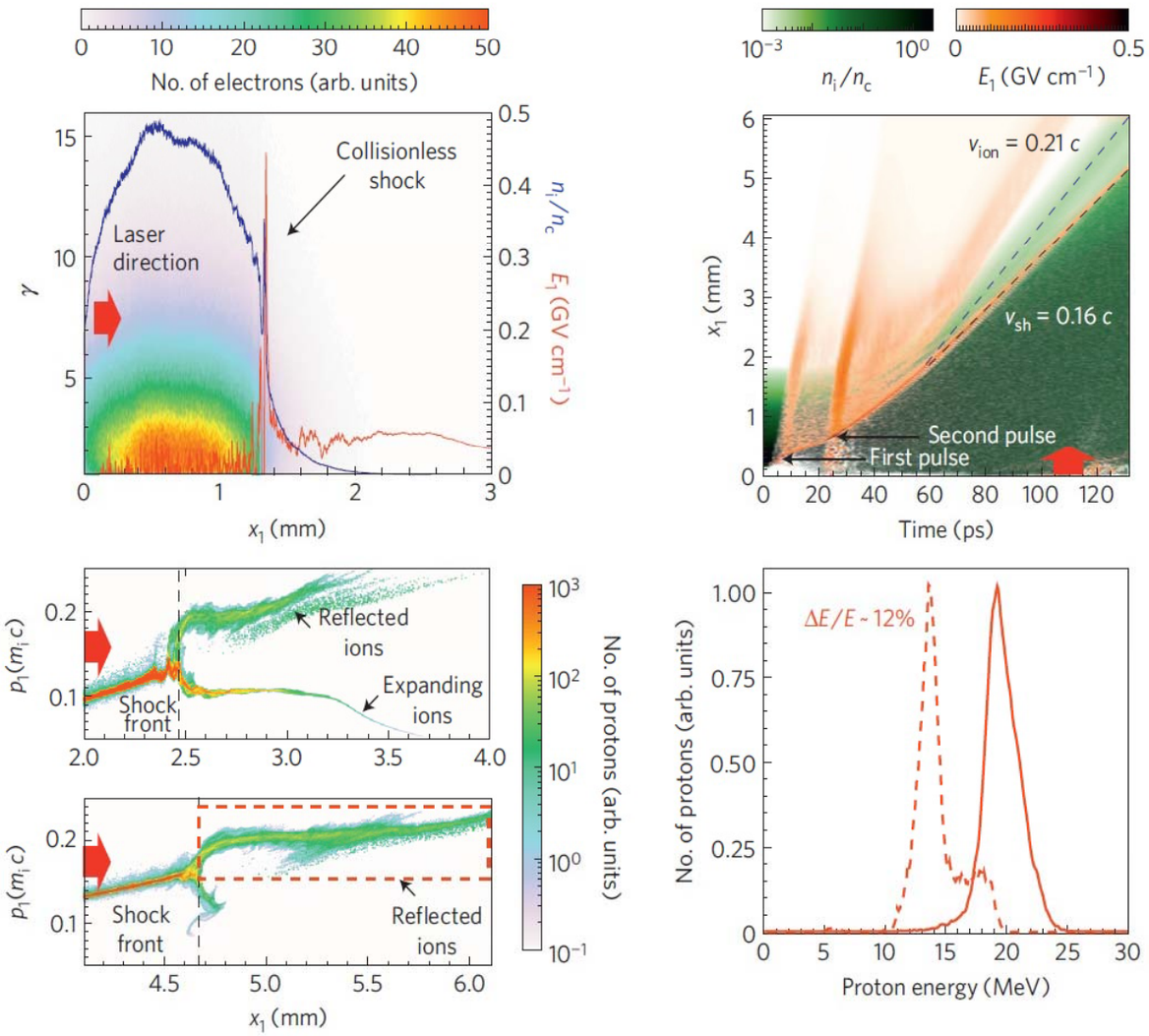

D. Haberberger et al., Nature Physics Nature Physics 8, 95 (2012)
F. Fiuza et al., Physical Review Letters 109, 215001 (2012)

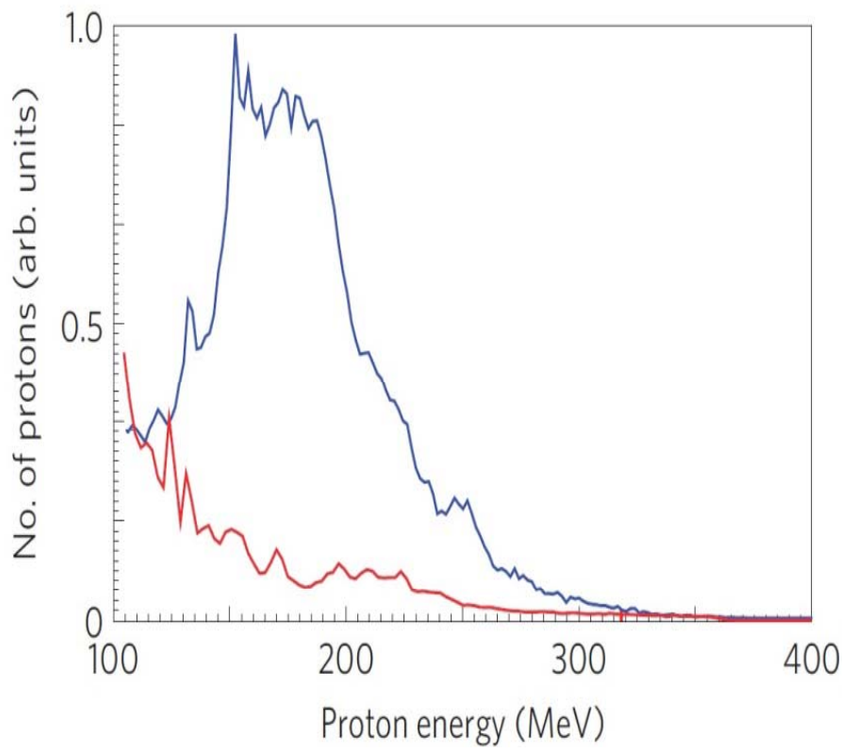

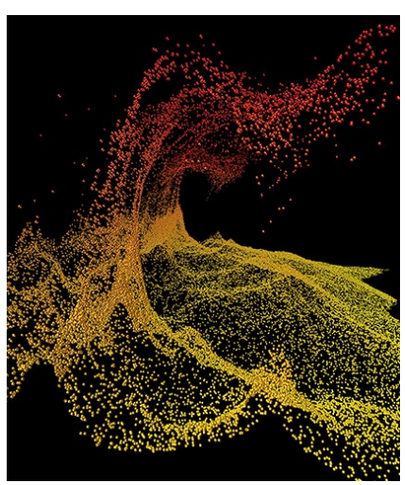

Fig. d.

Ion acceleration from a strong electrostatic shock wave driven by intense laser-plasma interactions. The spheres colored by energy (yellow – red) represent the ions that are reflected from the background by the fast moving shock wave.

Other possibility: hydrogen pellets

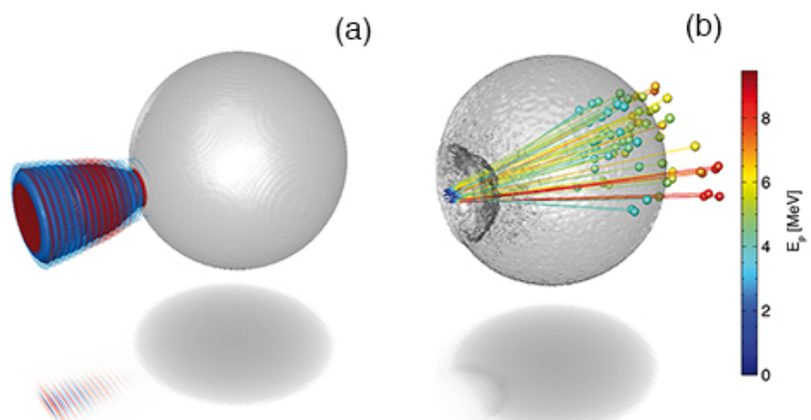

(a) A frozen hydrogen pellet is irradiated by a laser. (b) Ions are accelerated through the target. This work is currently prepared for publication by A. Stockem Novo et al. [NIC Symposium 2016 proc.]

Transition to electromagnetic shocks for particle acceleration

K. Mima et al. JPCS 717, 012070 (2016)

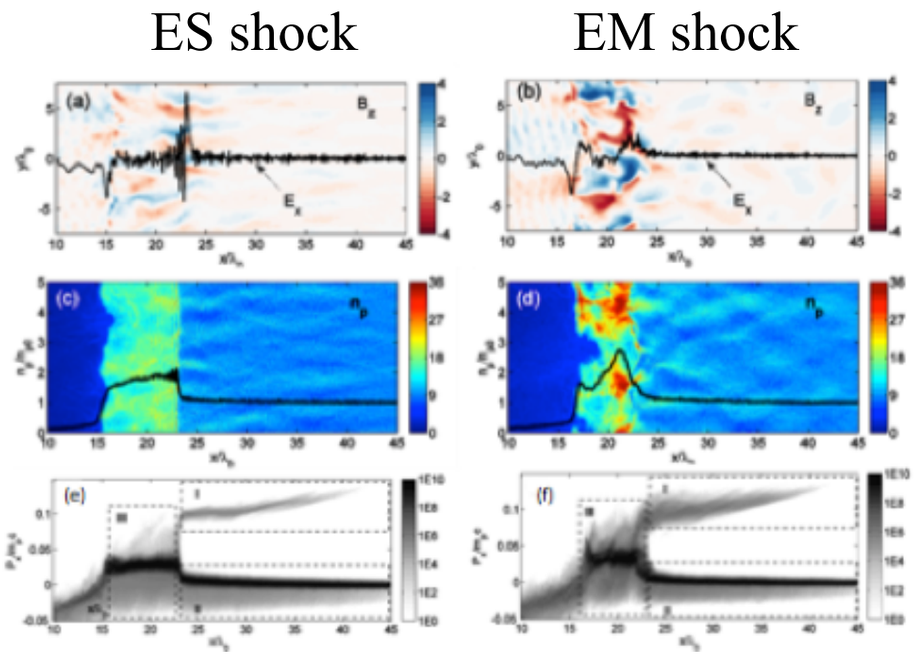

Comparison of ES and EM collisionless shock properties. PIC simulations for the laser intensity of 10^{19} W/cm^2 and the plasma density of 7 n_c with and without external magnetic field.
a) and b): electric field lineout and magnetic field structure.
c) and d): density profiles showing the strong filamentary compression in case of EM shock.
e) and f): ion phase space data. For ES shock ions are reflected at the shock front, for EM shock the reflection also happens behind the shock, in the highly magnetized region.

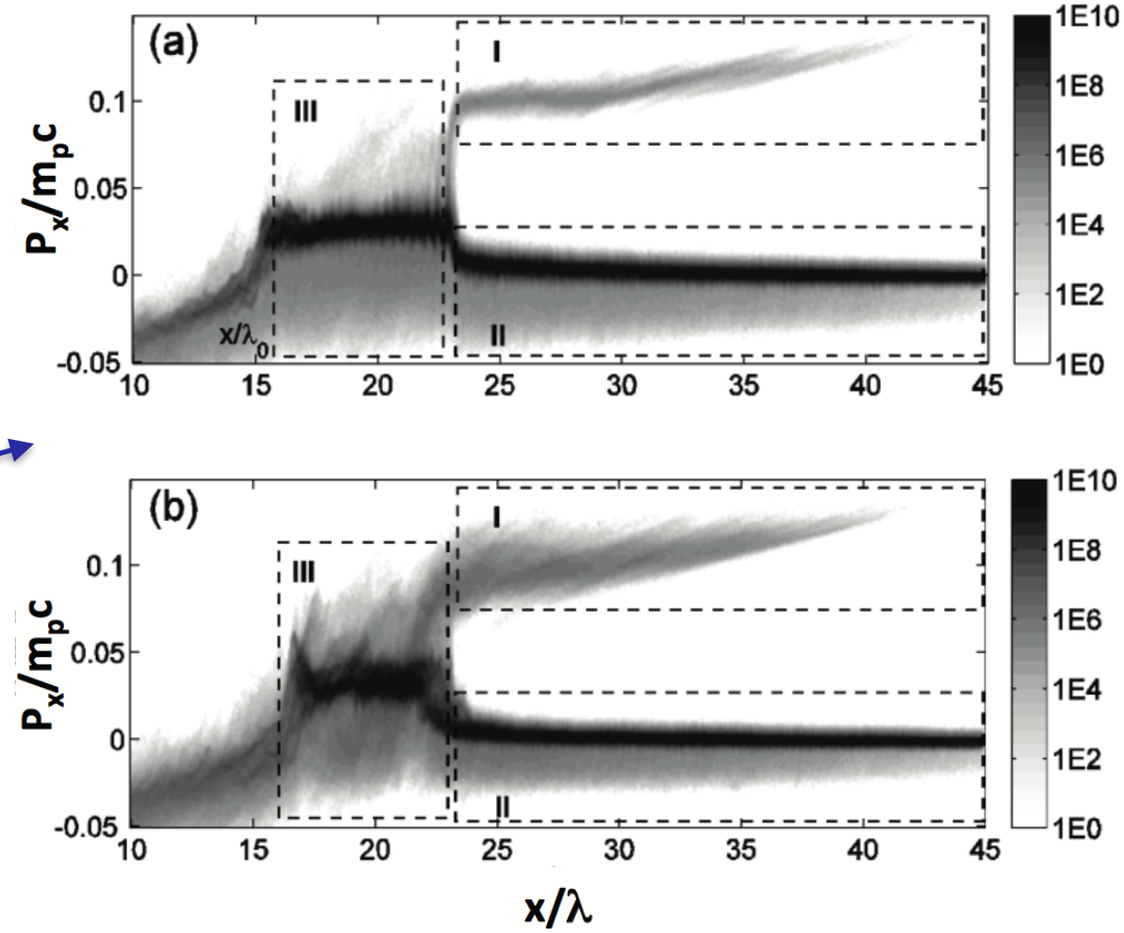

Ion phase space (x,Px), (a) without B field and (b) with B field. I, II, and III in (B) indicate reflected ion, up-stream ion and down stream ion, respectively

Outline

- High power laser systems and applications
- Collisionless shocks for laser particle acceleration
- **Importance of collisionless shocks in astrophysics**
- Experimental and numerical studies of collisionless shocks of interest for astrophysics
- Collision of plasmas in an external magnetic field as a platform to study magnetized collisionless shocks
- Collisionless shocks in electron-positron plasmas using extreme-light laser pulses
- Conclusions and perspectives

Collisionless turbulent shocks are held responsible for energetic particle and radiation generation in powerful astrophysical objects

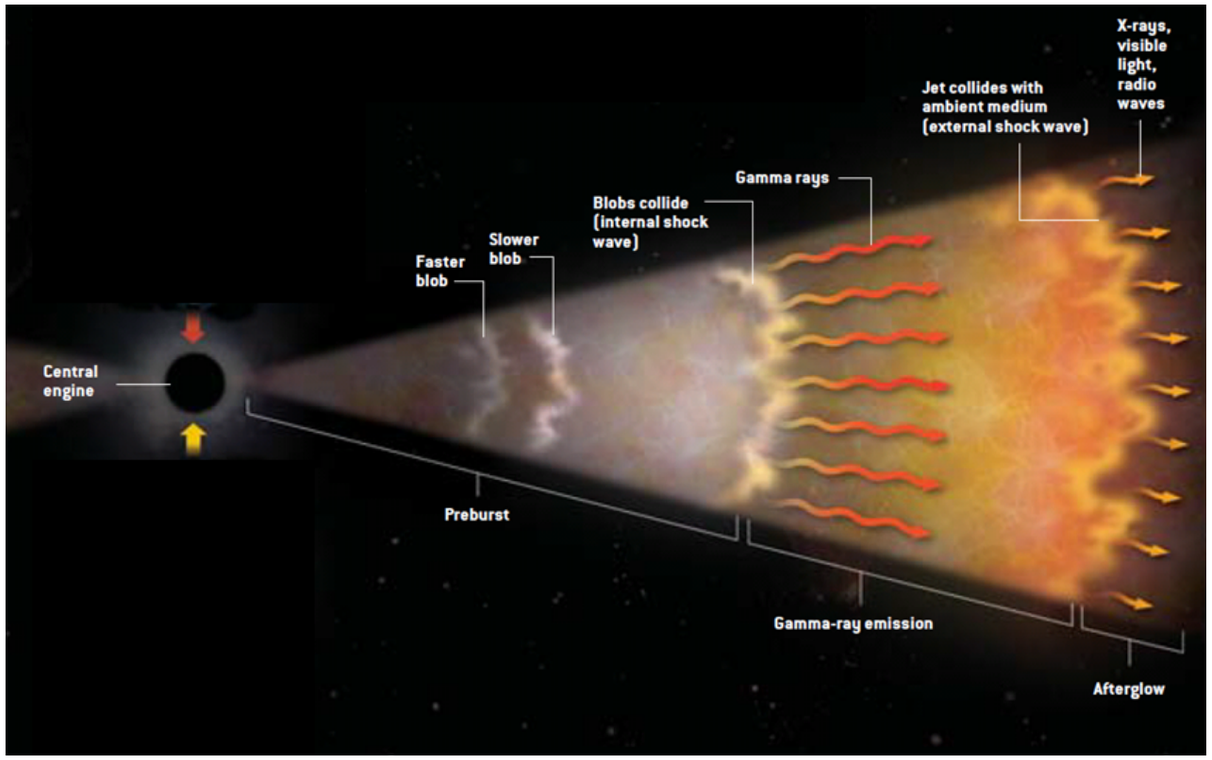

N. Gehrels *et al*., Scientific American **287**, 84 (2002)

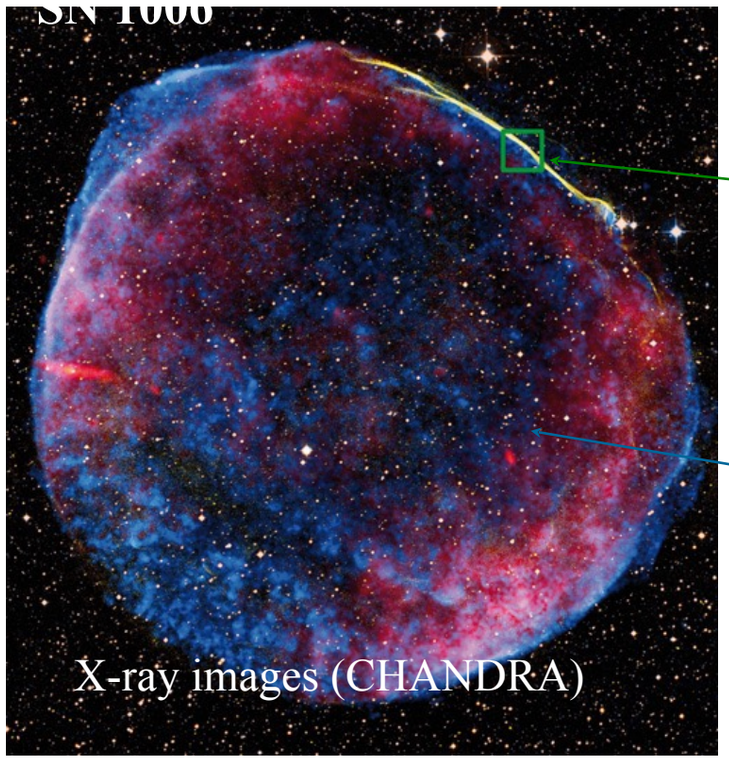

Shock transition region

Shock-heated ejecta in magnetic turbulence

Collisionless shocks are expected to form in violent astrophysical processes (SNR's, solar winds, pulsar winds, AGN's…) through:

- Explosion-driven blast waves induced by fast outflows encountering an obstacle or colliding with other flows;
- Nonlinear growth/steepening of unstable plasma waves excited inside these flows.

Typical SNR parameters[1,2]

- Shock velocity $v_{sh} \sim 3 \times 10^8$ cm/s
- Particle density $n \sim 1\ \mathrm{cm}^{-3}$
- SNR diameter $D \sim 10$ pc $= 3 \times 10^{19}$ cm
- Shock width $l_{sh} \sim 0.1$ pc $= 3 \times 10^{17}$ cm
- Collisional mean free paths:
  $\lambda_{ii} \sim 10^{22}\mathrm{cm} > \lambda_{ie} \sim 10^{20}\mathrm{cm} > D \gg l_{sh}$

[1]A. Bamba et al., Adv. Space Res. **33**, 376 (2004); [2]H. Völk et al., A&A **433**, 229 (2005).

Courtesy of Laurent Gremillet

Collisionless turbulent shocks are held responsible for energetic particle and radiation generation in powerful astrophysical objects

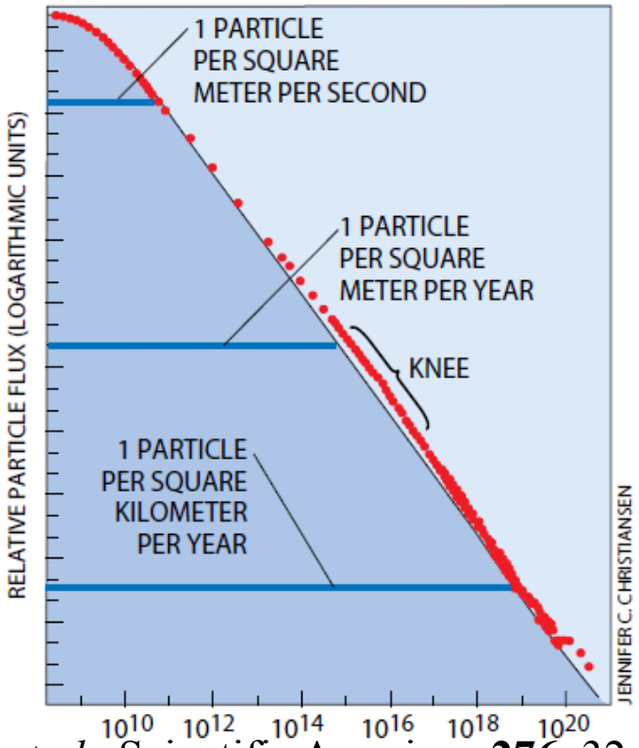

J.W. Cronin *et al.*, Scientific American **276**, 32 (1998)

Particle trajectories across the shock front
Fermi-type diffusive acceleration results from multiple reflections off *magnetic fluctuations* moving at different veloclities[1-3].

[1]A. R. Bell, MNRAS **182**, 147 (1978).
[2]R. Blandford & D. Eichler, Phys. Rep. **154**, 1 (1987).
[3]A. Spitkovsky, ApJ **682**, L5 (2008).

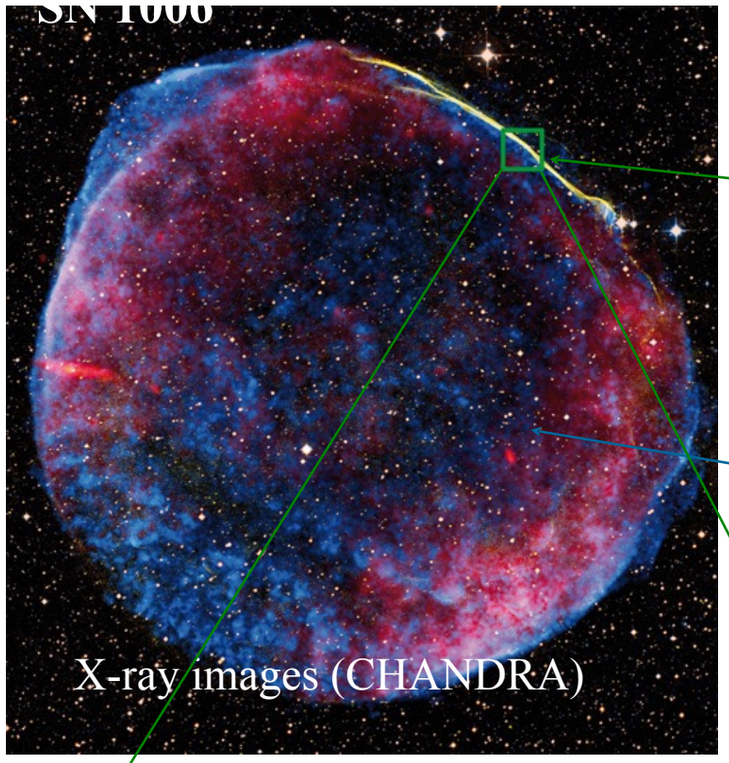

Shock transition region

Shock-heated ejecta in magnetic turbulence

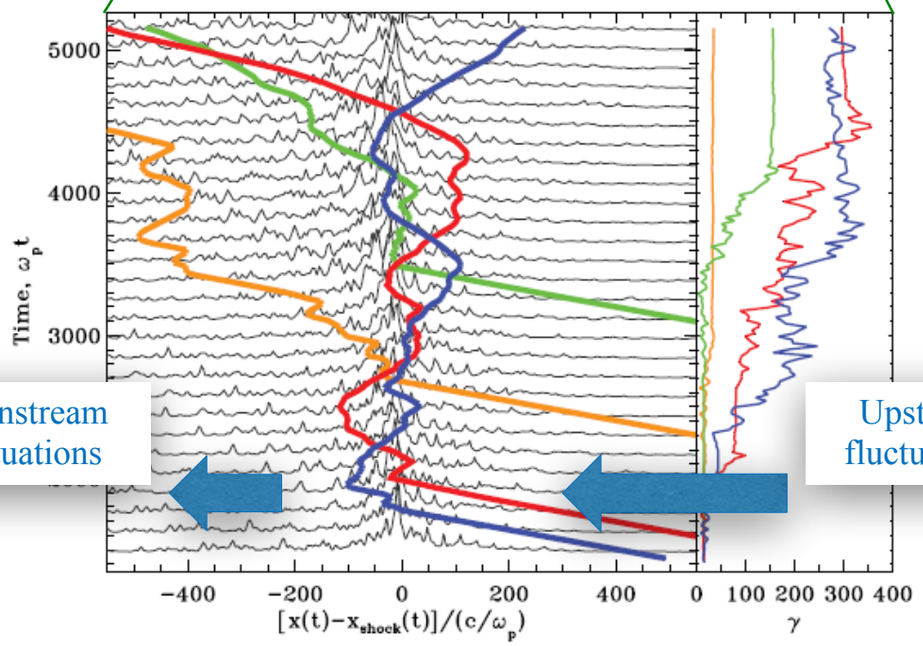

Courtesy of Laurent Gremillet

The Weibel-filamentation instability is a key player for turbulent shock formation in non/weakly-magnetized systems

- The Weibel/filamentation develops in plasmas with anisotropic momentum distributions (e.g. counterstreaming flows)[1].
- It generates magnetic filaments (on $c/\omega_{pe} - c/\omega_{pi}$ scales) through which particles are deflected/decelerated, hence dissipating their directed kinetic energy into (isotropic) thermal energy and initiating shock transition[2].
- It provides scattering centers causing (Fermi-type) nonthermal particle acceleration and synchrotron radiation emission[3].

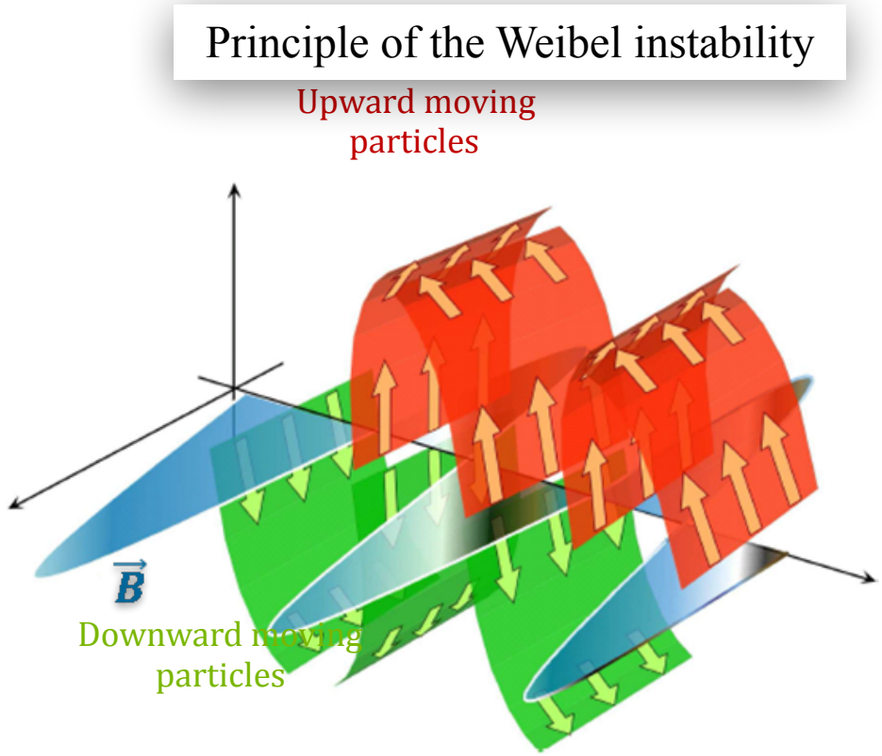

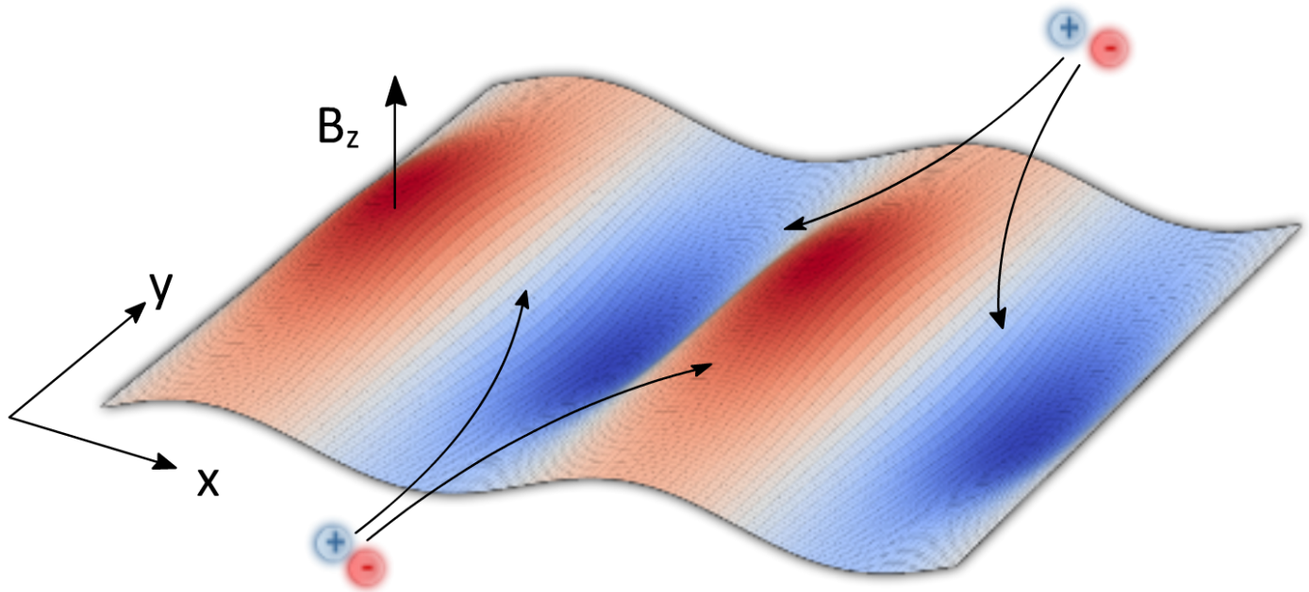

[1]E. S. Weibel, Phys. Rev. Lett. **2**, 83 (1959); B. D. Fried, Phys. Fluids **2**, 337 (1959).
[2]M.V. Medvedev & A. Loeb, ApJ **526**, 697 (1999).
[3]L. Sironi *et al*., ApJ **707**, L92 (2009); ApJ **771**, 54 (2013).

Courtesy of Laurent Gremillet

Scenario of turbulent shock formation in Weibel-unstable colliding plasmas

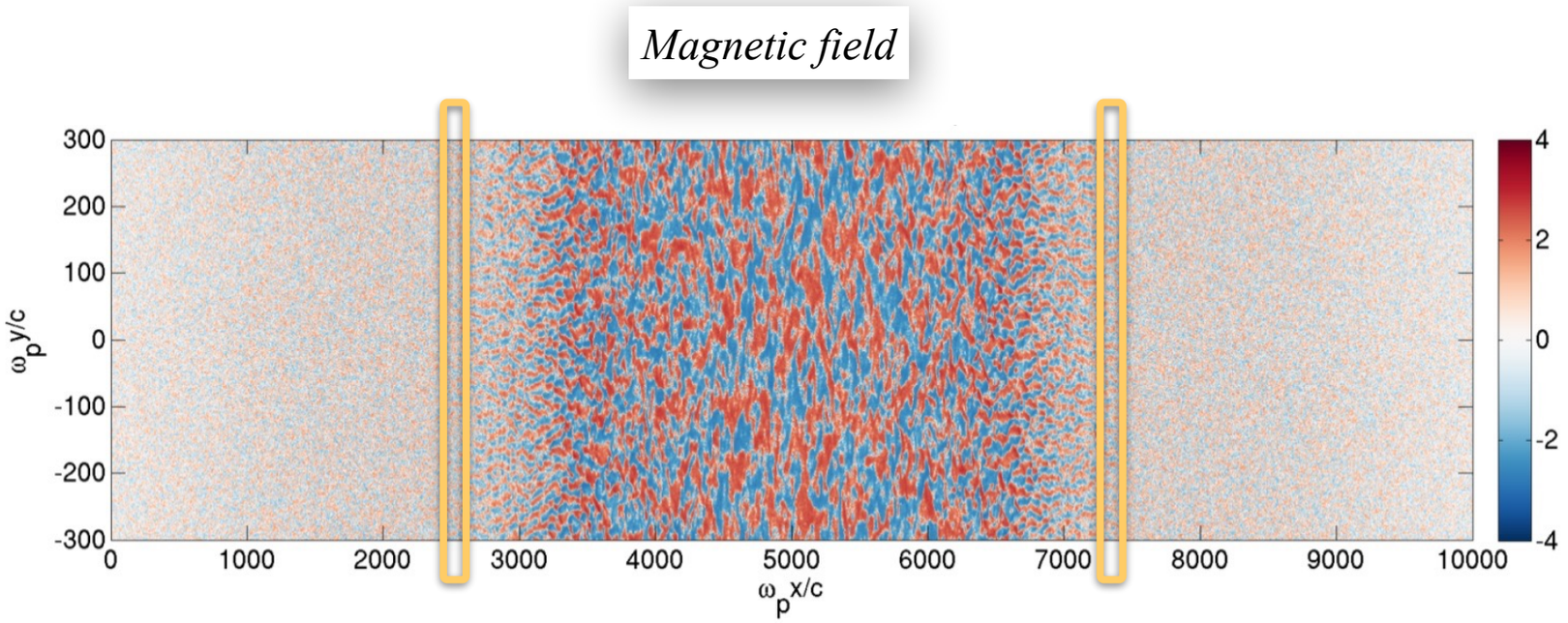

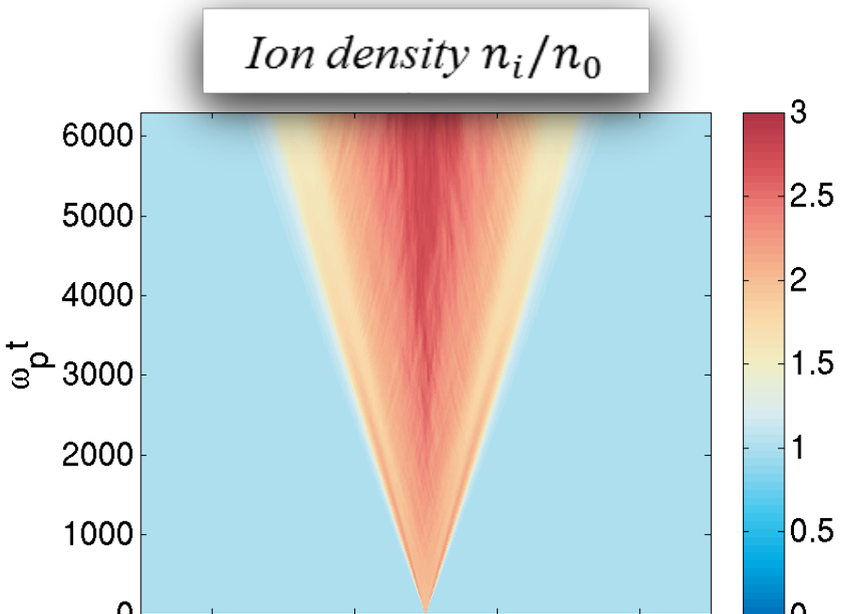

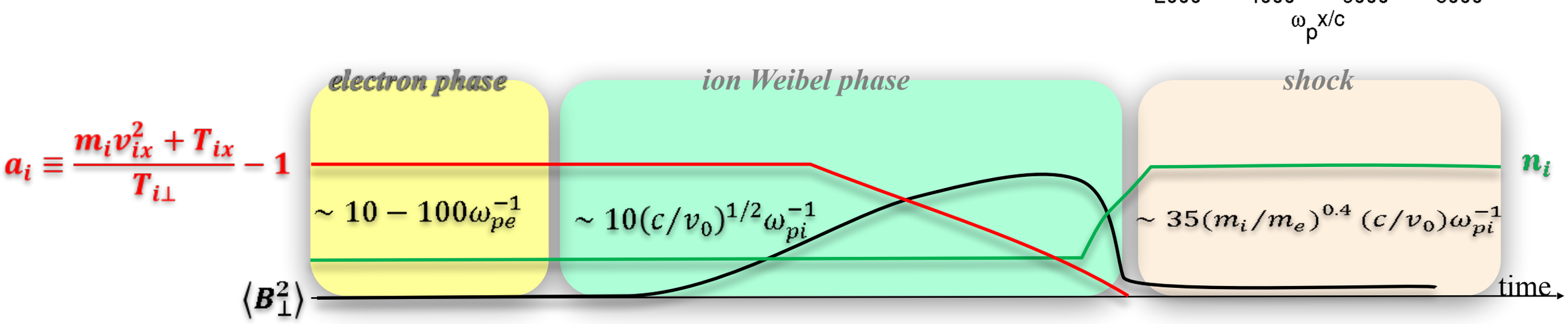

- Electron instabilities first develop and saturate, leaving the electrons mostly isotropized.

Courtesy of Laurent Gremillet

Scenario of turbulent shock formation in Weibel-unstable colliding plasmas

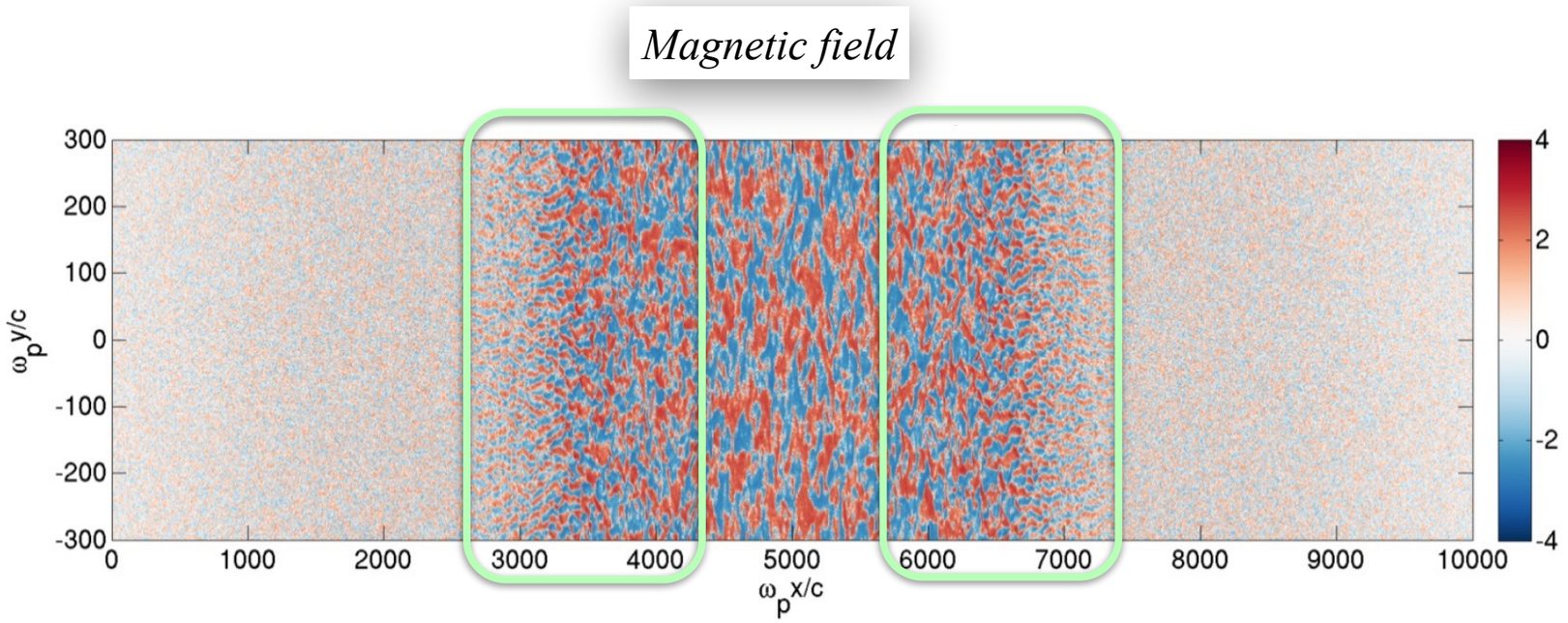

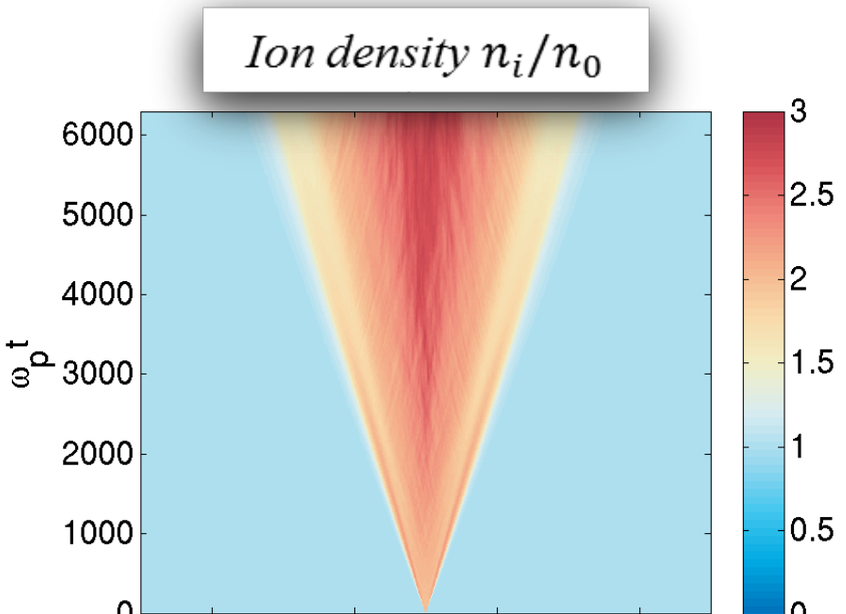

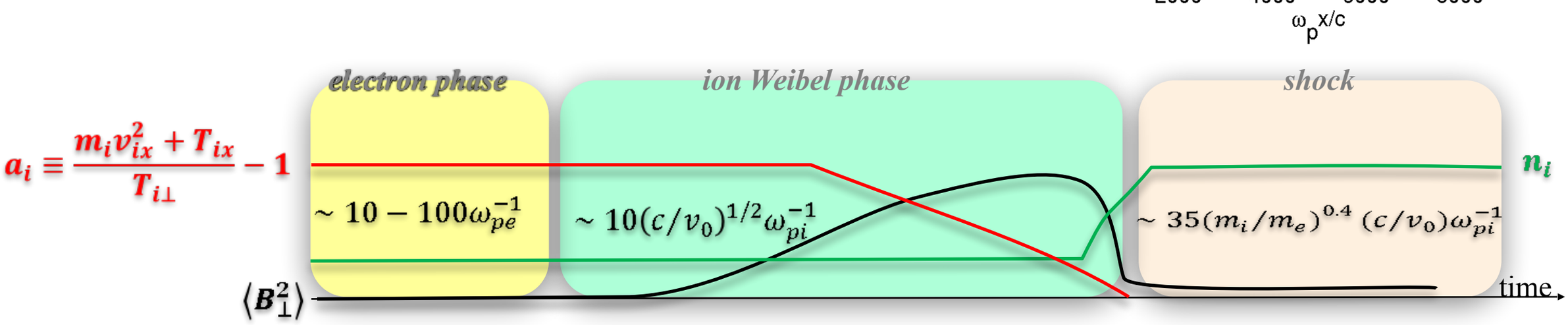

- Electron instabilities first develop and saturate, leaving the electrons mostly isotropized.
- The ion-ion Weibel-filamentation instability then grows up to $\sigma \equiv \langle B^2 \rangle / 2\mu_0 m_i c^2 (\gamma_i - 1) \sim 0.1$ (through filament coalescence and secondary kink instabilities), causing ion scattering off magnetic fluctuations.

Courtesy of Laurent Gremillet

Scenario of turbulent shock formation in Weibel-unstable colliding plasmas

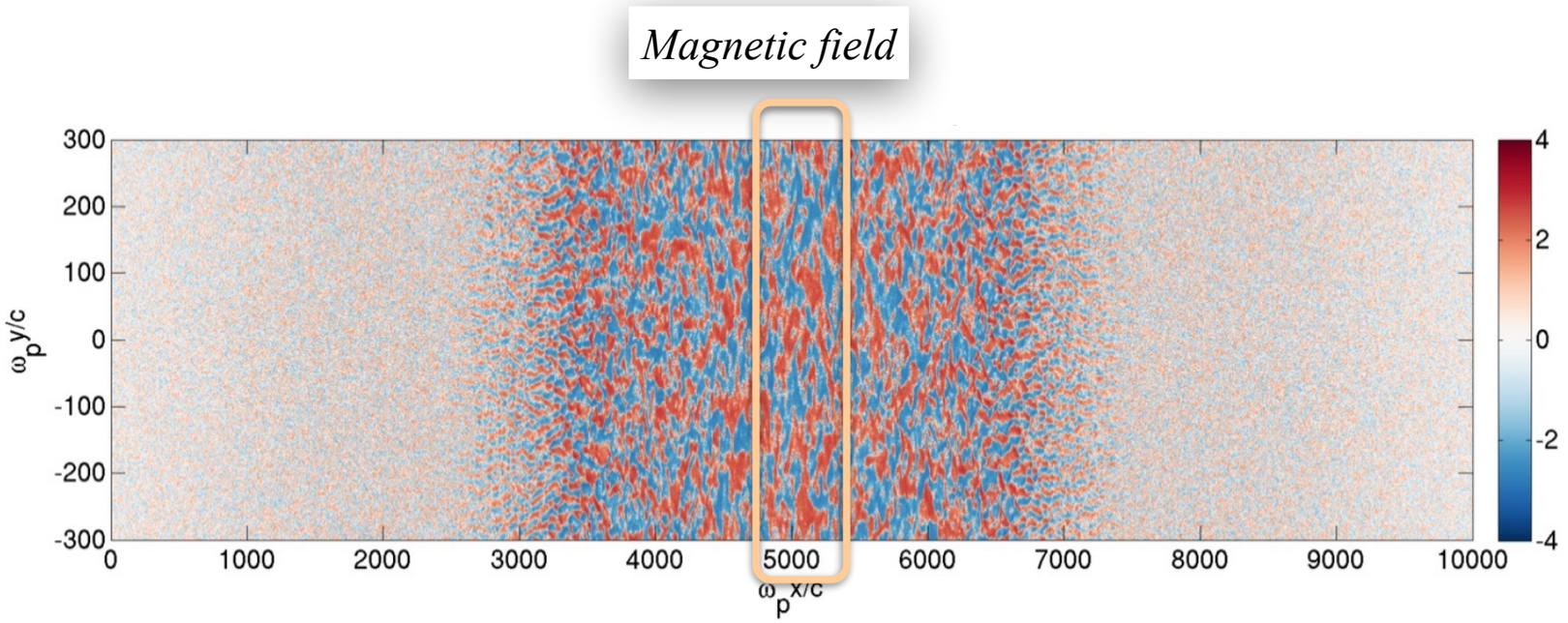

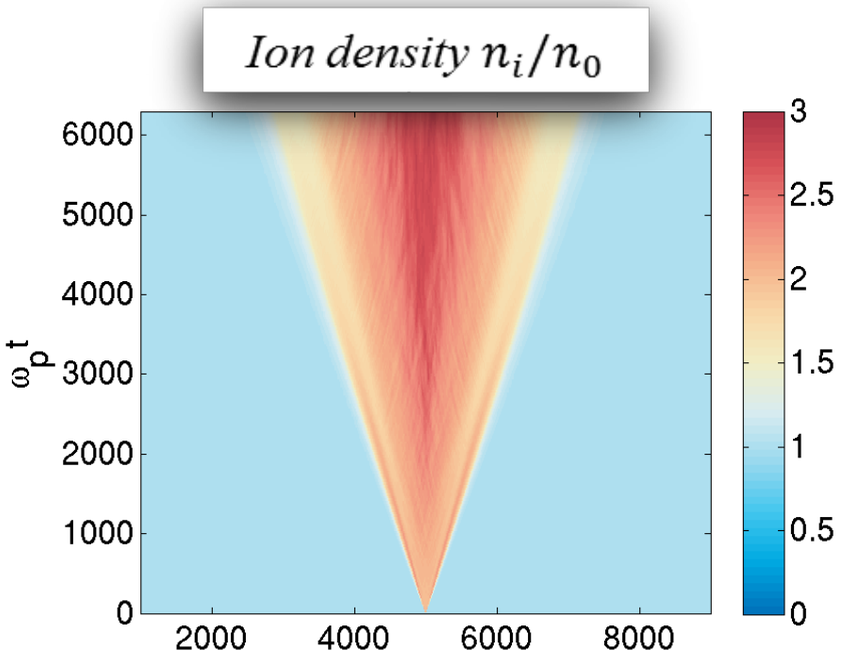

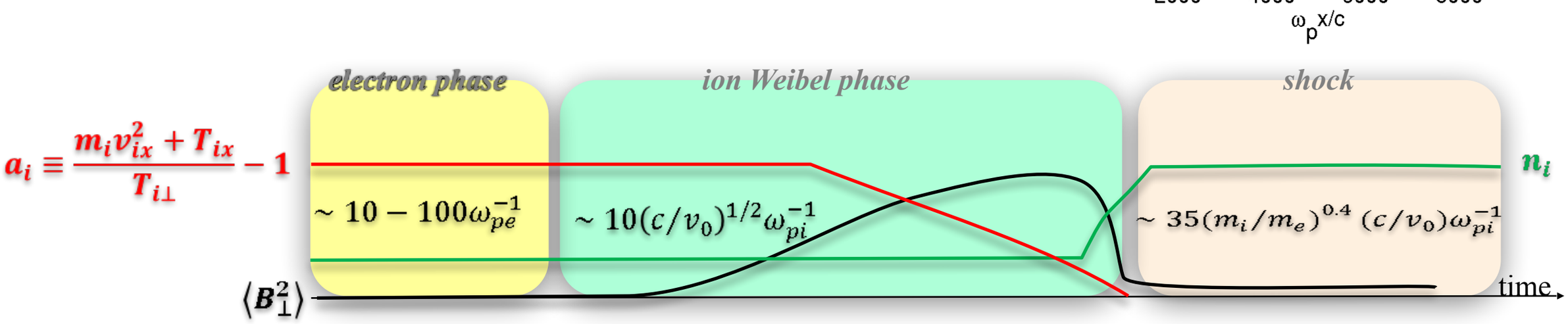

- Electron instabilities first develop and saturate, leaving the electrons mostly isotropized.
- The ion-ion Weibel-filamentation instability then develops up to $\sigma \equiv \langle B^2 \rangle / 2\mu_0 m_i c^2 (\gamma_i - 1) \sim 0.1$ (through filament coalescence and secondary kink instabilities), causing ion scattering off magnetic fluctuations.
- Isotropized particles accumulate in the overlap region until fulfilling the hydrodynamic-like (Rankine-Hugoniot) jump conditions of a stationary shock wave.

Moderately supersonic flows may develop laminar electrostatic shocks instead of turbulent Weibel-mediated shocks

$v_0 = \pm 0.01c$, $T_e = 20$ keV ($M_s \sim 3$)

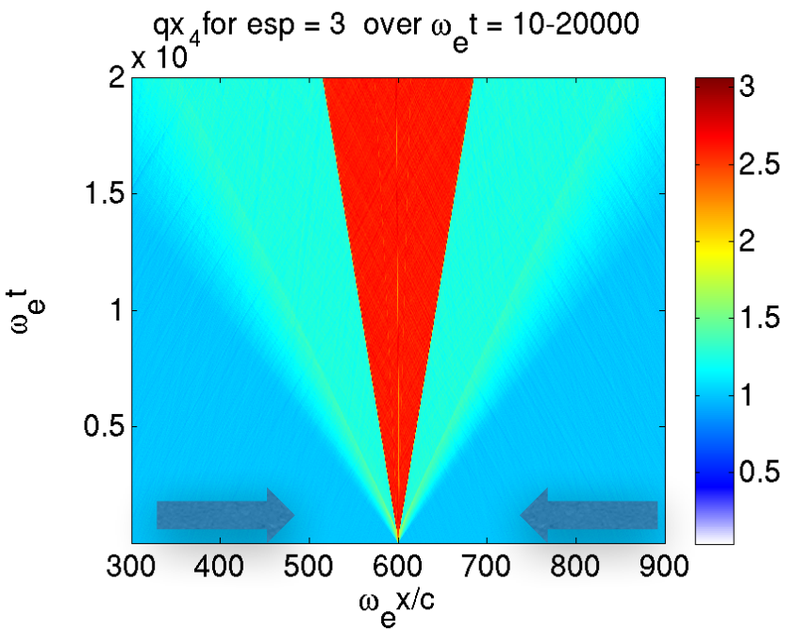

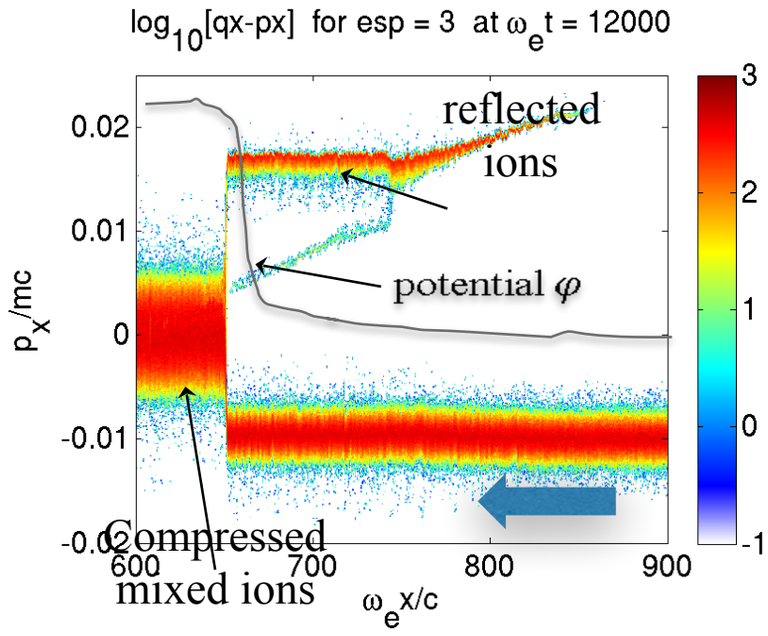

$v_0 = \pm 0.01c$, $T_e = 5$ keV ($M_s \sim 4.3$)

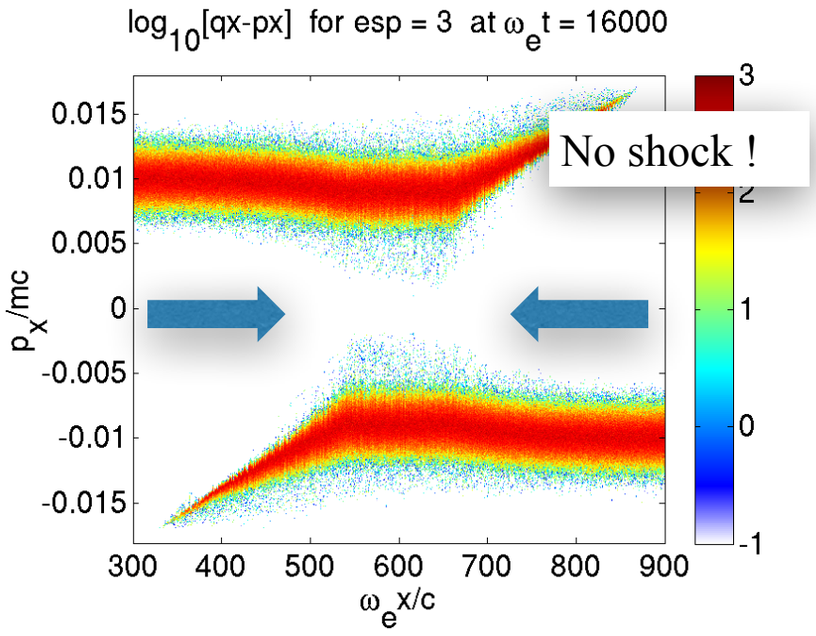

- Electrostatic shocks are mediated by the ambipolar electric field set up by the electrons across a plasma (pressure) discontinuity.
- They are characterized by *laminar* deceleration/reflection of the incoming ions, in contrast with the angular scattering underlying *turbulent* Weibel-mediated shocks
  ⇒ they do not lead to diffusive particle acceleration.
- An electrostatic laminar shock cannot (usually) form[1,2] if $M_s \equiv u_0/u_s > 3$, where $u_s = \beta_s \gamma_s$ and $u_s = \left(\frac{Z_i T_e}{m_i c^2}\right)^{1/2}$

[1]G. Sorasio, Phys. Rev. Lett. **96**, 045005 (2006)
[2]M. Dieckmann *et al*., Phys. Plasmas **20**, 042111 (2013)

Courtesy of Laurent Gremillet

The parameter space associated with electrostatic/Weibel-mediated shocks has been investigated[1]

Transition between electrostatic and electromagnetic shock regimes[1]

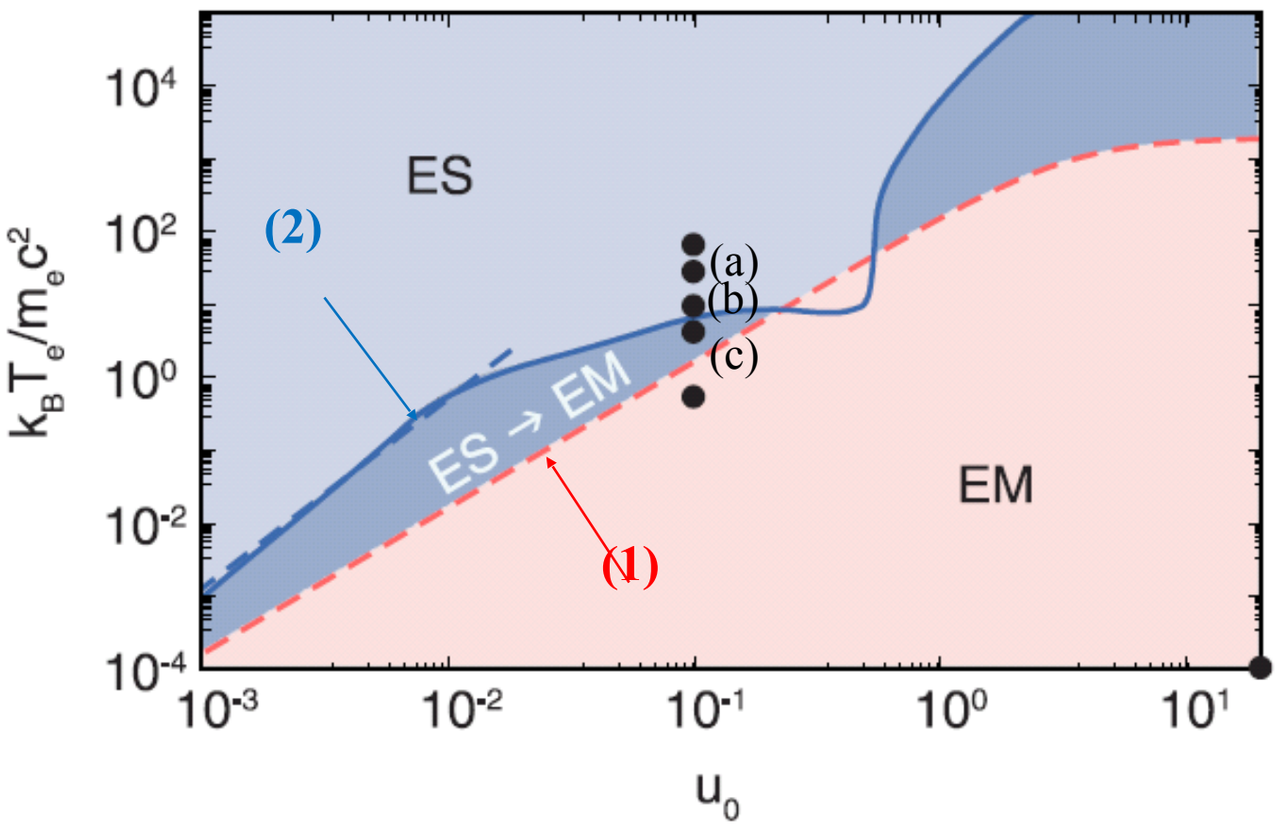

Proper flow velocity

Magnetic field map and electrostatic potential φ/E_{kin} for cases (a), (b), (c)[1]

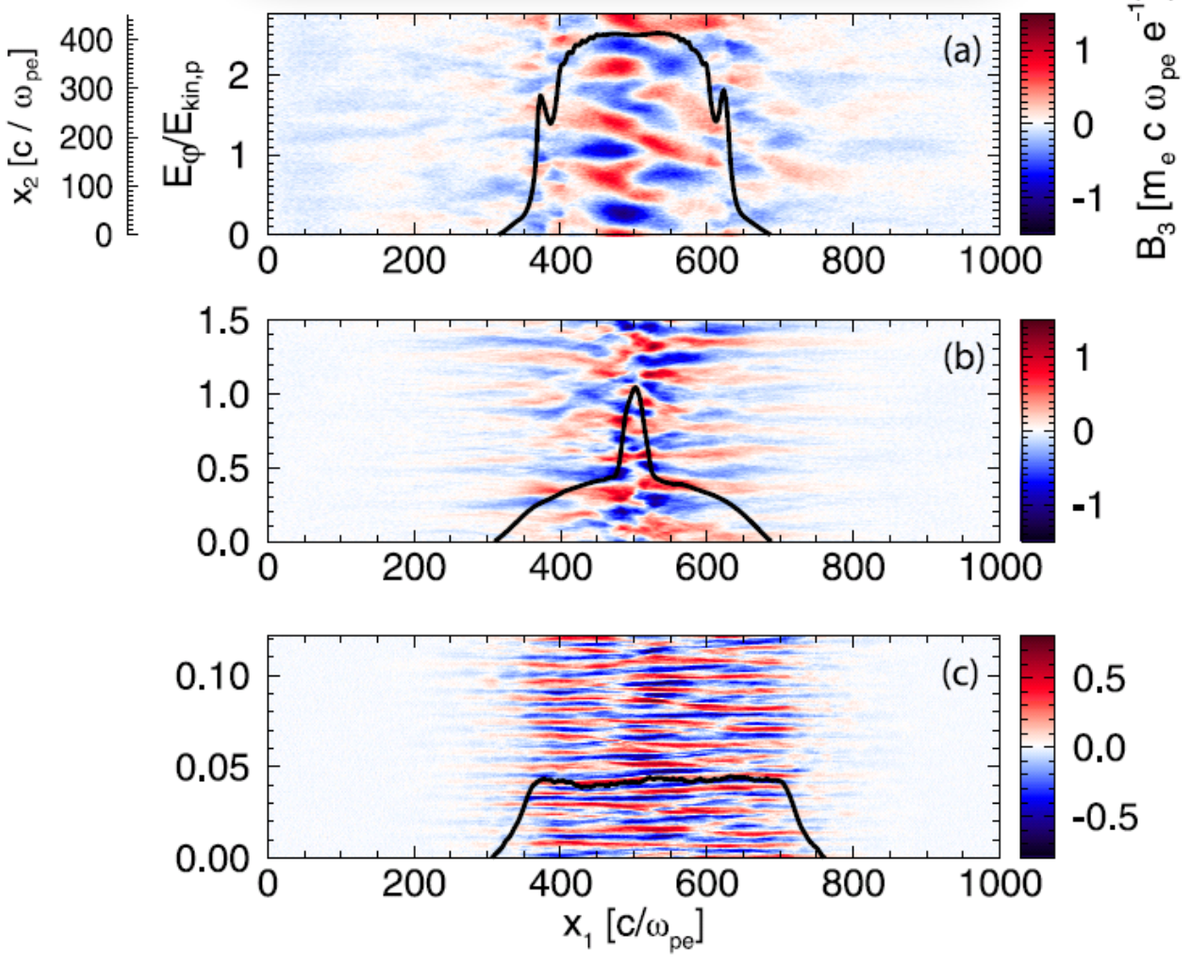

- An electrostatic laminar shock cannot form[1] if $M_s \equiv u_0/u_s > 3$, where $u_s = \beta_s \gamma_s$ and $u_s = \left(\frac{Z_i T_e}{m_i c^2}\right)^{1/2}$ **(1)**
- Weibel modes likely dominant if their growth time is shorter than the electrostatic shock formation time[1]:

$$\Gamma_W^{-1}(\varphi_{max}) < \tau_{sh,es} \sim 10\gamma_0^{3/2}\omega_{pi}^{-1} \quad \textbf{(2)}$$

[1]A. Stockem *et al.,* Sci. Rep. **4**, 3934 (2014)

Courtesy of Laurent Gremillet

Outline

- High power laser systems and applications
- Collisionless shocks for laser particle acceleration
- Importance of collisionless shocks in astrophysics
- **Experimental and numerical studies of collisionless shocks of interest for astrophysics**
- Collision of plasmas in an external magnetic field as a platform to study magnetized collisionless shocks
- Collisionless shocks in electron-positron plasmas using extreme-light laser pulses
- Conclusions and perspectives

Different scenarii of laser-induced unmagnetized collisionless shocks

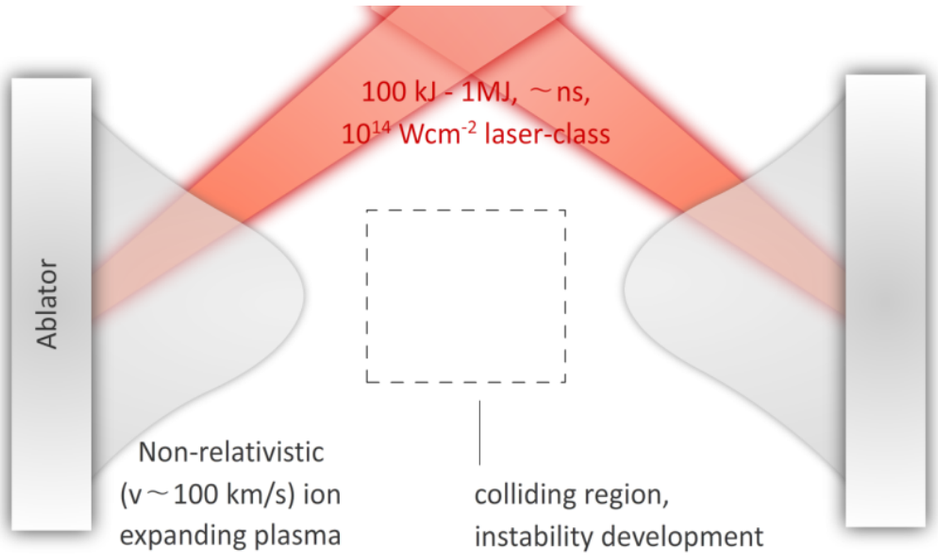

Non-relativistic regime: **Shocks between electron-ion *ablated* plasmas [1]**

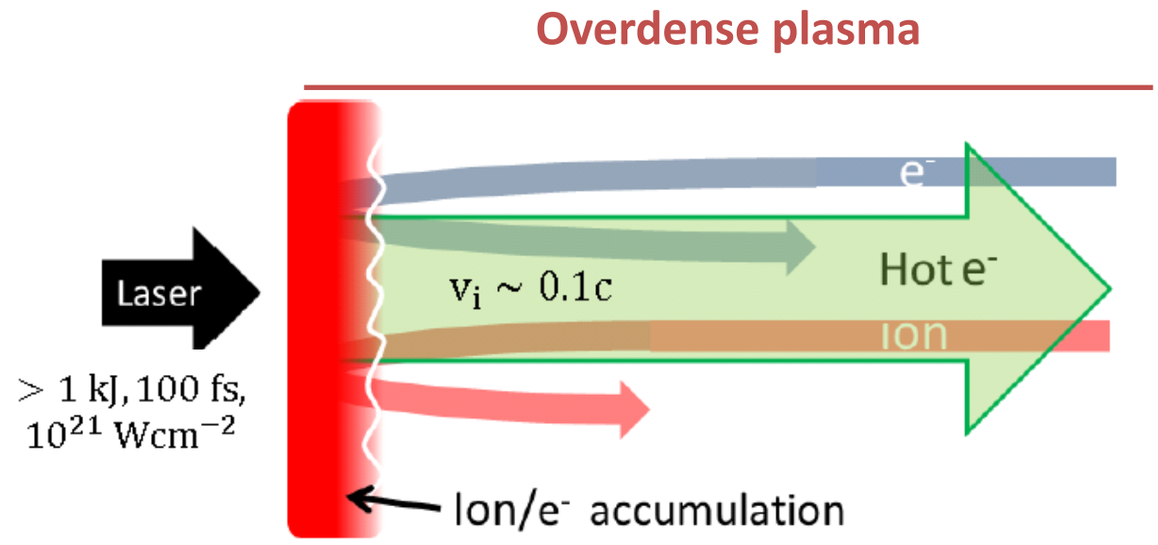

Relativistic regime: **Shocks induced by laser *radiation pressure* in overdense plasmas [2]**

Difficult to diagnose: not considered for laboratory astrophysics experiments yet

[1] – R. Drake *et al.,* AP **749**, 171 (2012), Fox *et al.,* PRL **111**, 225002 (2013)
[2] – F. Fiuza *et al.*, PRL **108**, 235004 (2012);

Weibel mediated shocks with high intensity lasers and dense targets

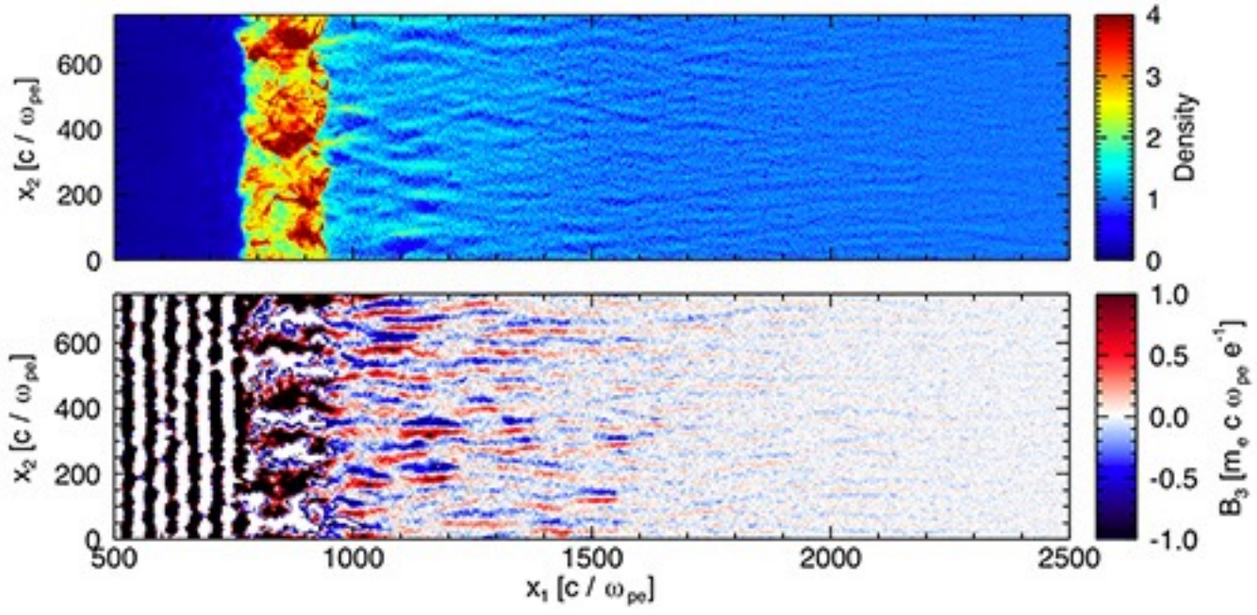

Structure of Weibel-mediated shock driven by the interaction of an intense laser with an overcritical target. The top panel shows the density compression behind the shock and the filamentary structure ahead of it. The bottom panel shows the strong filamentary magnetic fields associated with the Weibel instability

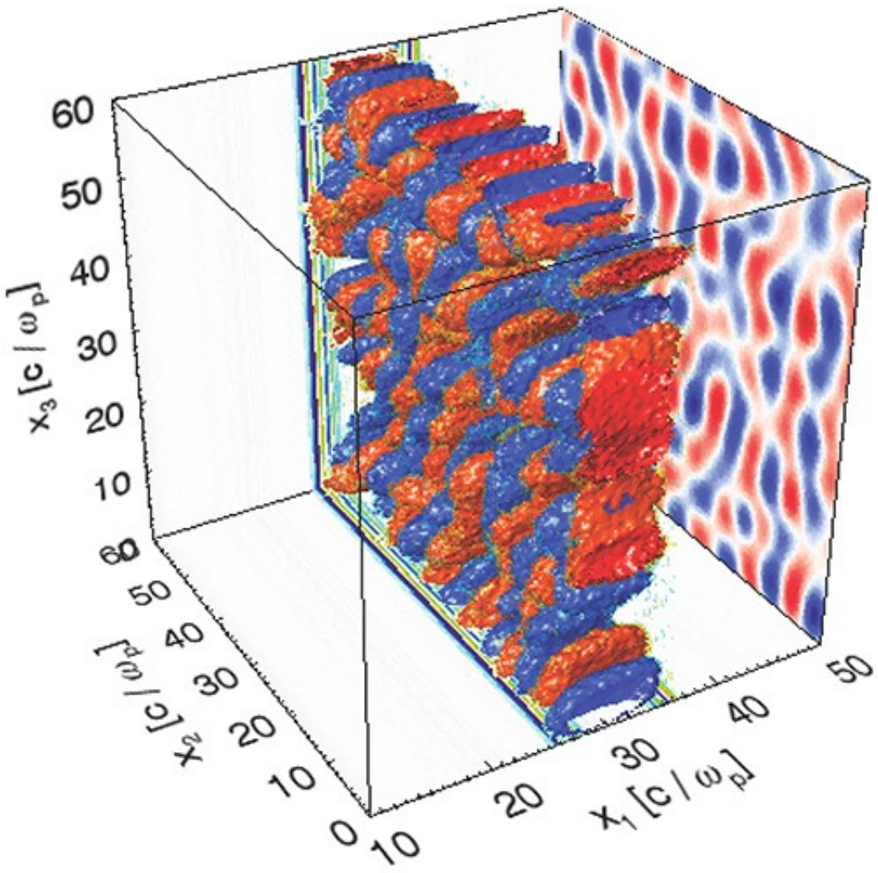

Perpendicular electromagnetic field in the course of shock formation. 2D projections show the electrostatic field in the planes parallel to shock propagation and the magnetic field projection in the perpendicular plane.

F. Fiuza et al., Physical Review Letters 108, 235004 (2012)
A. Stockem et al., Physical Review Letters 113, 105002 (2014)

Electrostatic shocks in lab plasma collisions

Sakawa et al. ADVANCES IN PHYSICS: X 2016

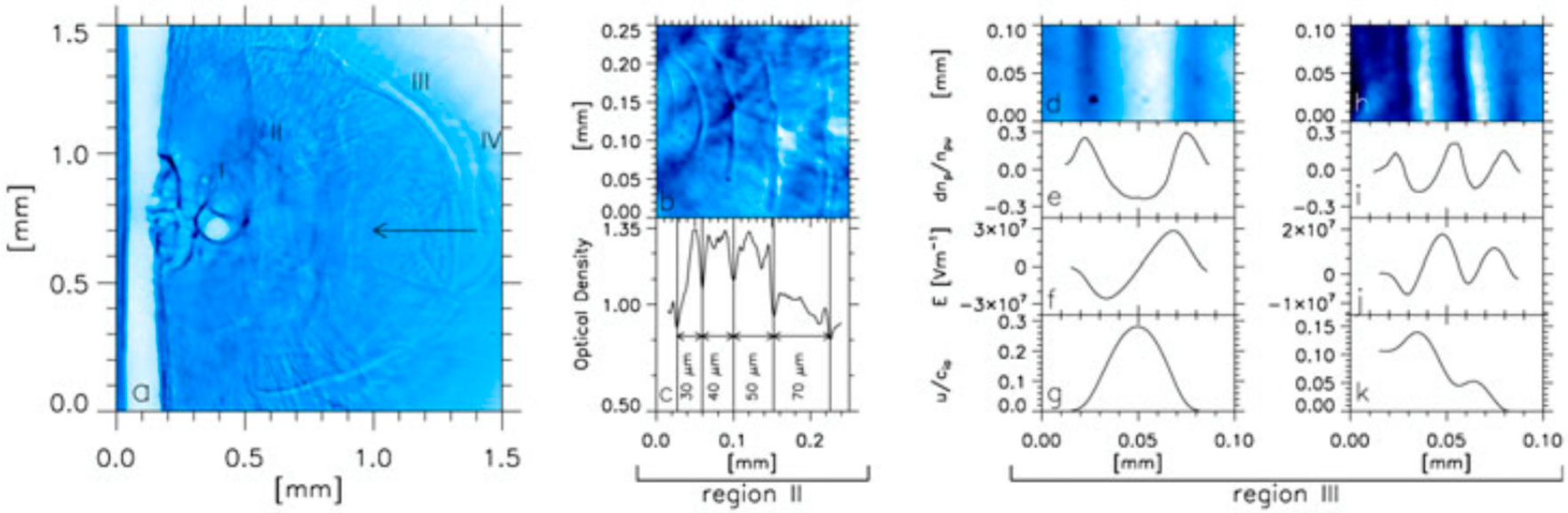

Typical proton imaging data with protons of 7 MeV energy. (b)–(c) Detail and RCF optical density lineout corresponding to the region II showing modulations associated with a train of solitons. (d)–(k) Details of the region III and correspondent lineouts of the probe proton density δnp/npu, reconstructed electric field E, and reconstructed normalized ion velocity u/cia in the case of (d)–(g) an ion acoustic soliton and (h)–(k) a collisionless shock [L. Romagnani et al. PRL 2008]

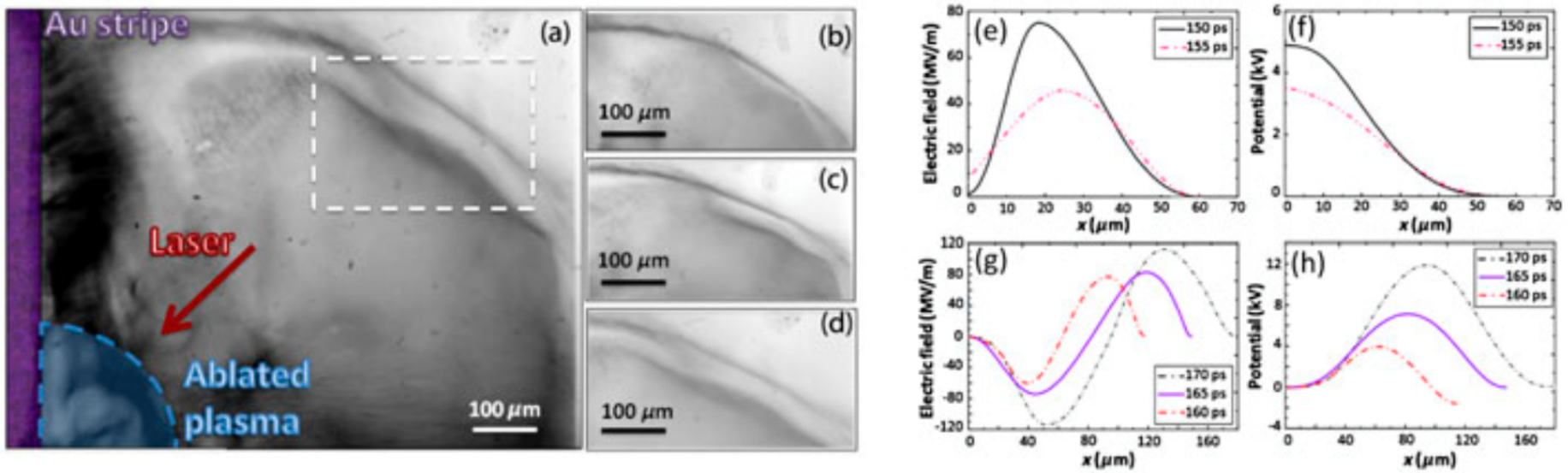

A proton radiograph of the interaction of the main laser pulse (red arrow) with a gold foil (left purple rectangle) at t = 17 ps. Notes: (b)–(d) Zooms of the proton radiographs of the region highlighted by the dashed white rectangle in (a) at (b) t = 150 ps (proton energy of 11.5 MeV), (c) 160 ps (10 MeV), and (d) 170 ps (9 MeV). (e), (g) Experimental electric field distribution and (f), (h) associated potential during the transition between the CFDL and the protoshock [H. Ahmed et al. PRL 2013]

Electrostatic shocks in lab plasma collisions

Sakawa et al. ADVANCES IN PHYSICS: X 2016

(a) The top view of experimental setup. SG and IF represent the ICCD cameras for shadowgraphy (SG) and interferometry (IF), respectively, WP is the Wollaston prism and PL is the polarizer. (b) Schematic view of the target design. (c) The interferogram and (d) shadowgraph measured at t = 9 ns. x = 0 and 4.5 mm are the surface of the first and second CH foils, respectively. Four beams were focused on the first CH at x = 0 and y = 2.5 mm. (e) The density profile at y = 3.5 mm derived from (c). A large density-jump is observed at x ≃ 3.1 mm. (f) The average intensity profile from (d) for y = 3.0–4.0 mm [T. Morita et al. POP 2010]

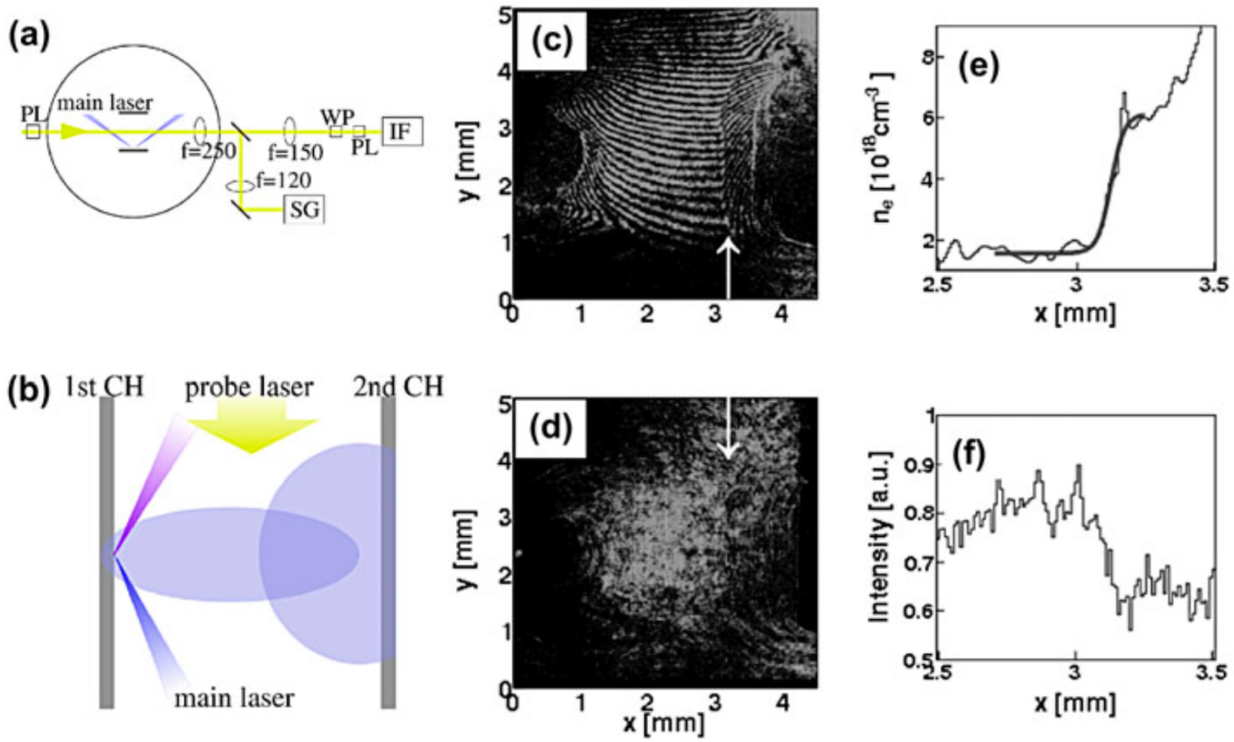

Schematic of double-plane target. The target normal lies 30◦ from the laser axis. (b) SOP image. The laser timing corresponds to the top of the image. (c) Stack plot of line profiles of the SOP image in (b) from 7 to 27 ns. x2 axis in (b) and (c) shows the spatial scale normalized to the ion inertial length. (d) Self-emission and (e) SG snapshots at t = 25 ns [Y. Kuramitsu et al. PRL 2011]

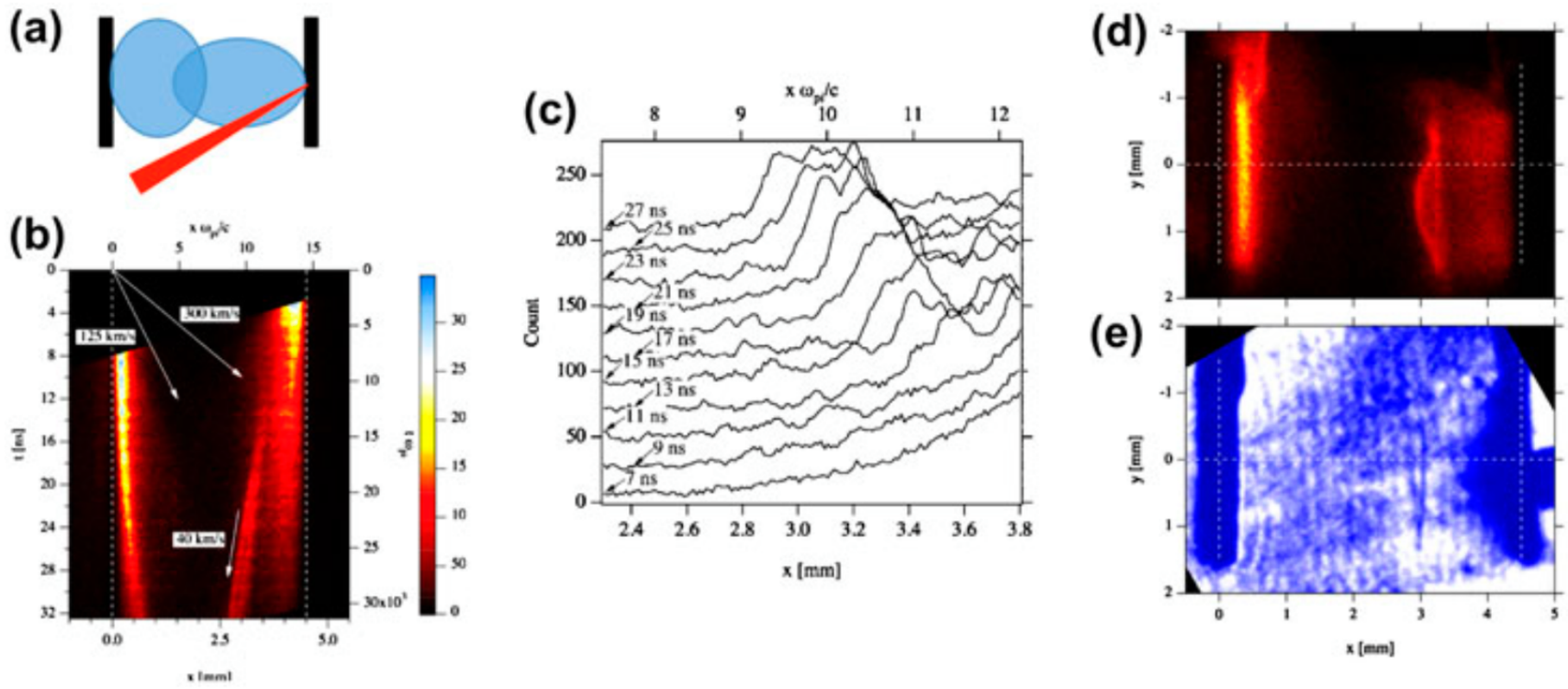

The experimental investigation of Weibel-mediated plasma collisions is becoming accessible to high-power lasers

- High-power lasers have the unique capability of driving high-velocity ($v_i \sim 0.005 - 0.1c$), high-density ($n_e > 10^{18}$ cm^{-3}) electron-ion plasmas from their interaction with solid targets.
- The simplest scheme consists in making collide two ablative plasma flows[1-3].

High-energy, long-pulse laser scheme[1-3]

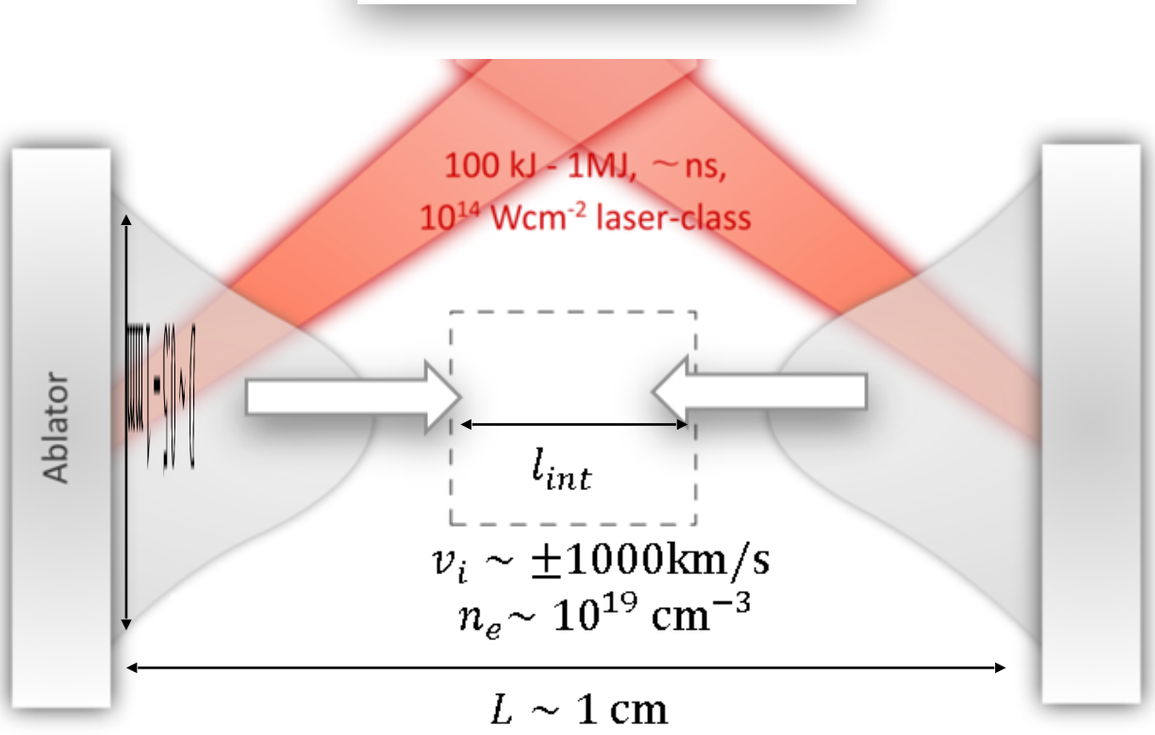

- The experimental generation of a Weibel-mediated shock implies:

$$c/\omega_{pi} \ll (D, l_{int}) \ll \lambda_{ii}$$

- For CH plasmas with $n_e = 10^{19}$ cm^{-3}, $v_i = \pm 1000$ km/s, $(T_e, T_i) \sim 1$ keV, one has
  - $M_s \sim 5 \Rightarrow$ Weibel-dominated
  - $c/\omega_{pi} \sim 0.1$ mm
  - $\boldsymbol{l_{int}} = ?$
  - $\lambda_{ee} \sim 2$ mm $\Rightarrow$ collisional electrons?
  - $\lambda_{Ce} \sim 7$ cm
  - $\lambda_{CC} \sim 70$ cm
  - $\lambda_{CH} \sim 300$ cm
  - $\lambda_{HH} \sim 400$ cm

  $\Rightarrow$ collisionless ions

[1]Kuramitsu et al., PRL. **106**, 175002 (2011); PRL **108**, 195004 (2012)
[2]W. Fox *et al.,* PRL **111**, 225002 (2013)
[3]C.M. Huntington *et al*., Nat. Phys. **11**, 173 (2015)

Courtesy of Laurent Gremillet

Formation and early nonlinear evolution of Weibel ion filaments recently observed in plasma-collision experiments[1,2]

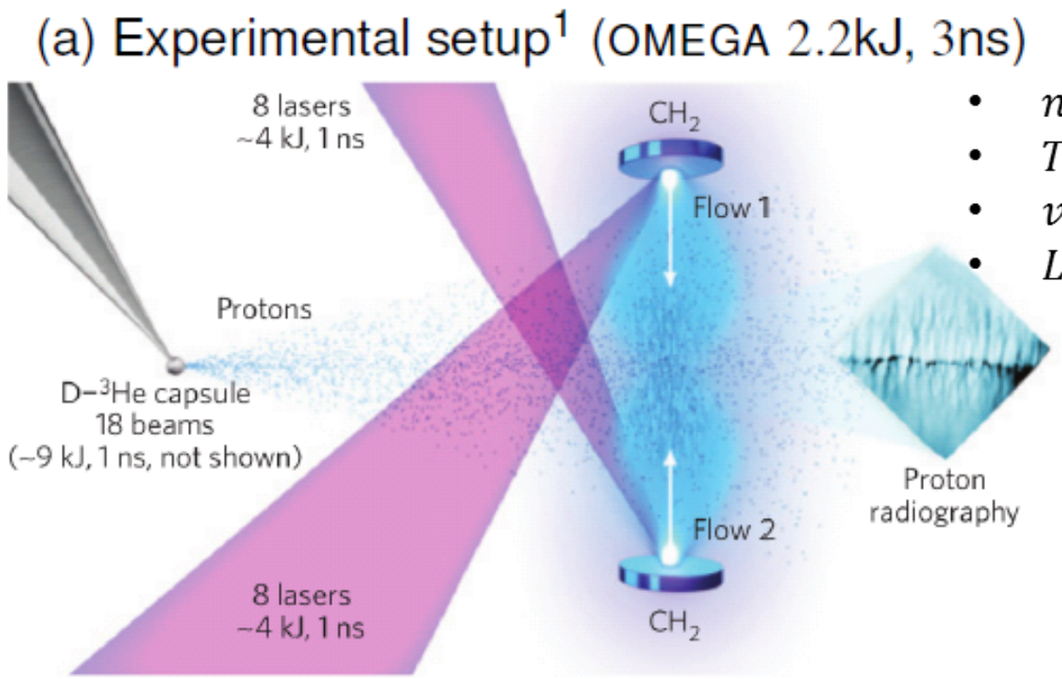

- $n_e \sim 5 \times 10^{18}$ cm^{-3}
- $T_e \sim 0.2$ keV
- $v_i \sim 2000$ kms^{-1} ($M_s \sim 20$)
- $L_{int} \sim 1$ cm $\sim 50 c/\omega_{pi}$

3D PIC (OSIRIS) simulation at $t = 1$ ns: Isosurfaces of n_e(orange) and B (blue-red)

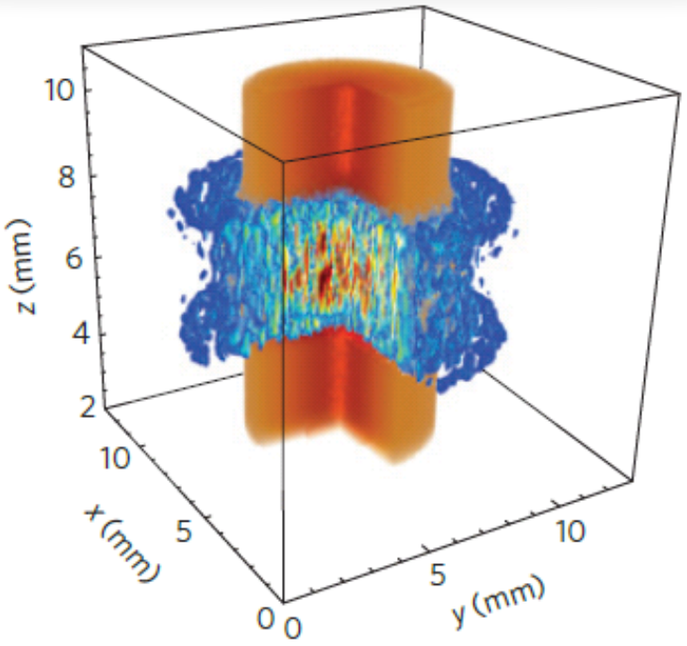

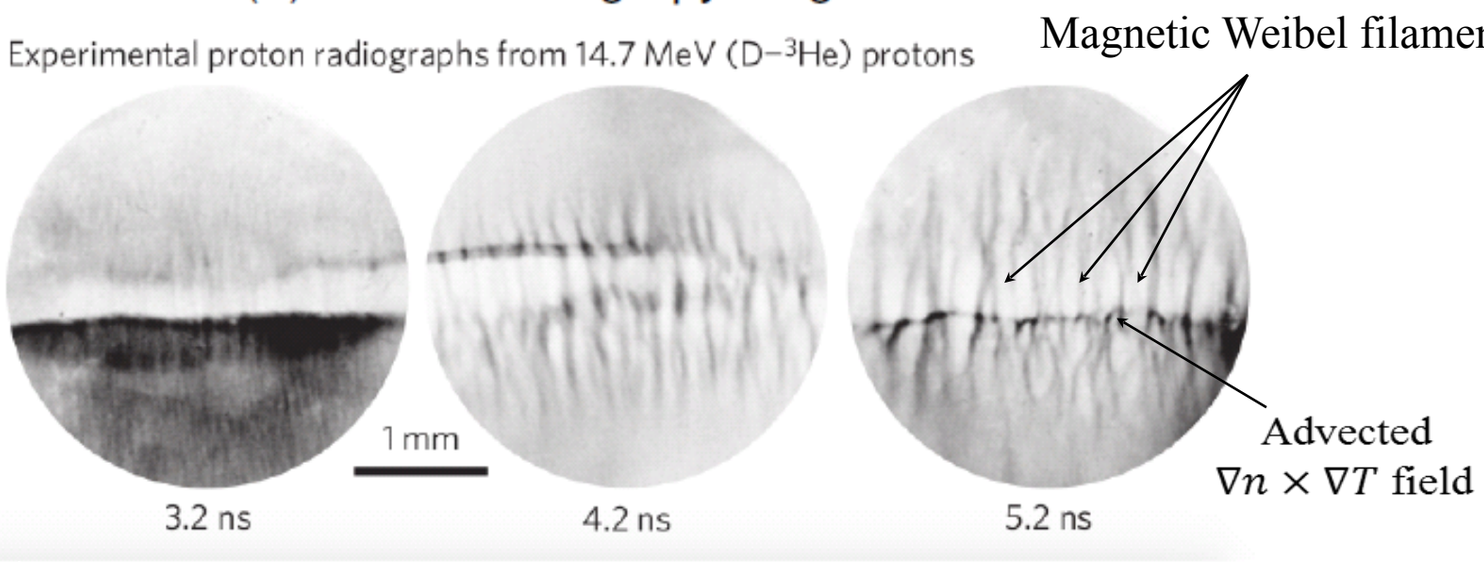

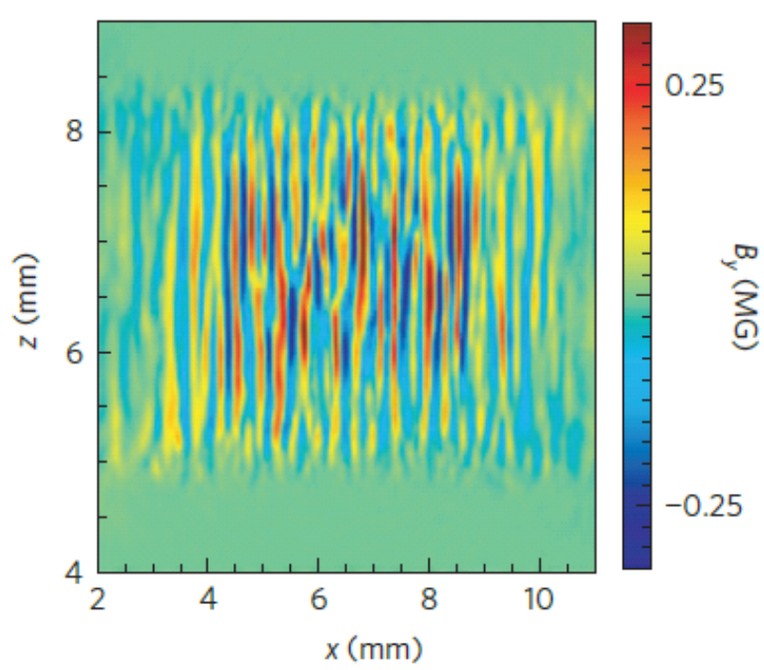

[1]C.M. Huntington *et al.*, Nat. Phys. **11**, 173 (2015)
[2]W. Fox et al., Phys. Rev. Lett. **111**, 225002 (2013)

Courtesy of Laurent Gremillet

Shock formation expected to be within the reach of the National Ignition Facility

NIF target design[1]

150 - 250 kJ per target
6 mm apart
Fe/Ni (0.1%) doped CD/CH foils

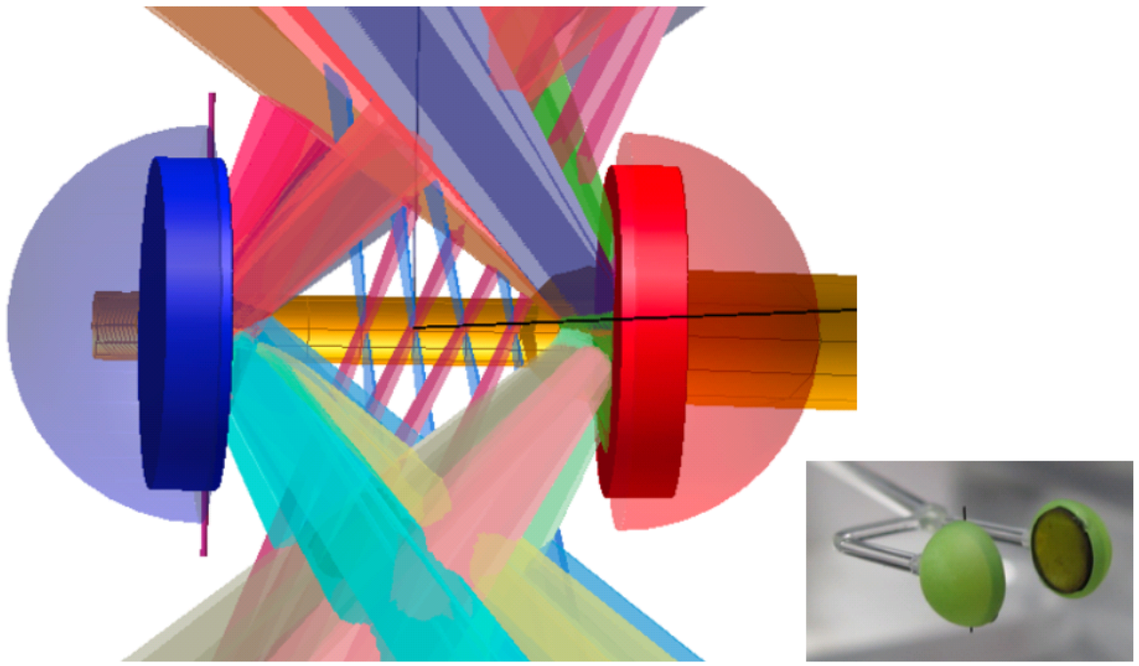

3D PIC (OSIRIS) simulation[1]

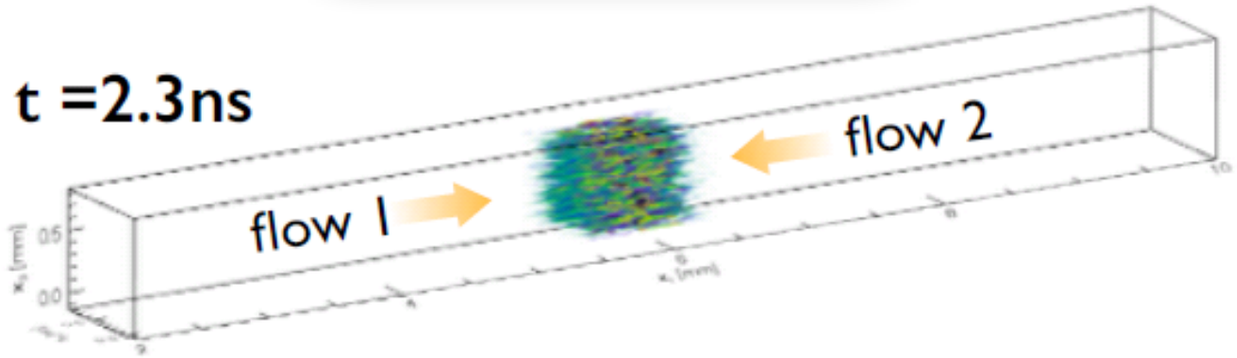

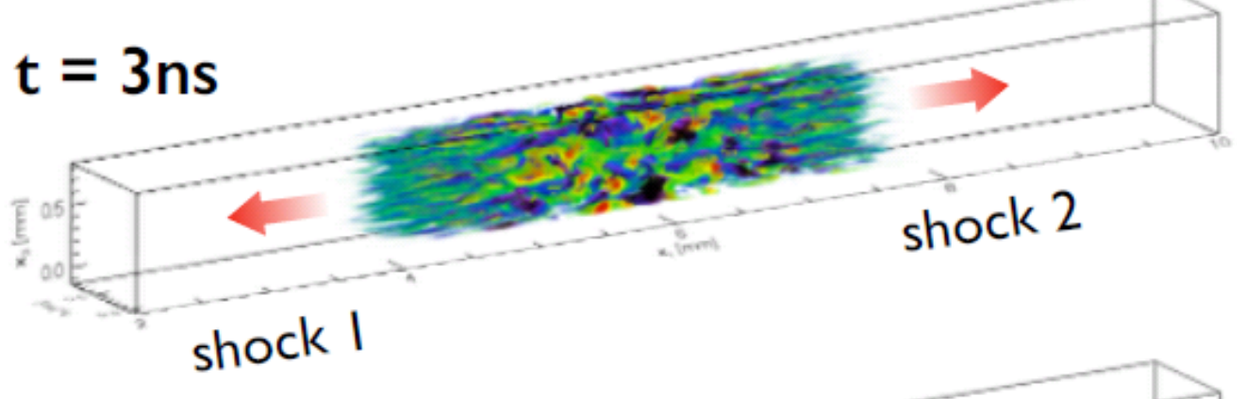

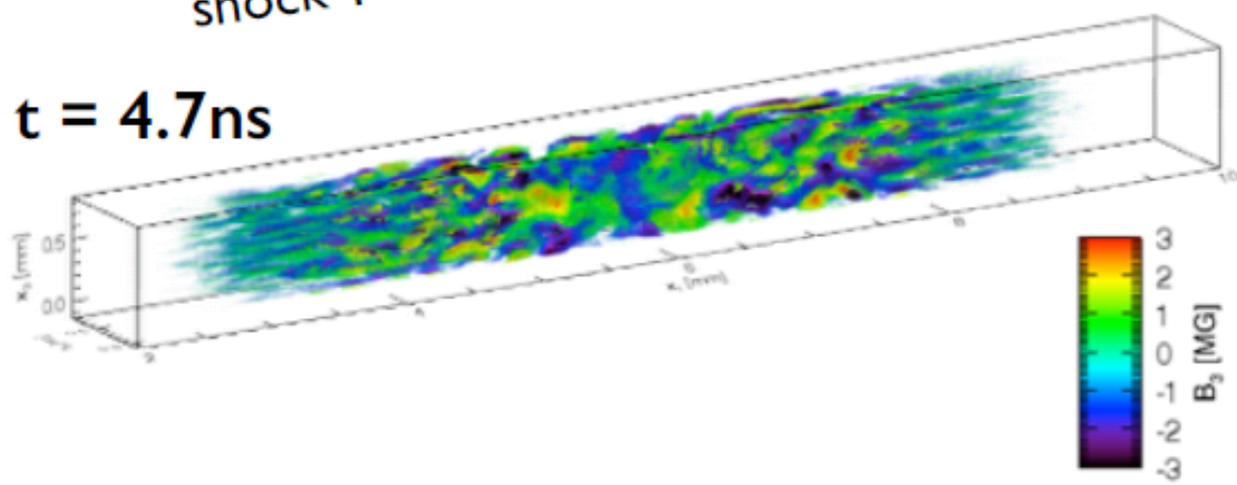

- Larger plasma densities ($\sim 2 \times 10^{20}$ cm^{-3}) are expected $\Rightarrow$ longer effective interaction length ($\sim 500c/\omega_{pi}$), yet instability development may be affected by Coulomb collisions.
- PIC simulations performed with 'heavy' electrons ($m_{e,PIC} = 28m_e$) to reduce computing time.

[1]F. Fiuza, NIF/JLF Users Meeting 2015

Courtesy of Laurent Gremillet

Energy transfer in couter-propagating plasmas at sub-relativistic velocities

→ Astrophysics (emission of high energy photons and production of energetic particles linked to collisionless shocks)
→ ICF (Ion Fast Ignition)

160 MeV obtained more recently at LANL [M. Hegelich et al., arXiv, 1310.8650 (2013)].

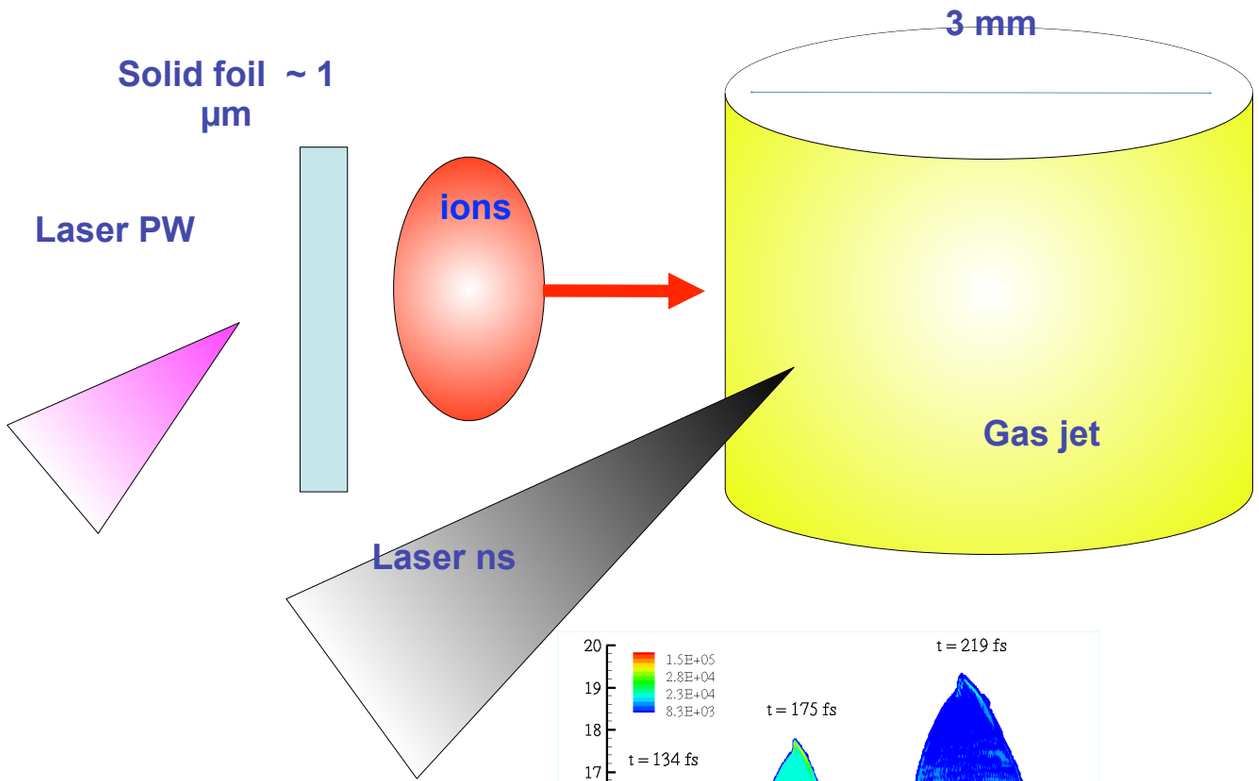

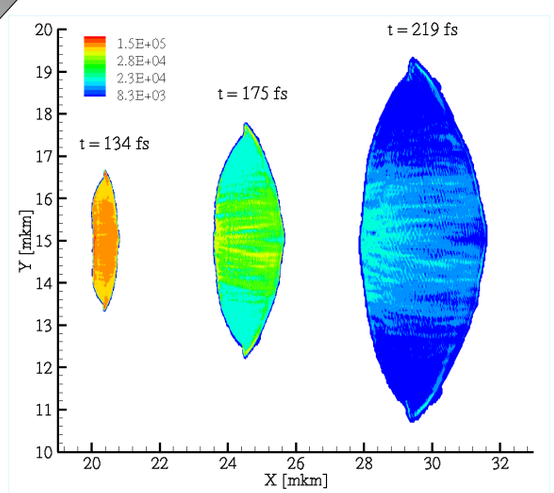

Detection system:
- ion energy loss
- X-ray emission
- interferometer

Laboratory realization of plasma collisions

Stage 1: Laser ion acceleration from a thin solid foil: 1 kJ, 1 ps, Ø 50 μm (PETAL)
Total ion energy 30 J, 20 MeV,
10^{15} protons Ø 100 μm
Stage 2: Ion ballistic transport to the secondary target: v ~ 0.1 c, distance ~
1 mm, density 10^{18} cm^{-3} × 10^{-3} mm^3
Stage 3: Formation of a secondary plasma with a second laser: 1 kJ, 1 ns, Ø 1 mm
Stage 4: Plasma collision: interaction
~ 100 ps, electron heating, shock formation

S. Davis et al. JPCS 2010

Simulation of collision of two sub-relativistic plasmas

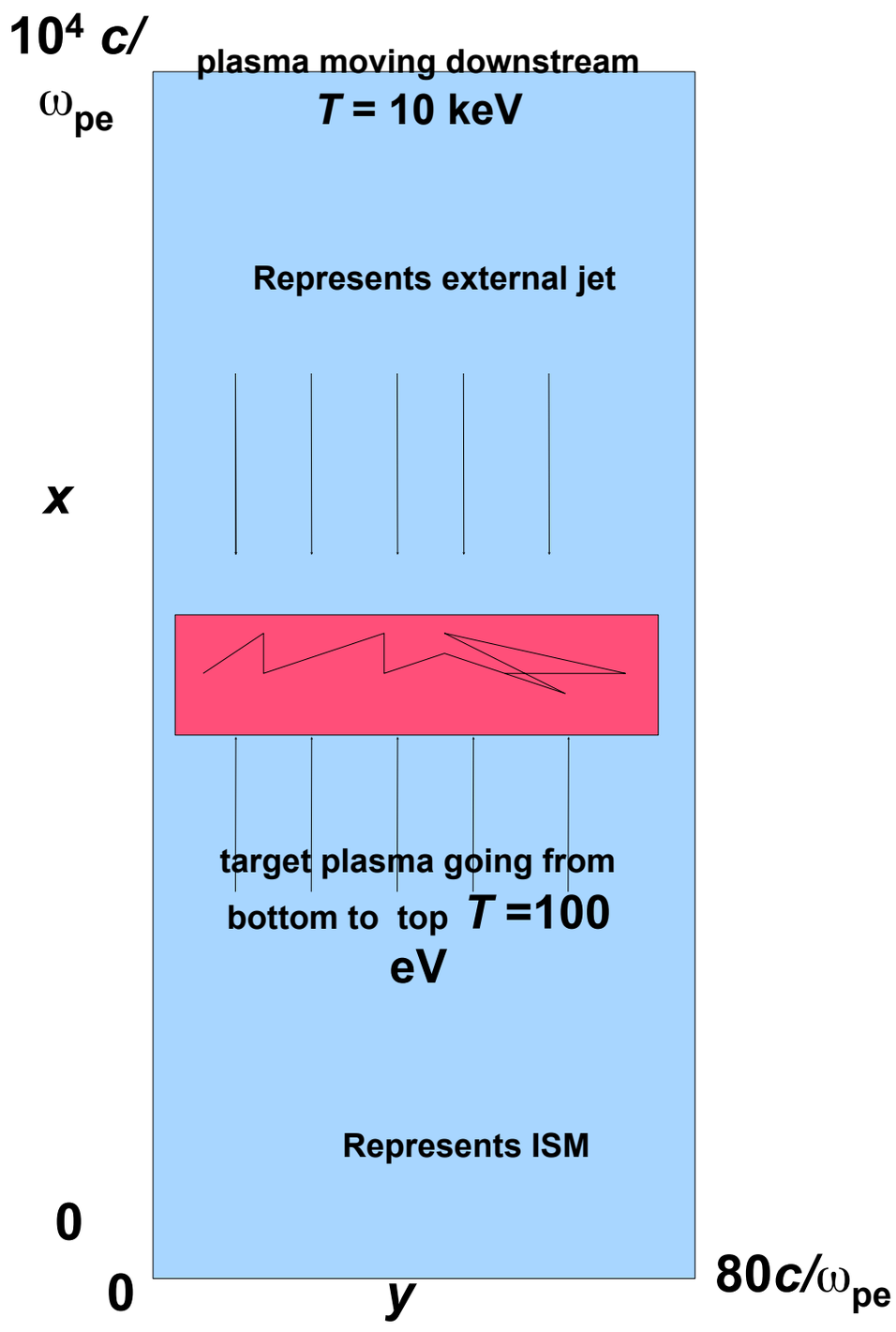

$\beta = u_p/c = 0.2$ $\varepsilon_p \approx 20$ MeV
for $n_0 = 10^{18}$ cm^{-3}
size 0.5×60 mm^2
time $\omega_{pi}^{-1} = 1$ ps $c/\omega_{pi} = 220$ μm

2D version of PICLS [Y. Sentoku and A. Kemp, JCP 2008]

Simulation of the plasma interaction in the center of mass reference frame in the ion filamentation-dominated regime

$$u_p \gg c_s \simeq c\sqrt{m_e / m_i}$$

- Sequence of instabilities (expected)
  - First stage of interaction – electron instabilities (Two-stream & Weibel instabilities)
  - Second stage of interaction – ion-electron instability
  - Ion Weibel instability

- electron heating
- ion slowing down
- magnetic field generation
- energy repartition in the upstream flow
- shock front formation

Ion phase space – time evolution and Global properties: filaments and fields

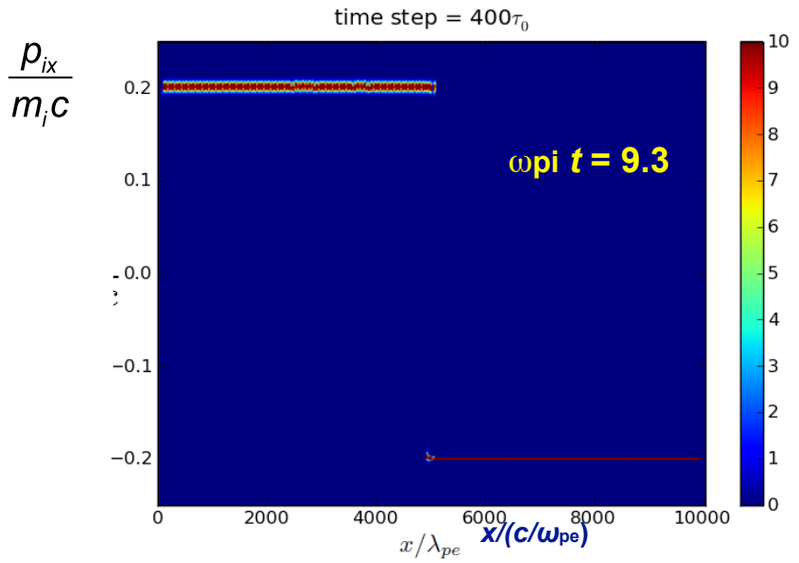

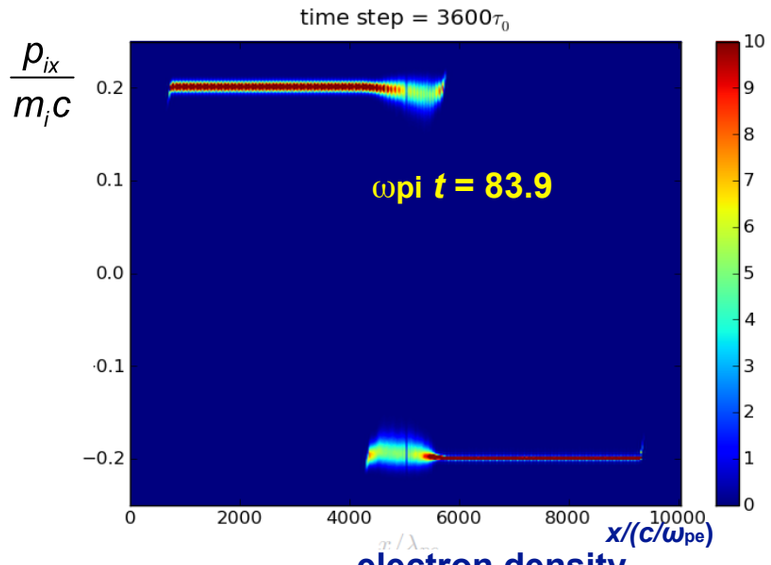

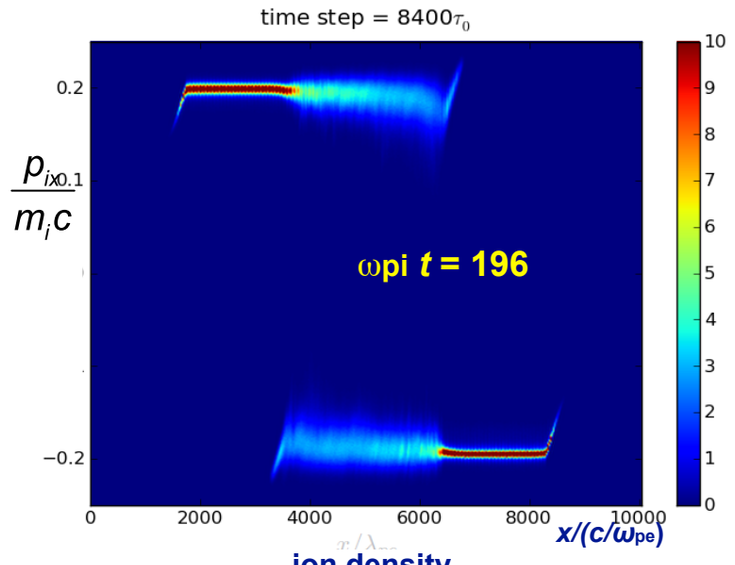

Shock front formation takes a long time after a significant ion heating
In the time scale of 200 ω_{pi}^{-1} they are loosing less than 10% of their energy

Plasma filamentation develops in the electron spatial c/ω_{pe} and temporal $1/\omega_{pe}$ scales.
Current filaments are associated with strong small scale magnetic fields.
Large amplitude charge density modulations produce strong electrostatic fields.
How the filaments have been generated?

S. Davis et al. HEDP 2013

electron density

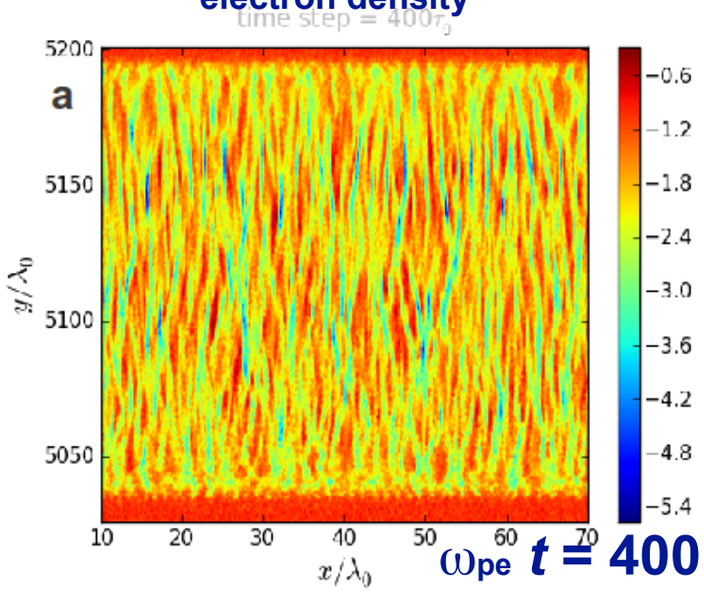

ion density

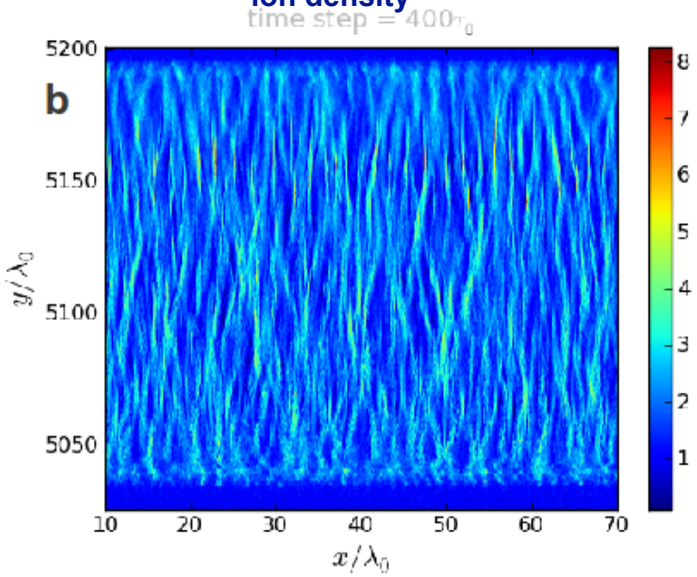

magnetic field B_z

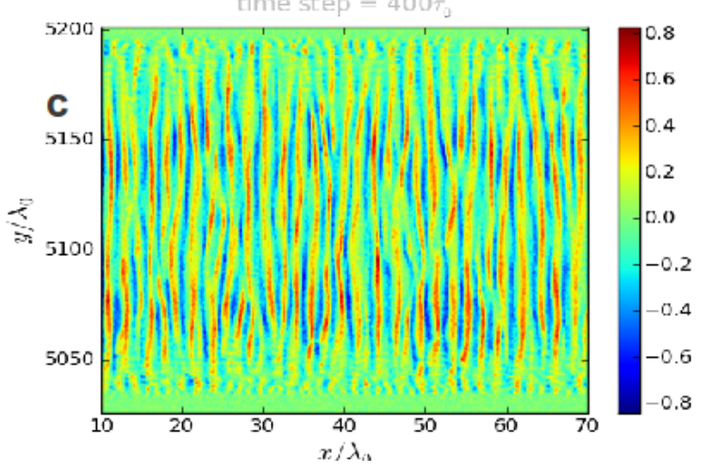

electric field E_y

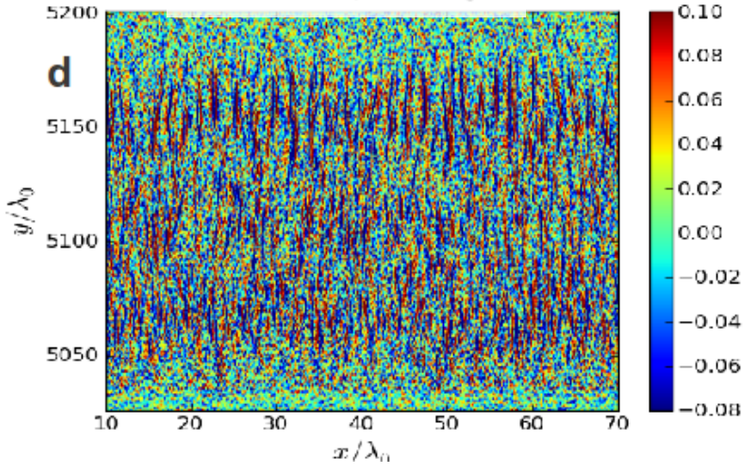

Outline

- High power laser systems and applications
- Collisionless shocks for laser particle acceleration
- Importance of collisionless shocks in astrophysics
- Experimental and numerical studies of collisionless shocks of interest for astrophysics
- **Collision of plasmas in an external magnetic field as a platform to study magnetized collisionless shocks**
- Collisionless shocks in electron-positron plasmas using extreme-light laser pulses
- Conclusions and perspectives

UHI laboratory astrophysics

Important parameters in Space (magnetized & collisionless) plasma interaction

- Characteristic plasma velocity, $\beta = v/c$
- Magnetization, $\sigma = \frac{B^2/4\pi}{\gamma n m c^2}$

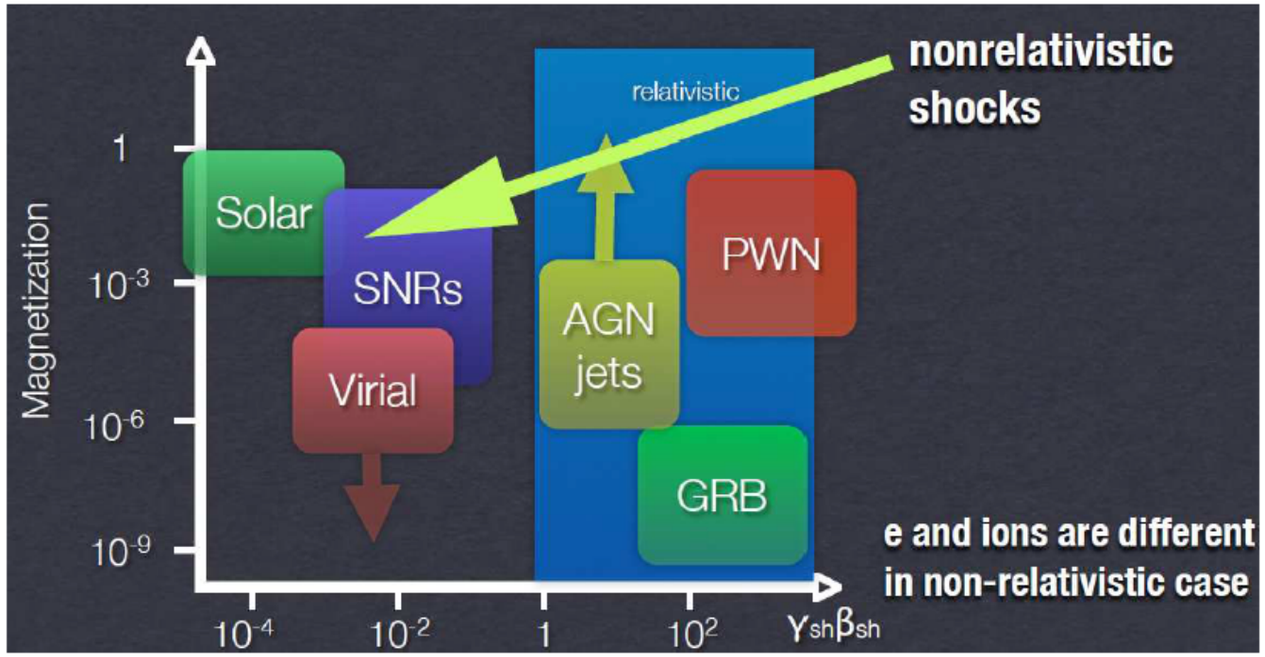

The scheme by A.Spitkovsky.

Crucial need to increase collision velocities and magnetic field amplitudes

Central Question: How is the Energy Transferred to the Particles?

➢Diffusion by shocks may be the energy source for cosmic ray acceleration

➢Instabilities that produce large amplitude current filaments and amplified magnetic fields can induce acceleration of ions through reflections on the fields

➢Experiments using high-power long –pulse lasers have been performed to investigate such instabilities

Our focus:

1. **Exploit high-velocity colliding flows**

2. **Add an ambient magnetic field (transverse to the flows)**

→ Allows to move closer to astrophysical situations

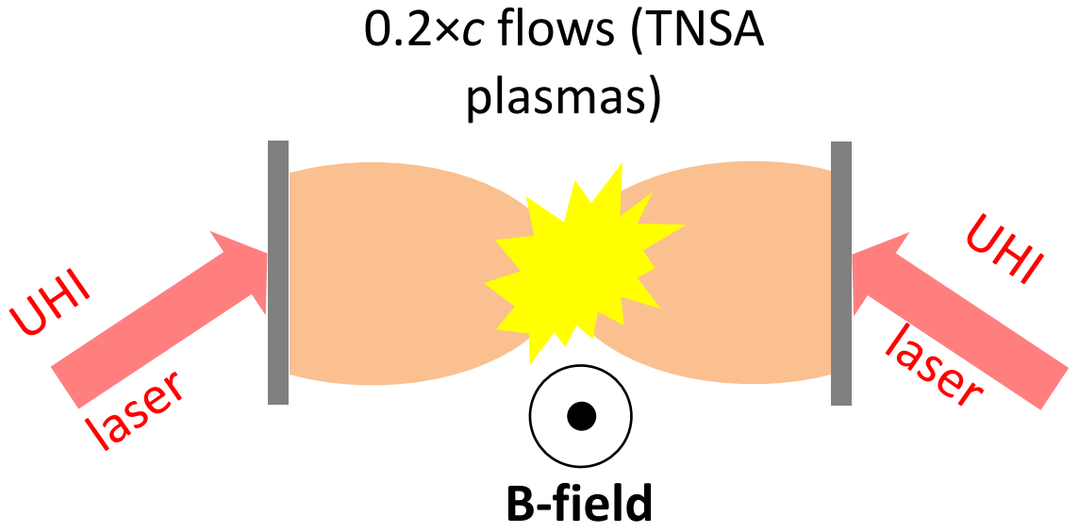

E. S. Weibel, Phys. Rev. Lett. **2,** 83 (1959)
A. Bret, The Astrophys. J. **699**, 990 (2009)
S. Davis et al., High Energy Density Physics **9**, 231 (2013)

Y. Kuramitsu et al., Phys. Rev. Lett. **106**, 175002 (2011); C. M. Huntington et al., Nat. Phys. **11**, 173 (2015)

The Titan Laser in Split Configuration Provides Double TNSA beam Production

Titan Laser
in Split Configuration
60 J / beam -- 700 fs

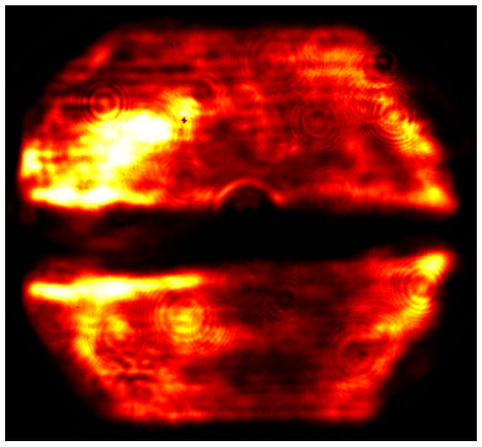

Two main observables with and without B-field :

1. **Electron density**: We used a 1ω interferometry probe to obtain electron density at different times.
2. A Thomson Parabola records the **proton and ion spectra**.

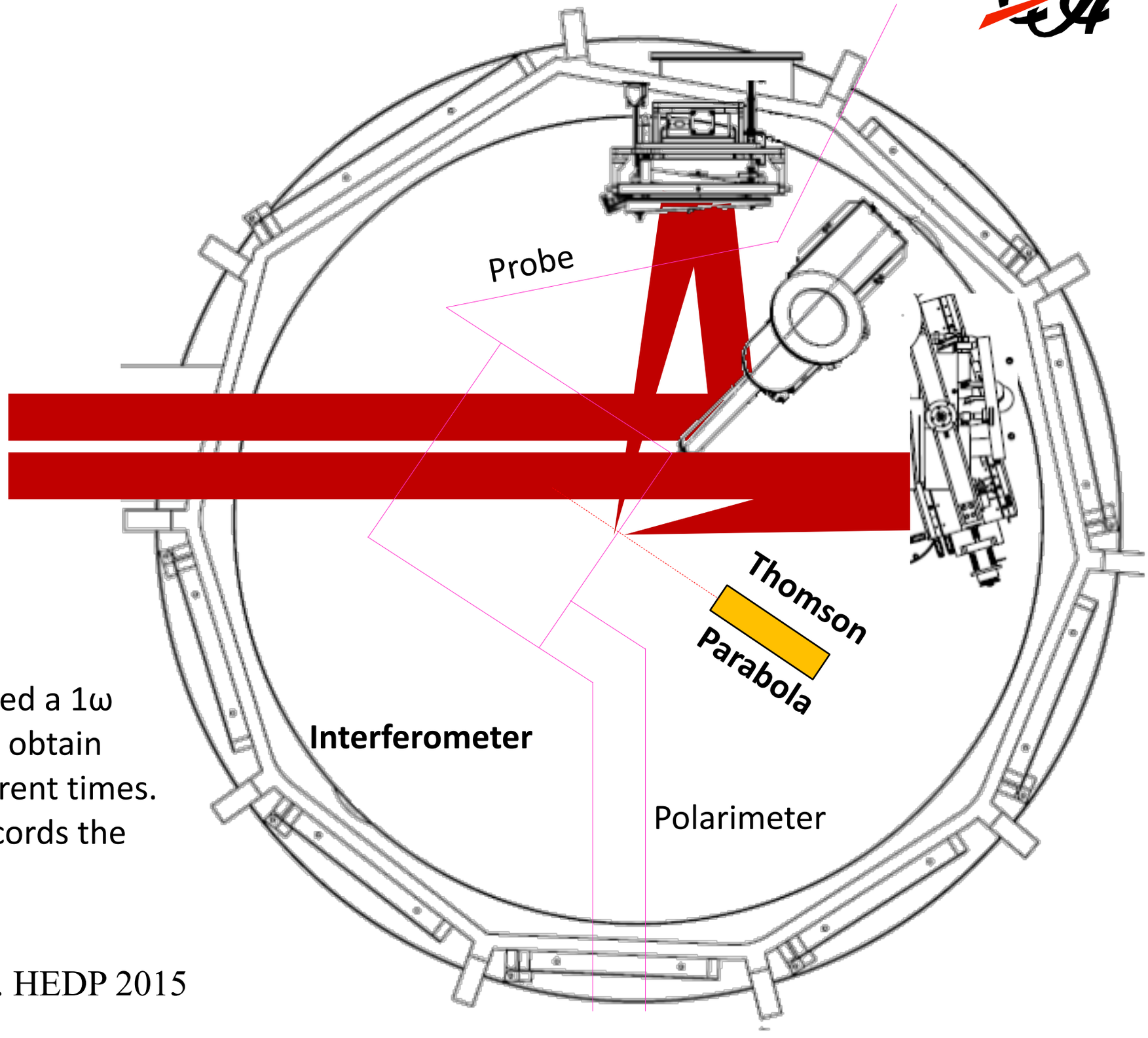

D. Higginson et al. HEDP 2015

Coil Developed at LNCMI for Titan Geometry

Coil provides **20 T external fields** which are constant in time (many µsec) and space (many mm).

The coil allows the f/3 short-pulse laser beams driving the TNSA plasmas to access the central magnetized zone

D. Higginson et al. HEDP 2015

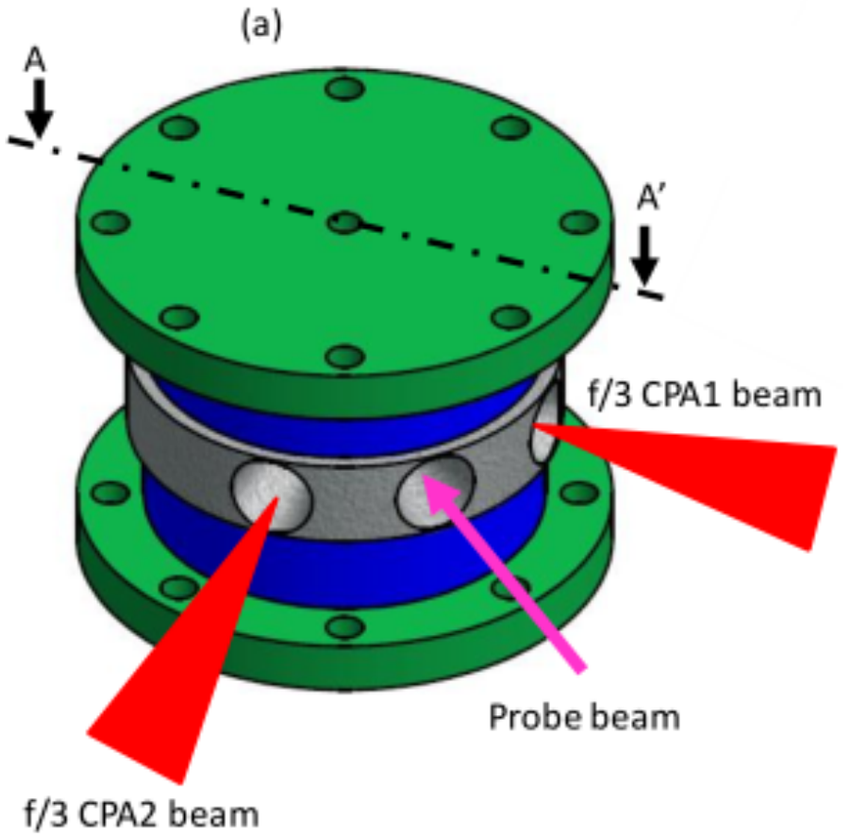

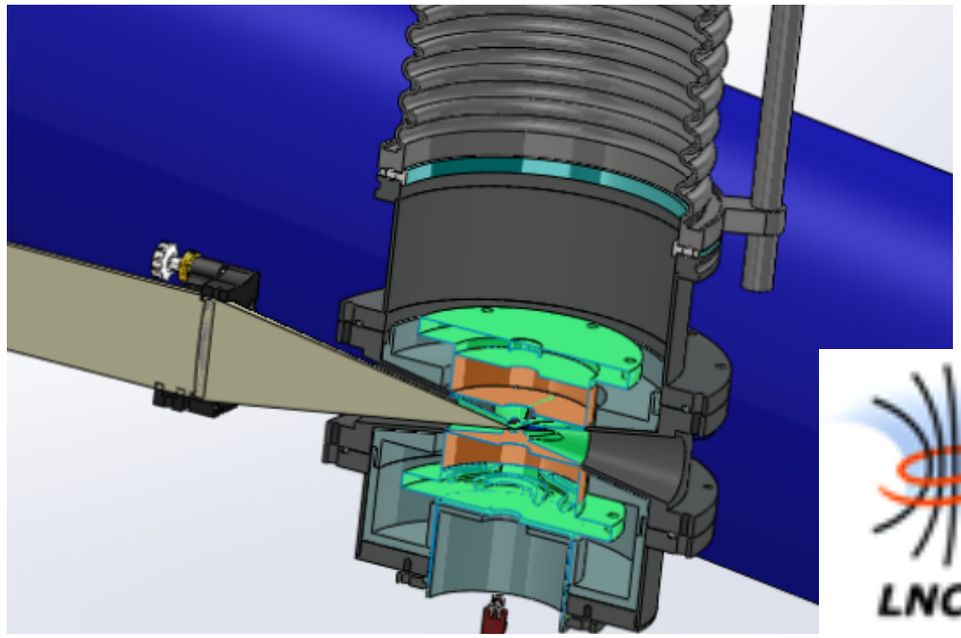

B = 20 T

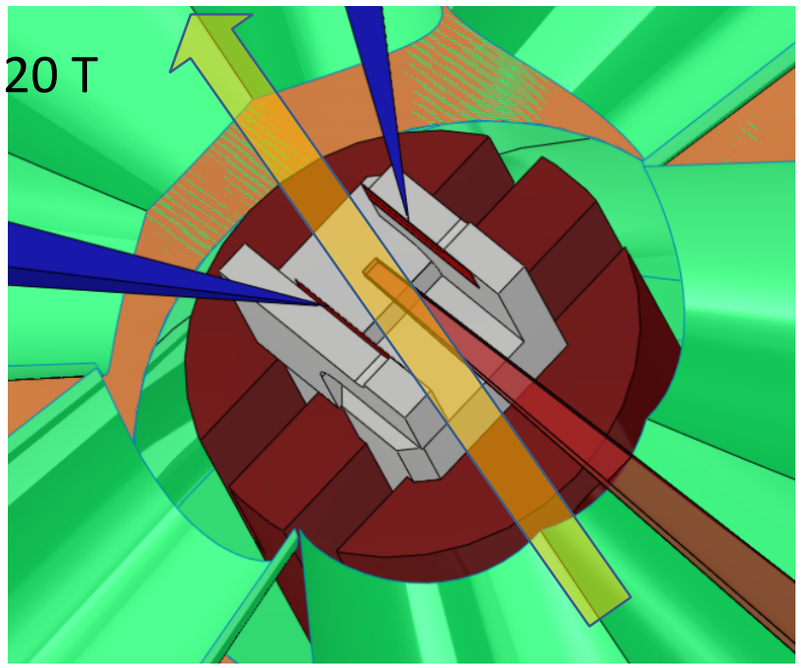

First signature produced by colliding the plasmas within the B-field: density increase of the center

B=20T, thickness=4.5 µm and separation=250 µm

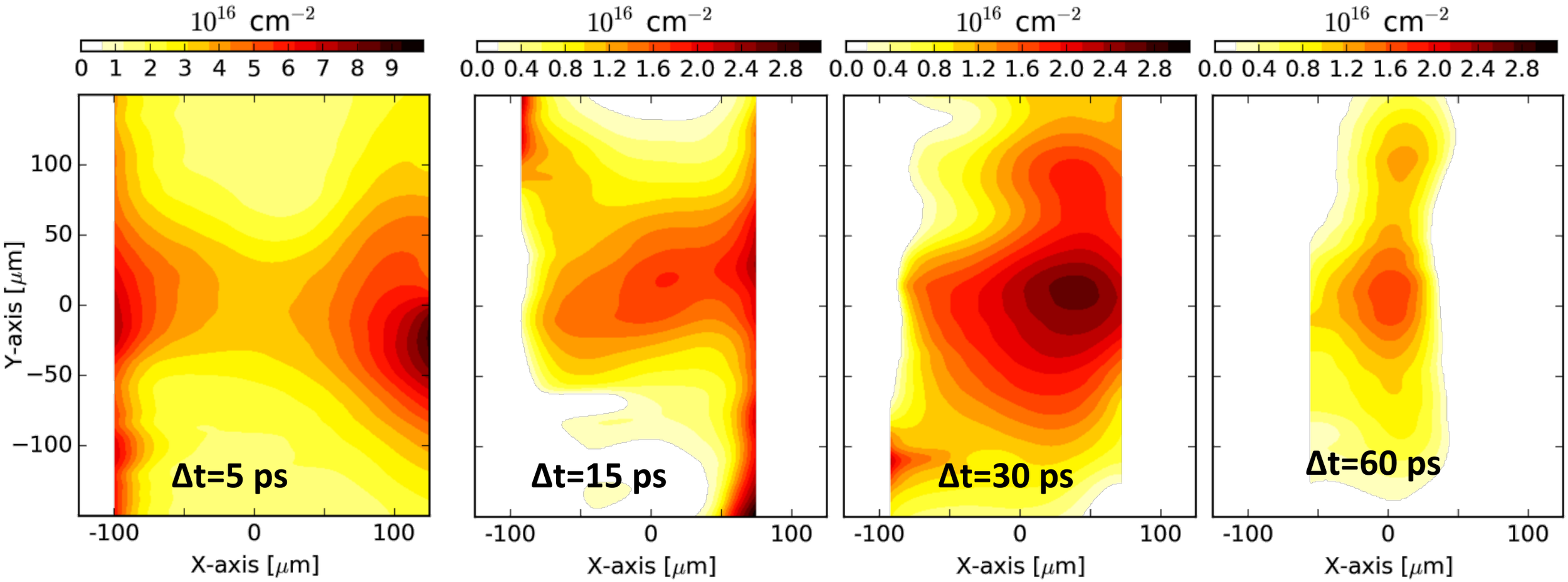

- Density bump cannot result from linear overlap of TNSA beams
- Density bump is not observed w/o B-field
- Closer distance leads to higher densities, and thus a stronger bump.
- When separating the targets by 500 µm, bump creation time is increased by about 2x, as expected from the change in distance.

Second signature: protons resulting from the magnetized collision emerge with higher energy

- For a single foil shot (no B-field) the maximum energy is 20 MeV.
- For a double foil shot (no B-field) the signal is reduced on the TP due to scattering in the foil. (We have verified this with TRIM).
- For a double foil shot (w/ B-field) the maximum energy increases up to 35 MeV.
- This shows that the protons have gained energy in the process

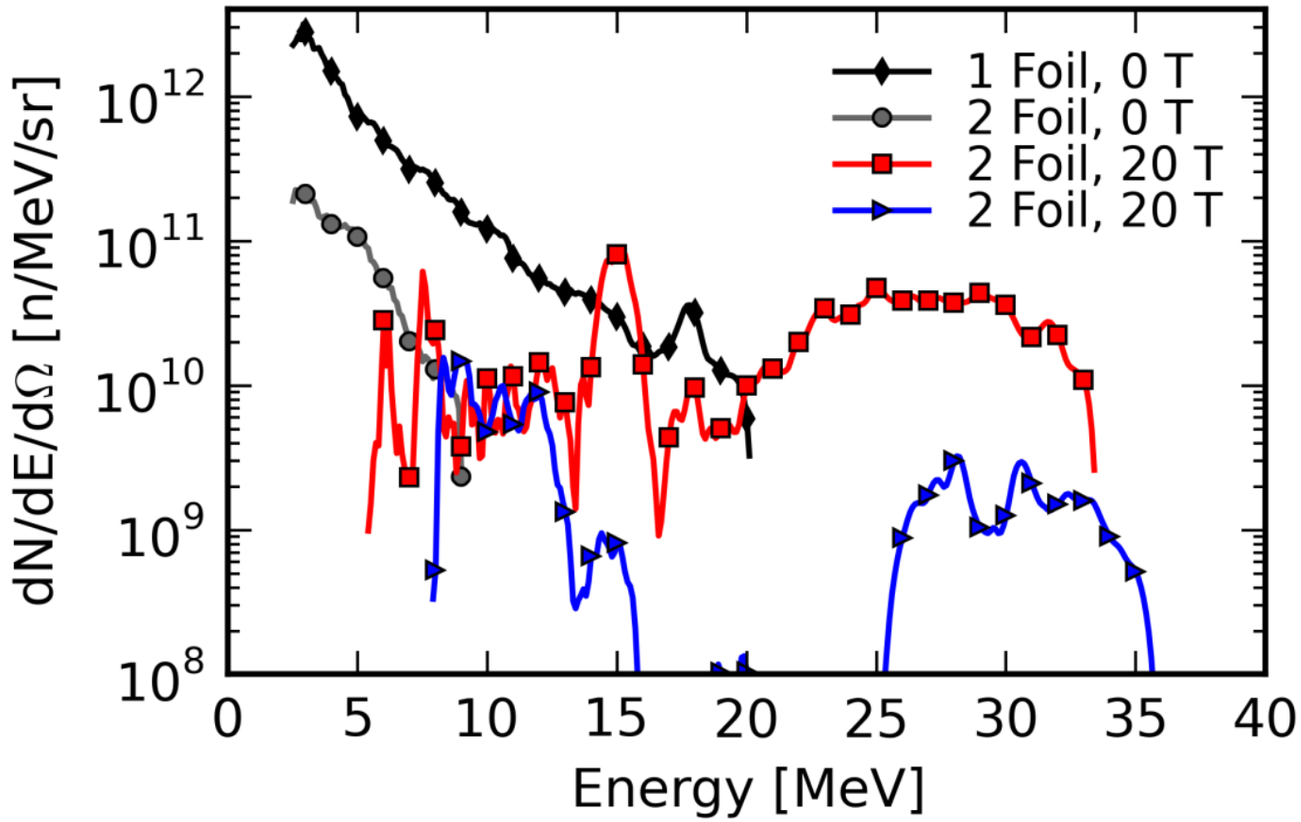

We are testing different mechanisms of energy exchange from the B-field to the protons

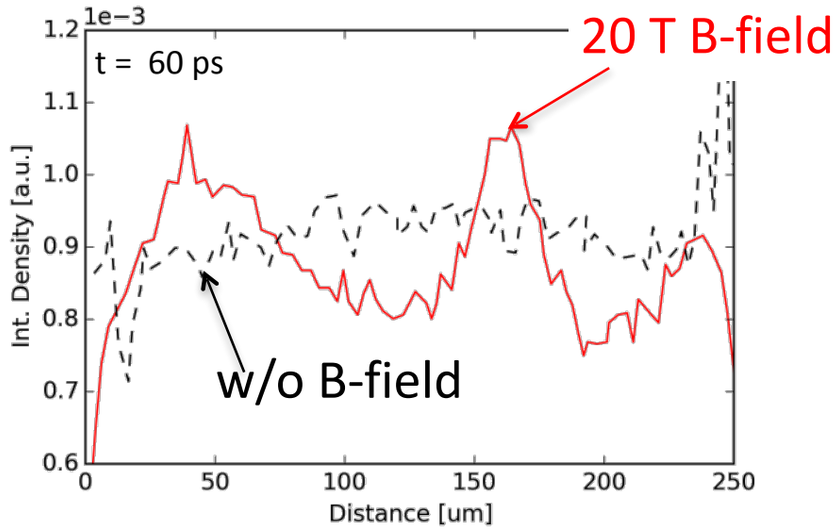

• At present, the PIC simulations exhibit some electron density enhancement at the center, as the experimental data.

• The PIC simulations show the formation of strong magnetic islands. At this stage some acceleration is observed but not enough to explain the experimental results. One notices that the magnetic energy stored at 500 T is comparable to the proton energy of 35 MeV.

• Other mechanisms (not present in the simulations) that could explain the acceleration process are being tested:

- ❖Further compression of the magnetic field islands followed by a magnetic piston ion acceleration
- ❖3D effect of magnetic island “tube” amplification

Experiments on the generation and Evolution of High-Mach Number, Laser-Driven Magnetized Collisionless Shocks in the Laboratory

Schaeffer et al. arXiv:1610.06533

PRINCETON UNIVERSITY

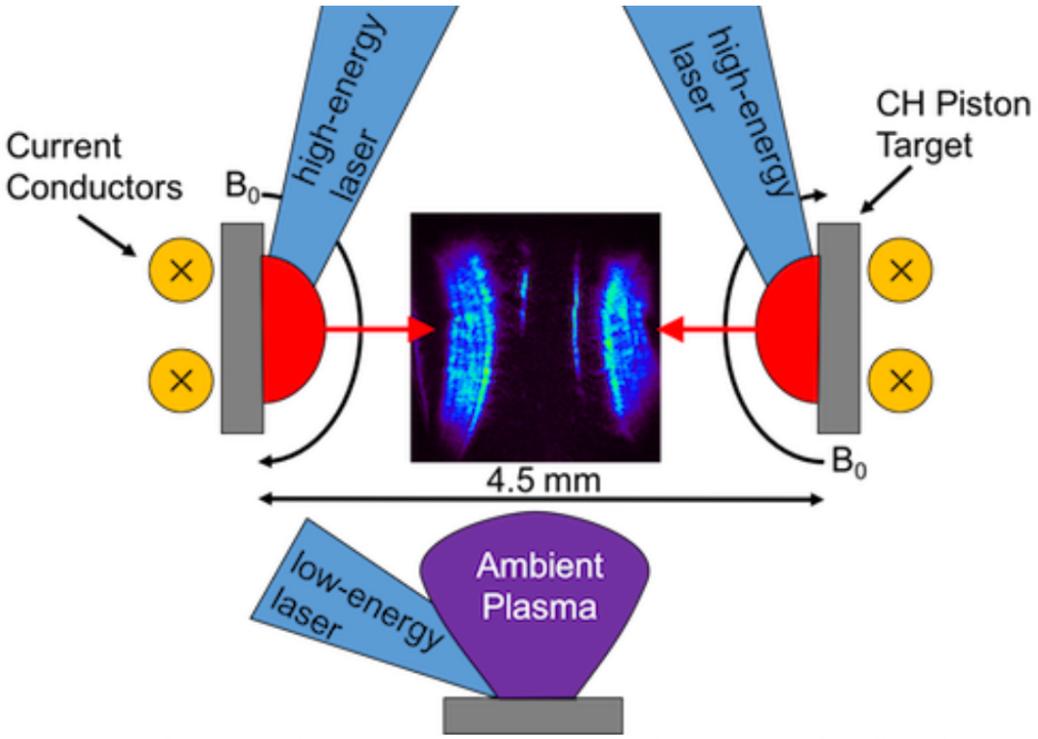

Experimental setup. An external magnetic field (B_0 = 8 T) in an anti-parallel geometry was applied by pulsing current through conductors located behind opposing plastic (CH) piston targets.

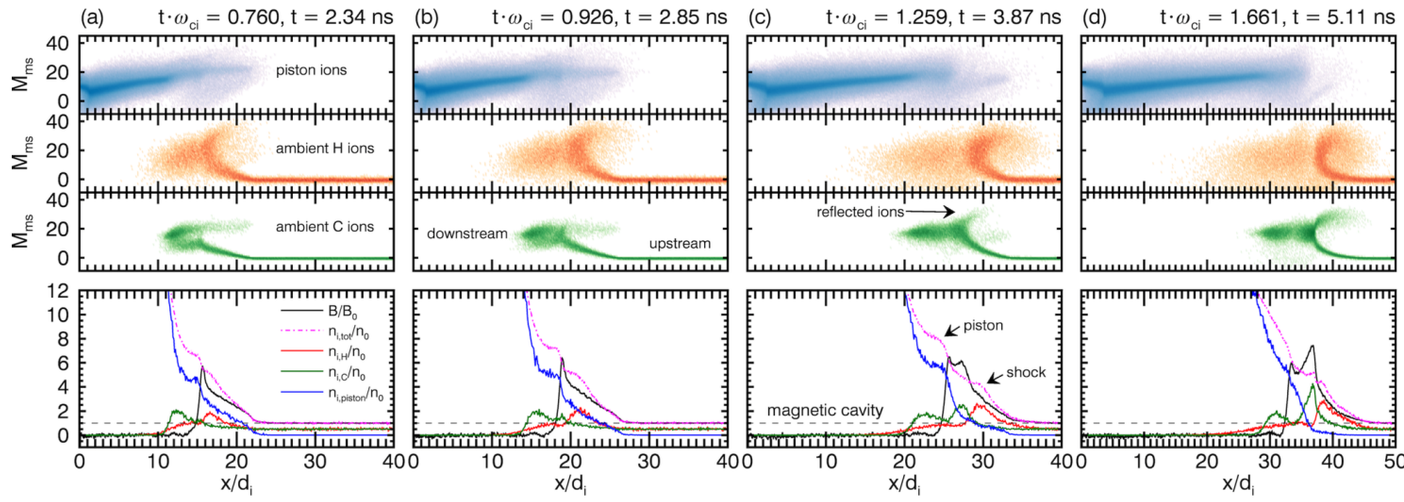

Results from 2D particle-in-cell simulations that show the formation of a high-Mach number, magnetized collisionless shock

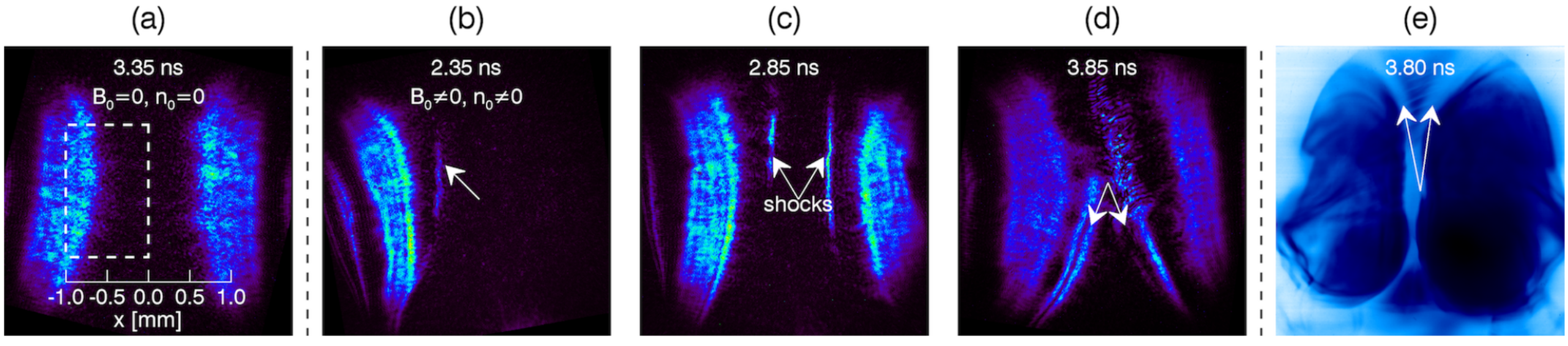

Refractive and proton radiographic images of collisionless shock evolution

Simulations of the formation of collisionless shocks in magnetized plasma interaction with kinetic-scale obstacles

F. Cruz et al. arXiv:1701.05802

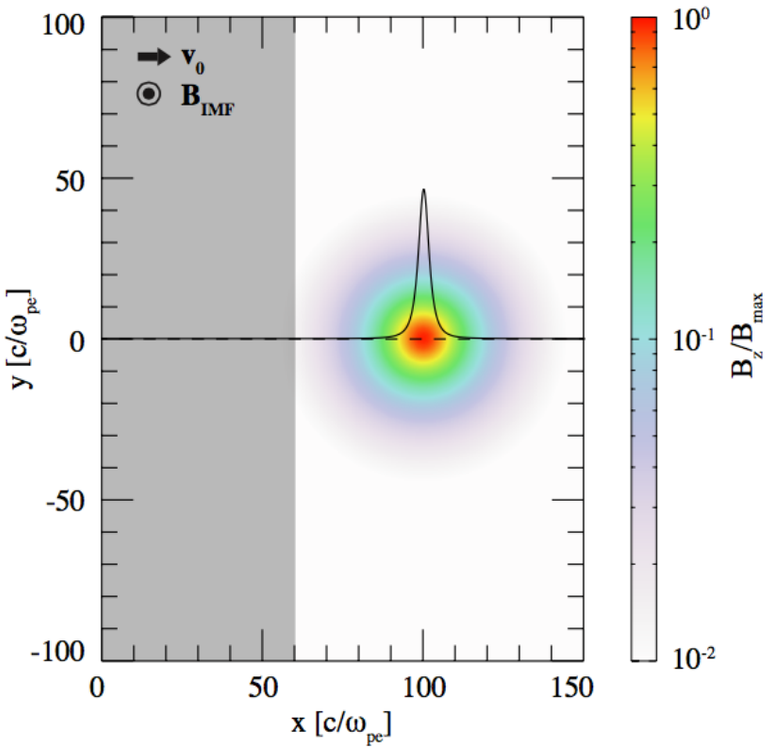

Schematic illustration of the initial setup of the 2D simulations. The plasma is continuously injected from the left boundary and flows along the x direction. Part of the plasma is initialized inside the box (indicated in grey), to reduce the computation effort. The colour map indicates the dipole field strength normalized to its maximum value, determined by a cutoff introduced in the dipolar field. A lineout (at y = 0) of this field is also indicated.

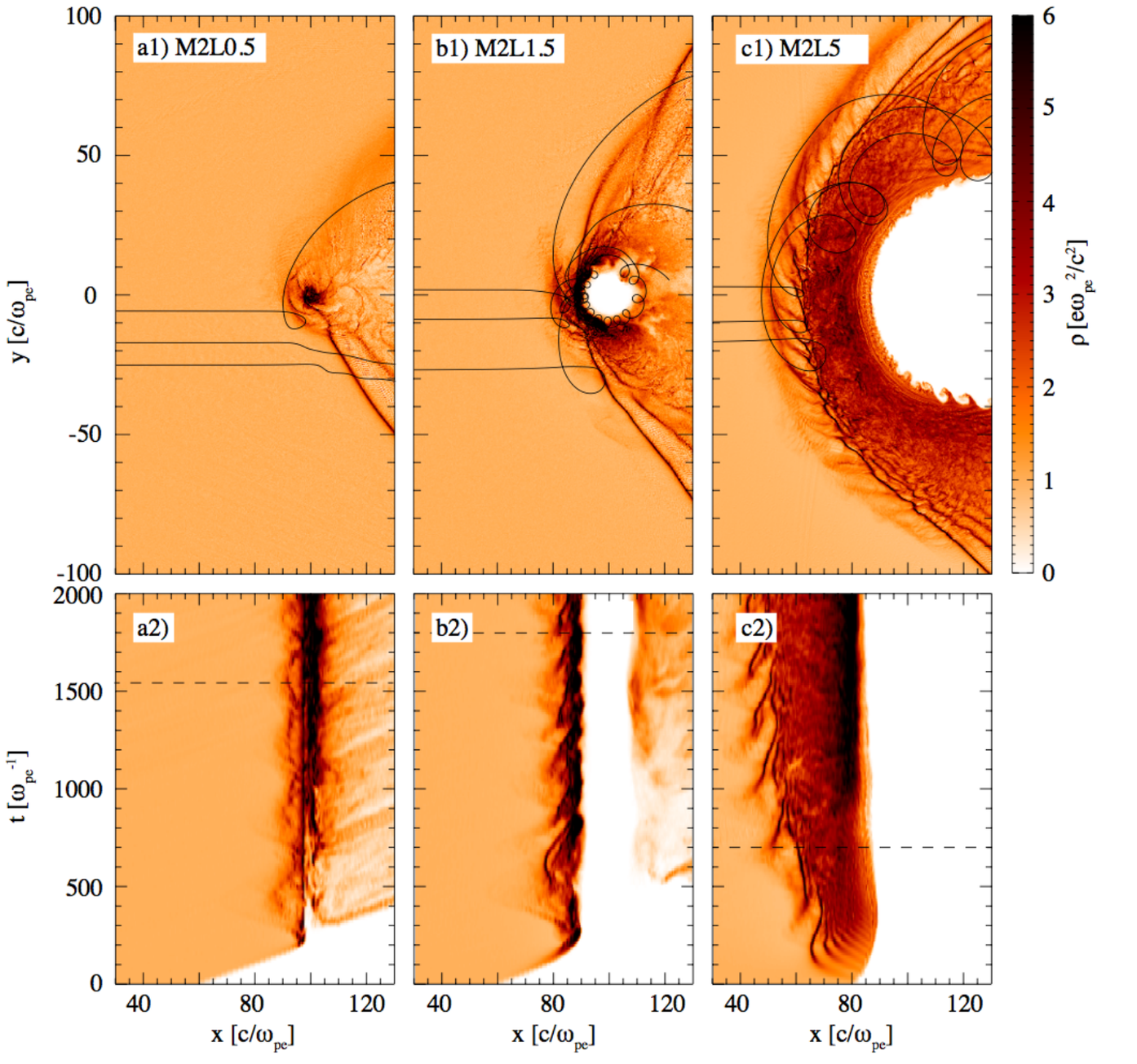

Critical cavity size for formation of miniature magnetized shocks. A plasma flow with v_0=0.2 c and M_A=2 interacts with magnetic dipoles that standoff the plasma at a distance (a) $L_0 = 0.25\varrho_i$, (b) $0.75\varrho_i$ and (c) $2.5\varrho_i$. Along with the ions density, black lines are representing ion trajectories are shown in panels a-c1, illustrating the typical Larmor radius scale after the particles are reflected. Panels a-c2 show the time evolution of the same density along the y = 0 lineout. The dashed lines in these panels indicate the time at which the frames shown above were taken.

Laser assisted high amplitude magnetic field generation to tailor ion beams

i)

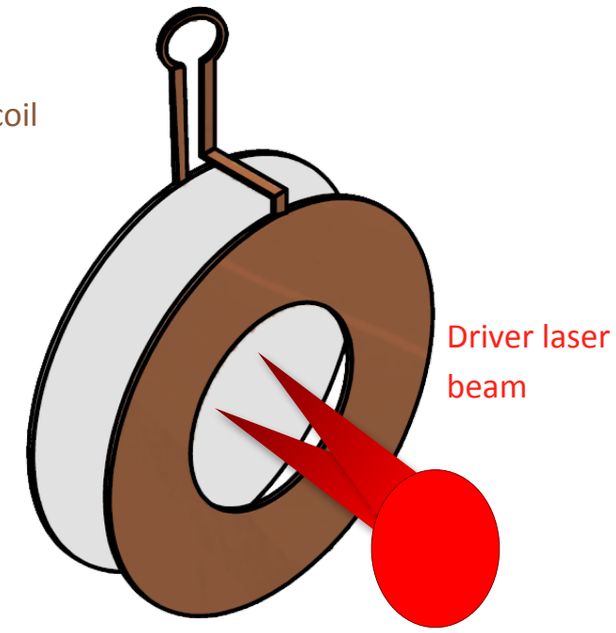

ii)

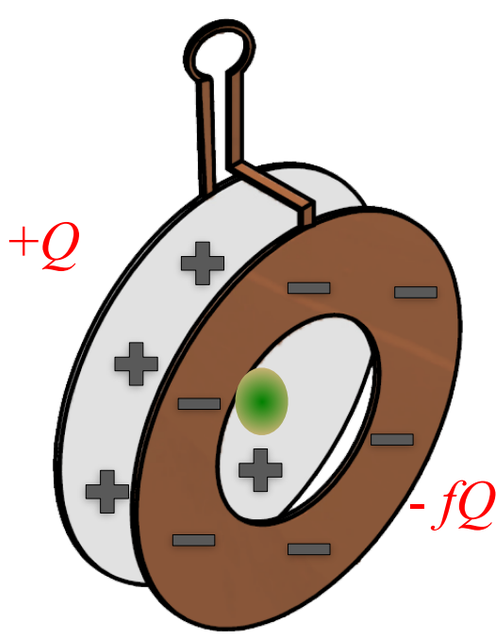

iii)

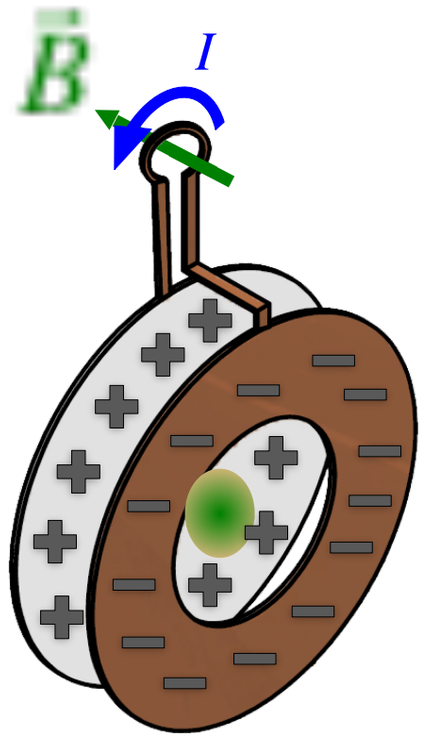

J. Santos et al., Laser-driven platform for generation and characterization of strong quasi-static magnetic fields, NJP 17, 083051 (2015)

- Experiments performed at LULI with ns pulses.
- kT range fields obtained.

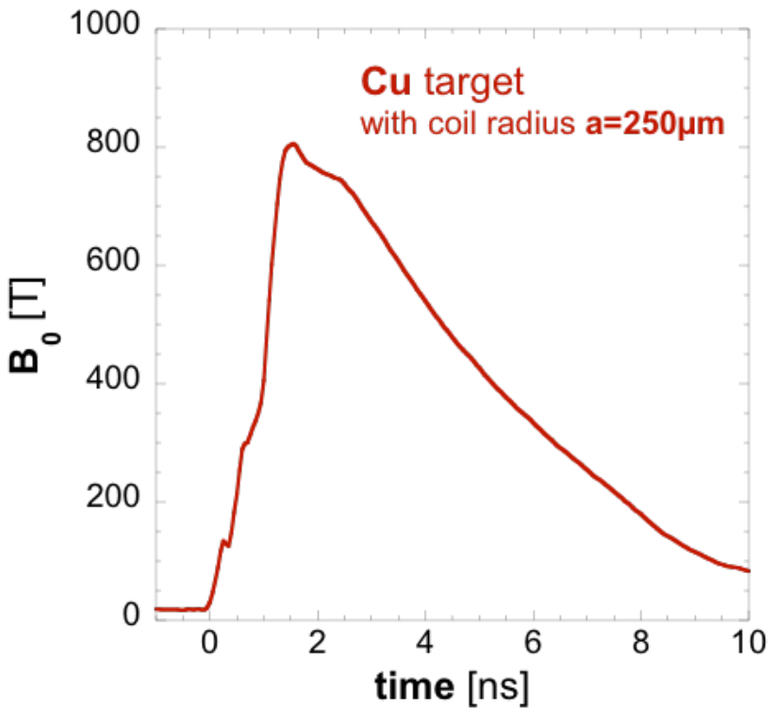

Plasma plumes collision in an external magnetic field

Parallel and perpendicular fields will be investigated

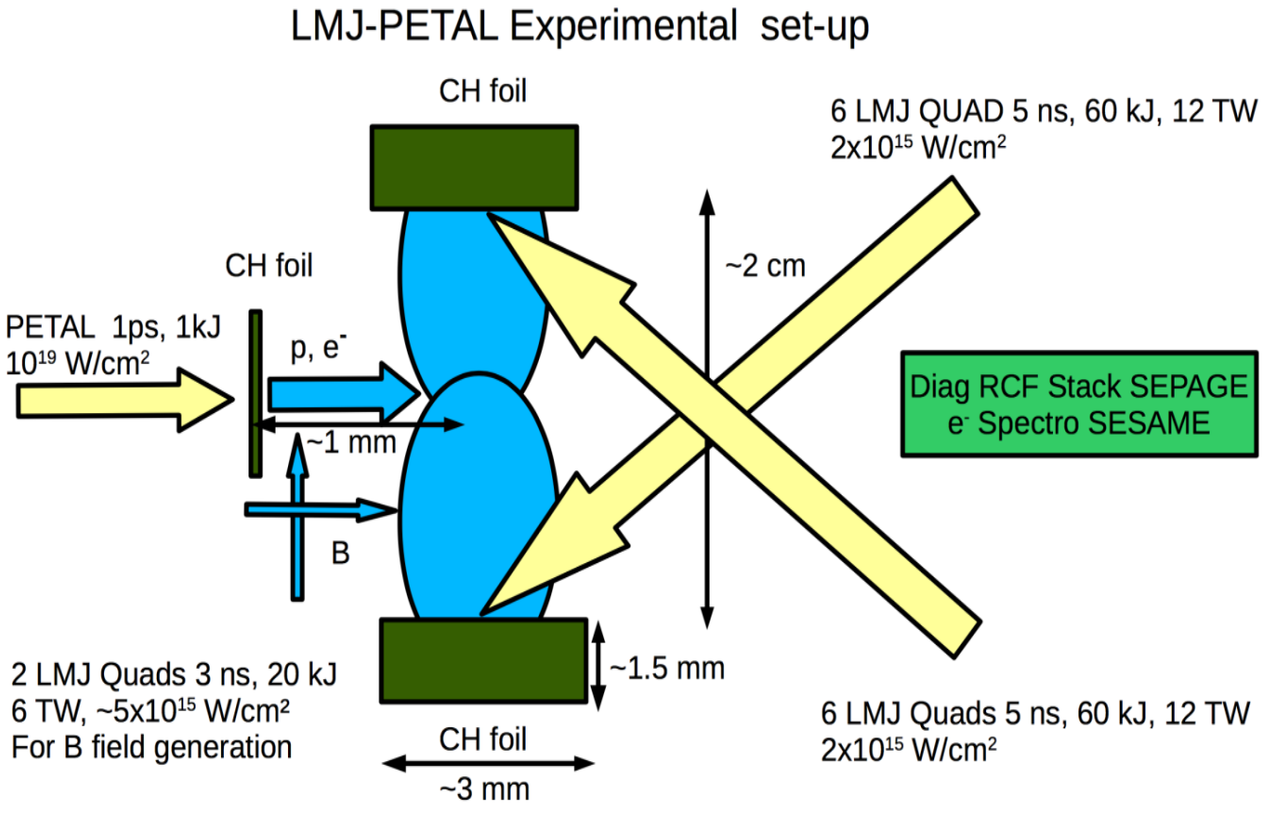

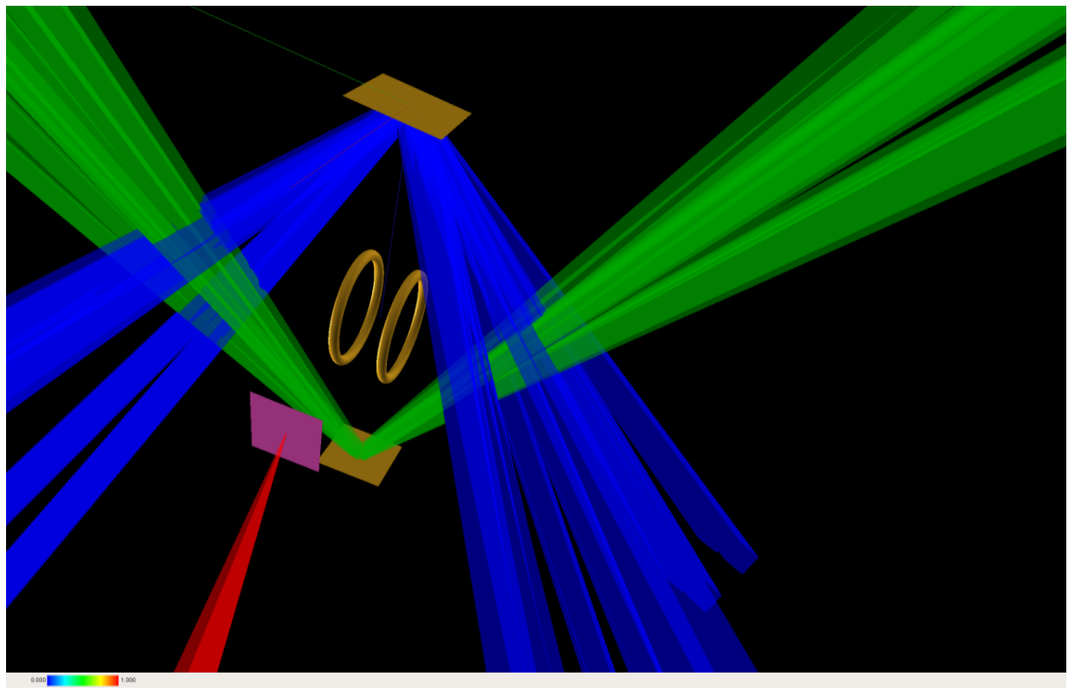

Diagnostics: proton radiography with Omega EP, particle and radiation spectrometers, Thomson scattering

Control of the synchronization between the laser beams generating the plumes and the ones generating the magnetic field is paramount

Outline

- High power laser systems and applications
- Collisionless shocks for laser particle acceleration
- Importance of collisionless shocks in astrophysics
- Experimental and numerical studies of collisionless shocks of interest for astrophysics
- Collision of plasmas in an external magnetic field as a platform to study magnetized collisionless shocks
- **Collisionless shocks in electron-positron plasmas using extreme-light laser pulses**
- Conclusions and perspectives

Future high-power short-pulse laser facilities [1]

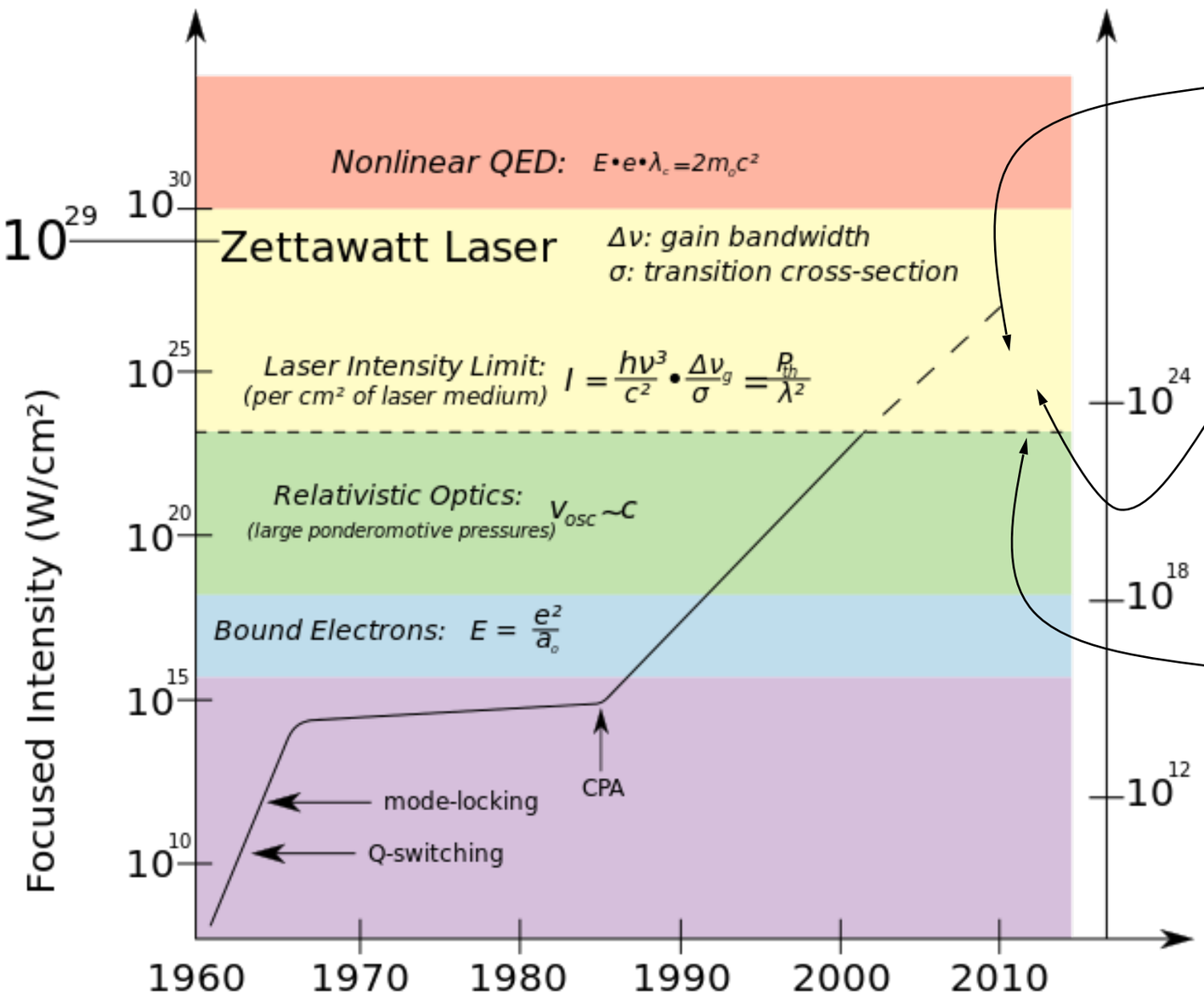

EXASCALE: IZEST
(compressed LMJ, NIF-class lasers?)

100 PW: ELI upgrade, XCELS
(10^{23}- 10^{24} $\mathrm{Wcm^{-2}}$, 10x10 PW beams)

10 PW: Apollon, Vulcan, ELI
(10^{22}- 10^{23} $\mathrm{Wcm^{-2}}$, 150-300 J, 15-30 fs)

1 PW: State of the art facilites
10^{21} $\mathrm{Wcm^{-2}}$, 30 J, 30 fs

[1] A. Di Piazza *et al.*, Rev. Mod. Phys. **84**, 1177 (2012)

Radiative and QED effects[1] in ultra-intense laser plasma interaction[2,3]

Apollon (10 PW, 100J, 15 fs) → **ELI** (100 PW) → **IZEST** (> 1EW)

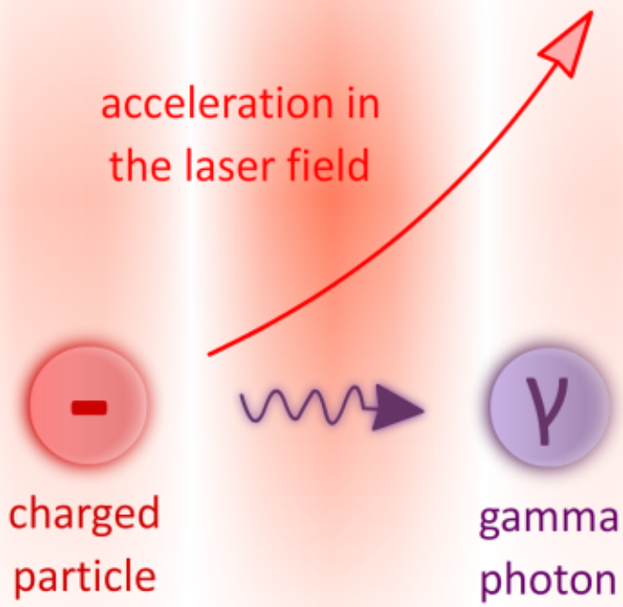

Non-linear Compton scattering: high-frequency photon emission in the laser field

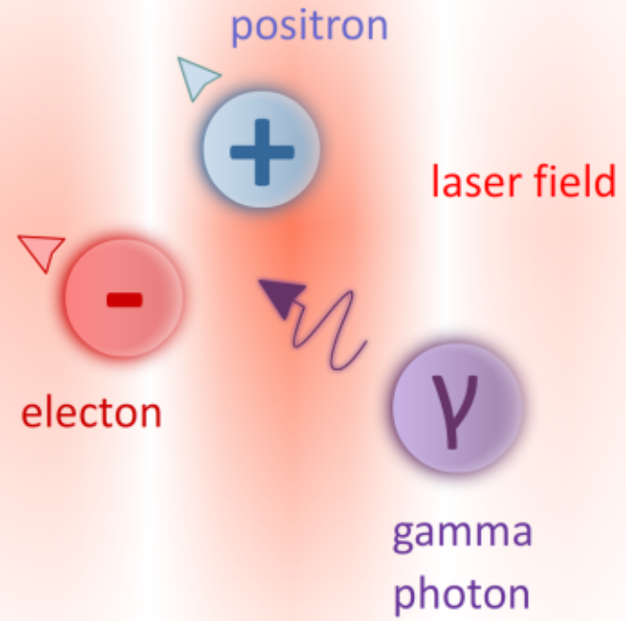

Multiphoton Breit-Wheeler: e^-e^+ pair generation in the laser field ($I > 10^{23}$ Wcm^{-2})

- Implementation of these mechanisms in the PIC code CALDER [M. Lobet et al. arXiv.1311.1107v2]

And competition with Bethe-Heitler and Trident processes when using solid foils

[1] – A. Di Piazza *et al.*, Rev. Mod. Phys. **84**, 1177 (2012) – A. Bell *et al.*, Phys. Rev. Lett. **101**, 200403 (2008).
[2] – A. Zhidkov *et al*, PRL **88**, 185002 (2002) – M. Tamburini *et al*, NJP **12**, 123005 (2010) – R. Capdessus *et al*, PRL **110**, 215003 (2013)
[3] – C. P. Ridgers *et al*, PoP **20**, 056701 (2013) – C. S. Brady *et al*, arXiv preprint 1311.5313 (2013) – L. L. Ji *et al*, PoP **21**, 023109 (2014)

The Particle-In-Cell (PIC) Method

capture collective effects by solving the Vlasov-Maxwell Eqs.

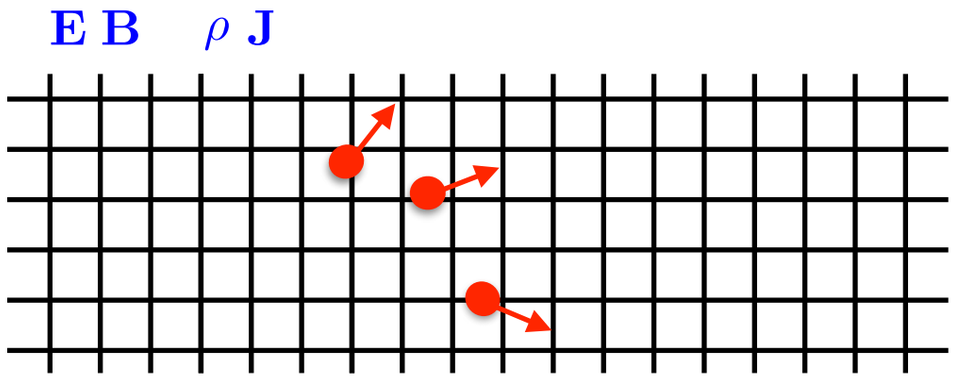

- Vlasov Eq. is solved using so-called macro-particles

$$f_s(t,\mathbf{x},\mathbf{p}) = \sum_N w^N \, S(\mathbf{x}-\mathbf{x}^N(t)) \, \delta(\mathbf{p}-\mathbf{p}^N(t))$$

Maxwell Solver

$$\partial_t \mathbf{E} = -\mathbf{J} + \nabla \times \mathbf{B}$$
$$\partial_t \mathbf{B} = -\nabla \times \mathbf{E}$$

Courtesy of M. Grech

Interpolation

$$\forall N \; [\mathbf{E},\mathbf{B}] \rightarrow [\mathbf{E}^N,\mathbf{B}^N]$$

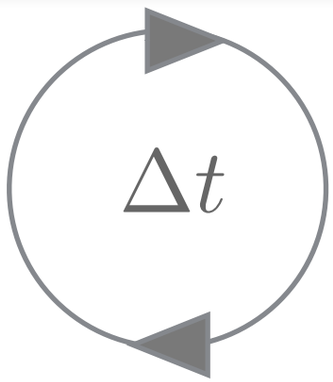

Projection

$$\forall N \; [\mathbf{x}^N,\mathbf{p}^N] \rightarrow [\rho,\mathbf{J}]$$

See also M. Tamburini et al, NJP 12, 123005 (2010), M. Vranic et al. (2014), C. S. Ridgers et al., Journal of Computational Physics 260, 273 (2014).

Modified Electron Pusher

$$\chi_e = \left| \frac{F^{\mu\nu}}{E_S} \frac{p^\nu}{m_e c} \right|$$

$\chi_e < 10^{-5}$ classical relativistic push.

$\chi_e < \chi_e^{th}$ radiation reaction force

$\chi_e > \chi_e^{th}$ Monte-Carlo method

Photon Pusher

for > 1.022 MeV photons:

$$\epsilon_\gamma > 2\, m_e c^2$$

$$\chi_\gamma = \left| \frac{F^{\mu\nu}}{E_S} \frac{\hbar k^\nu}{m_e c} \right|$$

multiphoton Breit-Wheeler process

Implemented in the PIC code CALDER

Lobet et al., arXiv:1311.1107 (2013)

Simulations of laser ion acceleration with low density targets in the ultra-high intensity regime

Proton phase space at various times for I=10^{22} W/cm^2, τ=30fs for a 2 n_c, H, 190 microns long cos^2 target. The laser comes from the left side of the simulation box.

→ Competition with radiation emission

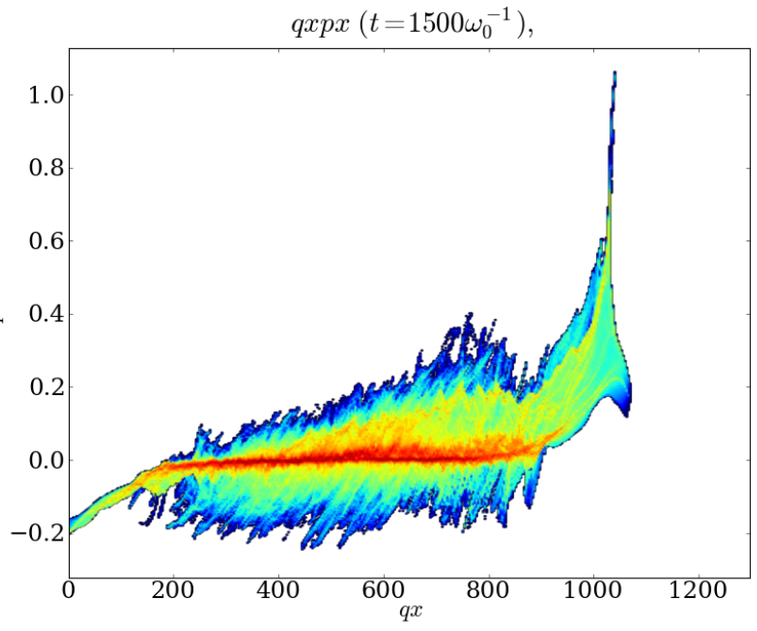

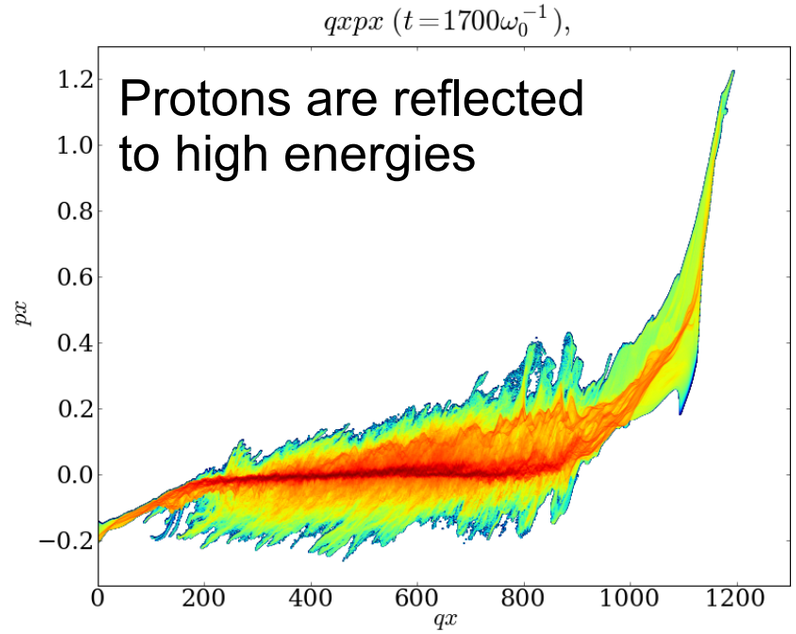

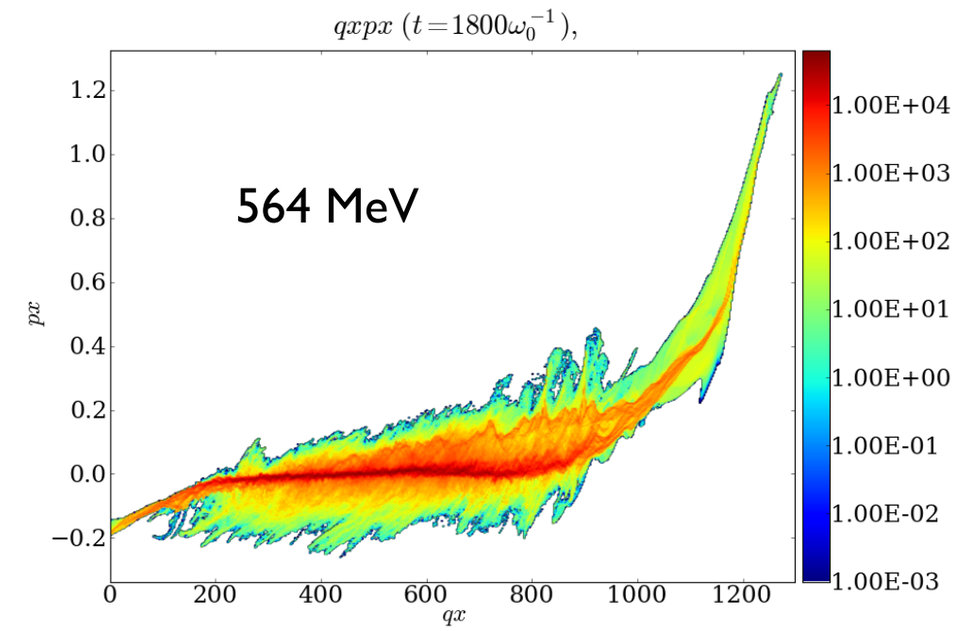

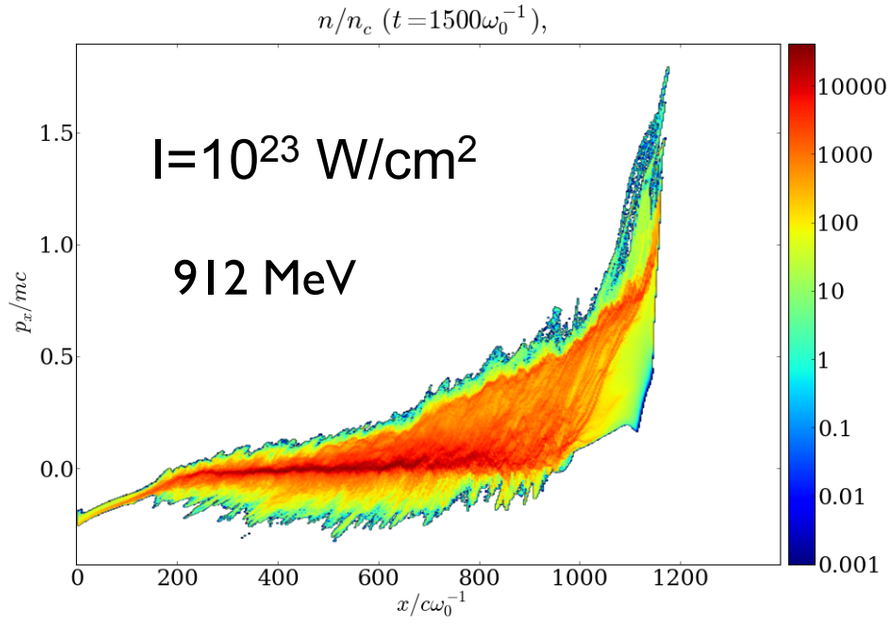

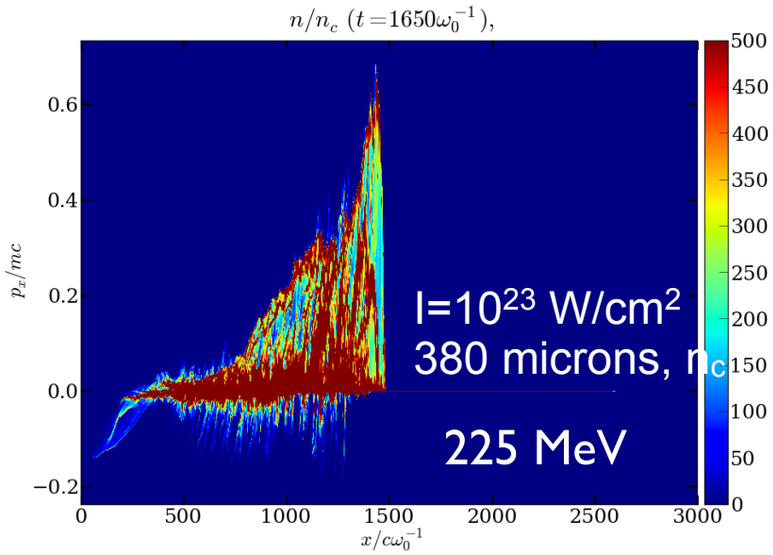

→ Relativistic ion beams

Simulations of laser ion acceleration with low density targets in the ultra-high intensity regime

Calder: Monte Carlo emission and pair production modules have been implemented

Energy time evolution and proton phase space for I =5×10^{23} W/cm^2 for a H, 4 n_c, 190 microns long cos^2 target. The laser comes from the left side of the simulation box.

I=5×10^{23} W/cm^2

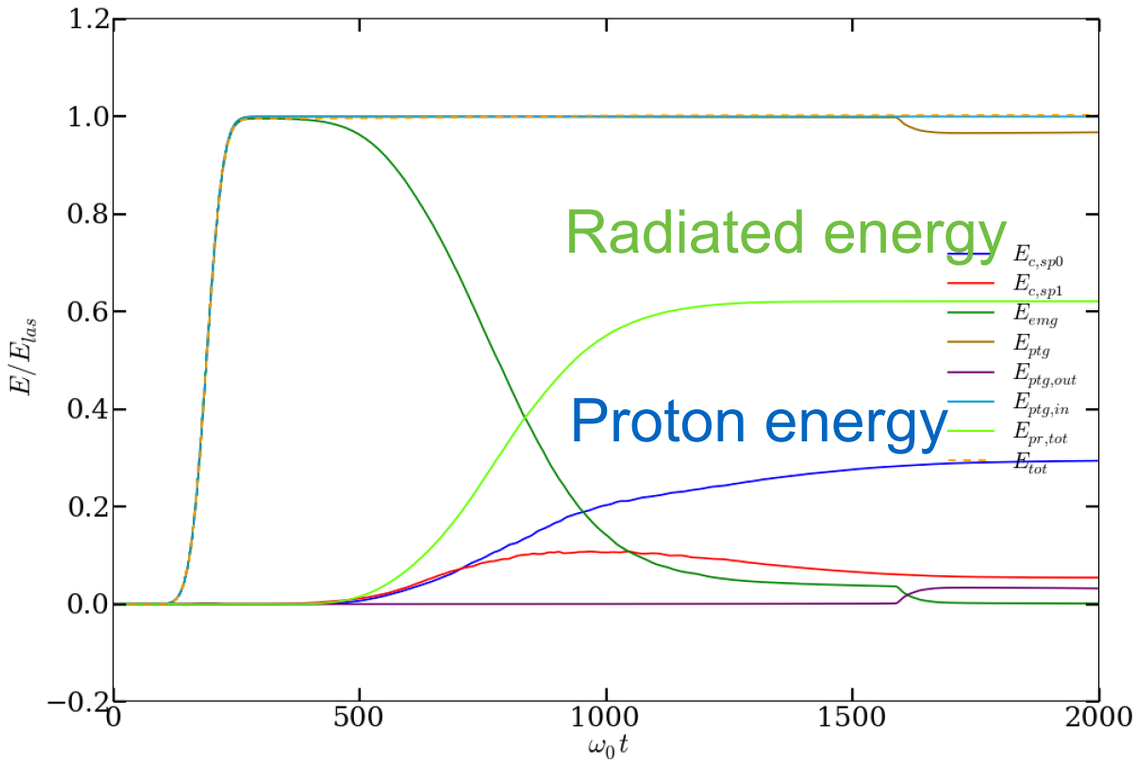

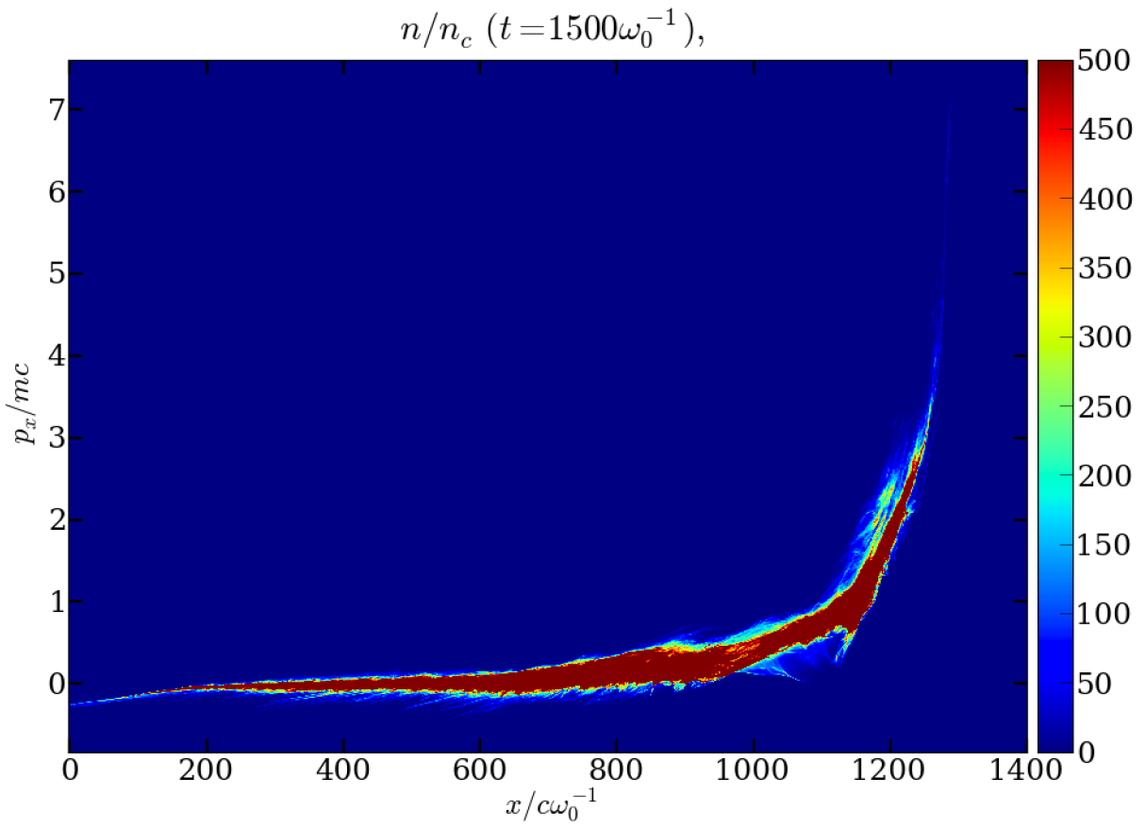

Maximum proton energy through shock acceleration: 6.25 GeV

→ Competition with radiation emission

Different scenarii of laser-induced unmagnetized collisionless shocks

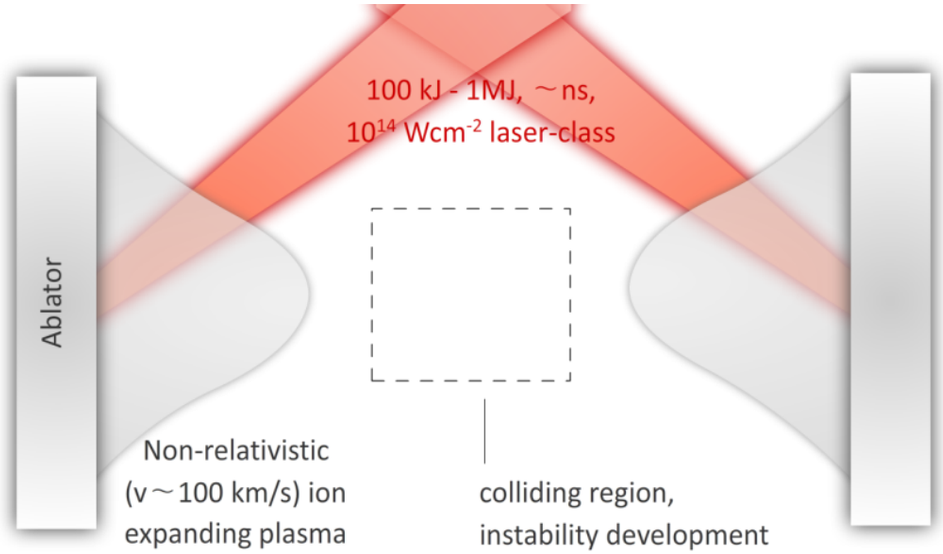

Non-relativistic regime: **Shocks between electron-ion *ablated* plasmas [1]**

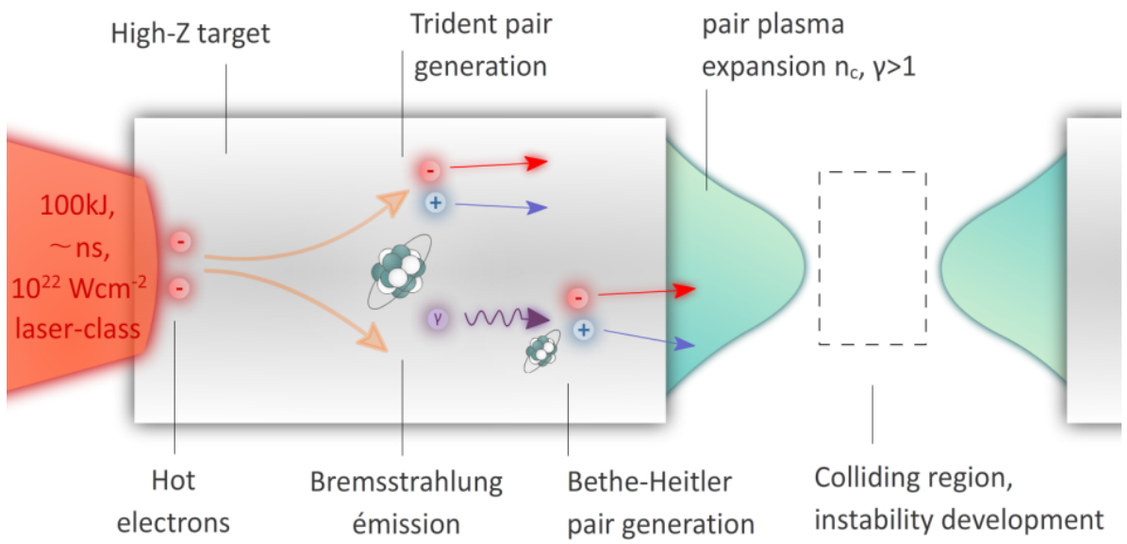

Relativistic regime: **Shocks between e^-e^+ plasma flows [3]**

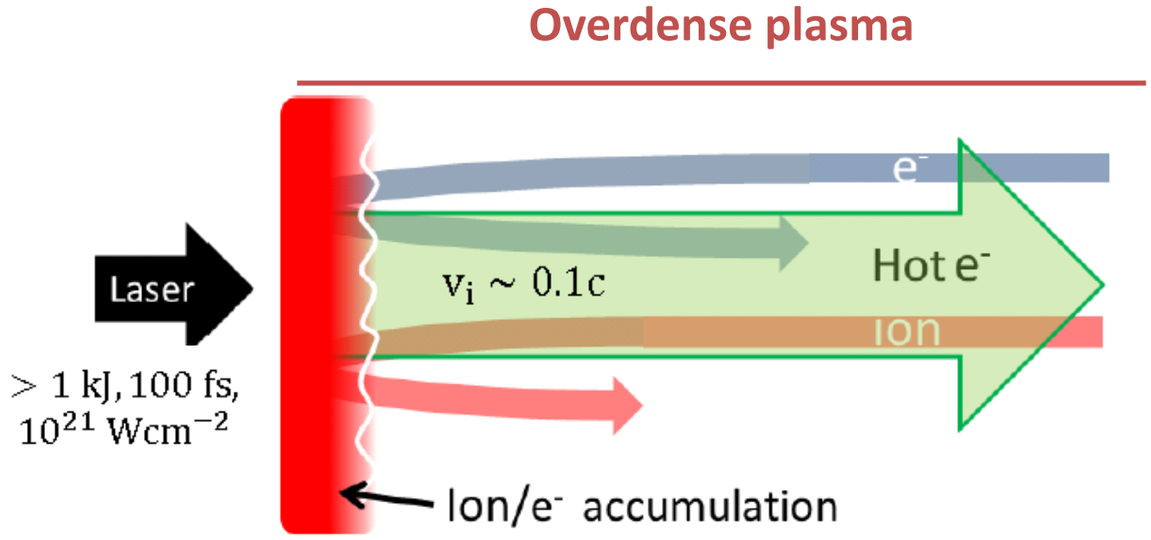

Relativistic regime: **Shocks induced by laser *radiation pressure* in overdense plasmas [2]**

Experimental study of e^-e^+ instabilities, let alone e^-e^+ shocks, is impaired by difficulty of creating dense enough pair plasmas:

- Previously proposed schemes are based on Bremsstrahlung/Bethe-Heither processes in thick (mm) high-Z targets.
- Here, we study an alternative setup based on synchrotron/Breit-Wheeler processes in thin (μm) targets.

[1] – R. Drake *et al.,* AP **749**, 171 (2012), Fox *et al.,* PRL **111**, 225002 (2013)
[2] – F. Fiuza *et al.*, PRL **108**, 235004 (2012); Poster of C. Ruyer *et al.*
[3] – Myatt *et al.,* PRE **79**, 066409 (2009) ; Chen et *al.*, HEDP **7**, 225-229 (2011)

Two-target configuration for the study of the Weibel instability in colliding e^-e^+ jets

Could be transposed to e^-p plasma collisions using low density targets

- High laser intensity necessary to generate sufficiently dense pair plasmas
- Large focal spot necessary to minimize transverse spreading of pair plasma and generate many filaments

⇒ Total laser energy > 200 kJ

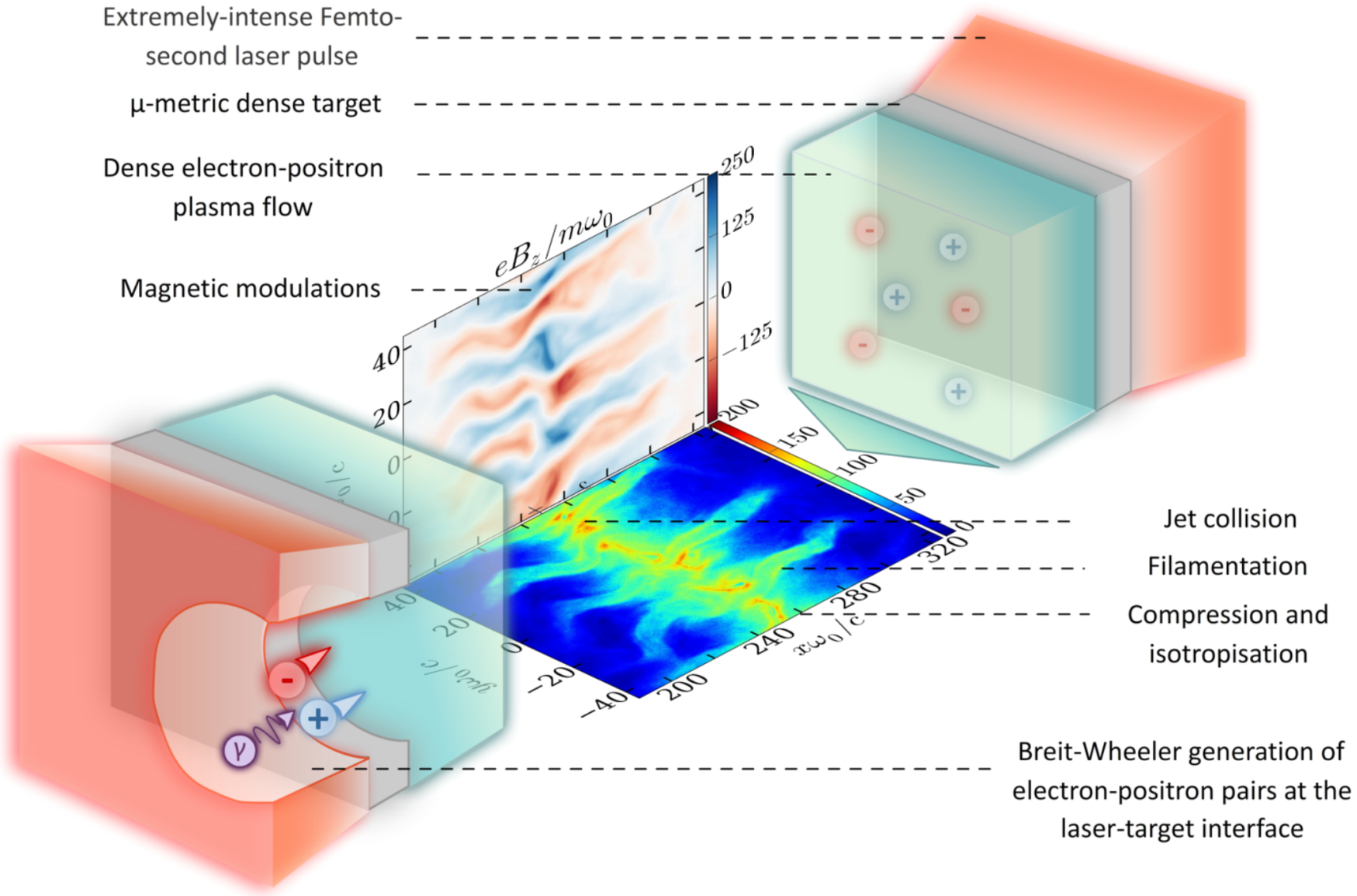

CALDER PIC Simulation

- **Laser:** plane wave, wavelength $\lambda_0 = 1\ \mu\mathrm{m}$, Gaussian profile of $125\omega_0^{-1}$ (65 fs) FWHM, linear polarization, amplitude $a_0 = 800$ $(I \sim 8.9 \times 10^{23}\ \mathrm{Wcm^{-2}})$

- **Target:** fully-ionized Al^{13+} slab of $32c\omega_0^{-1}$ $(5\ \mu m)$ thickness + preplasma of $12.5c\omega_0^{-1}$ $(2\ \mu m)$ thickness

M. Lobet et al. PRL 2015

e^-e^+ generation at the laser solid interface

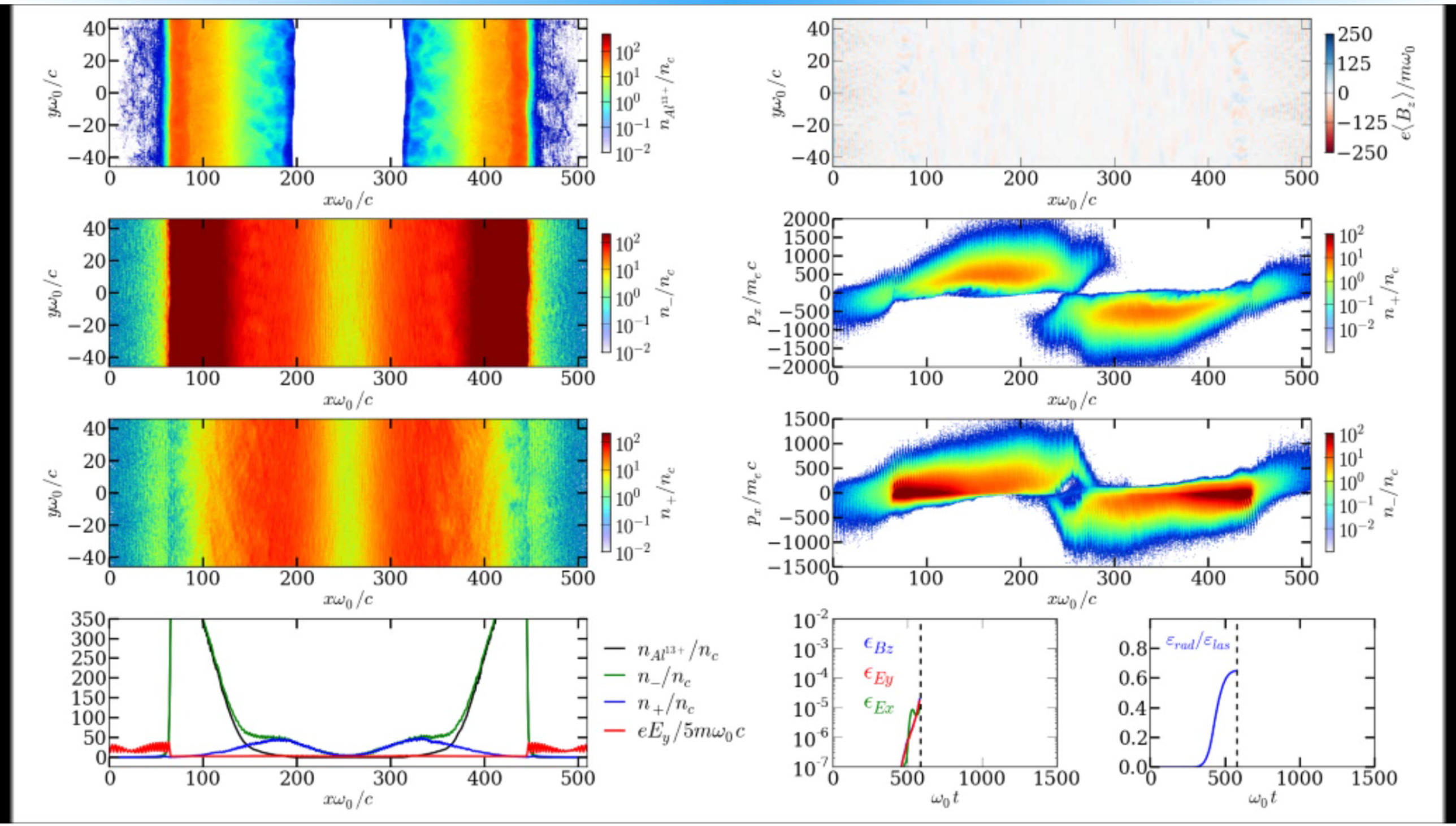

M. Lobet et al. PRL 2015

Saturated magnetic fluctuations exceed 10^6 T!

- Formation of magnetic and density filaments
- At saturation time,

$$B_z \simeq 150 \frac{m_e \omega_0}{e} \simeq 1.5 \times 10^6 \mathrm{T}\ !$$

- Estimate of the saturated magnetic field (in the Alfvén limit)

$$B_{z,sat} = (2\gamma_- n_-/n_c)^{1/2} \sim 100 m_e \omega_0 / e$$

- Estimate of the filament size

$$\lambda \sim 2\pi (n_c \gamma_-/n_-)^{1/2} \sim 20c/\omega_0$$

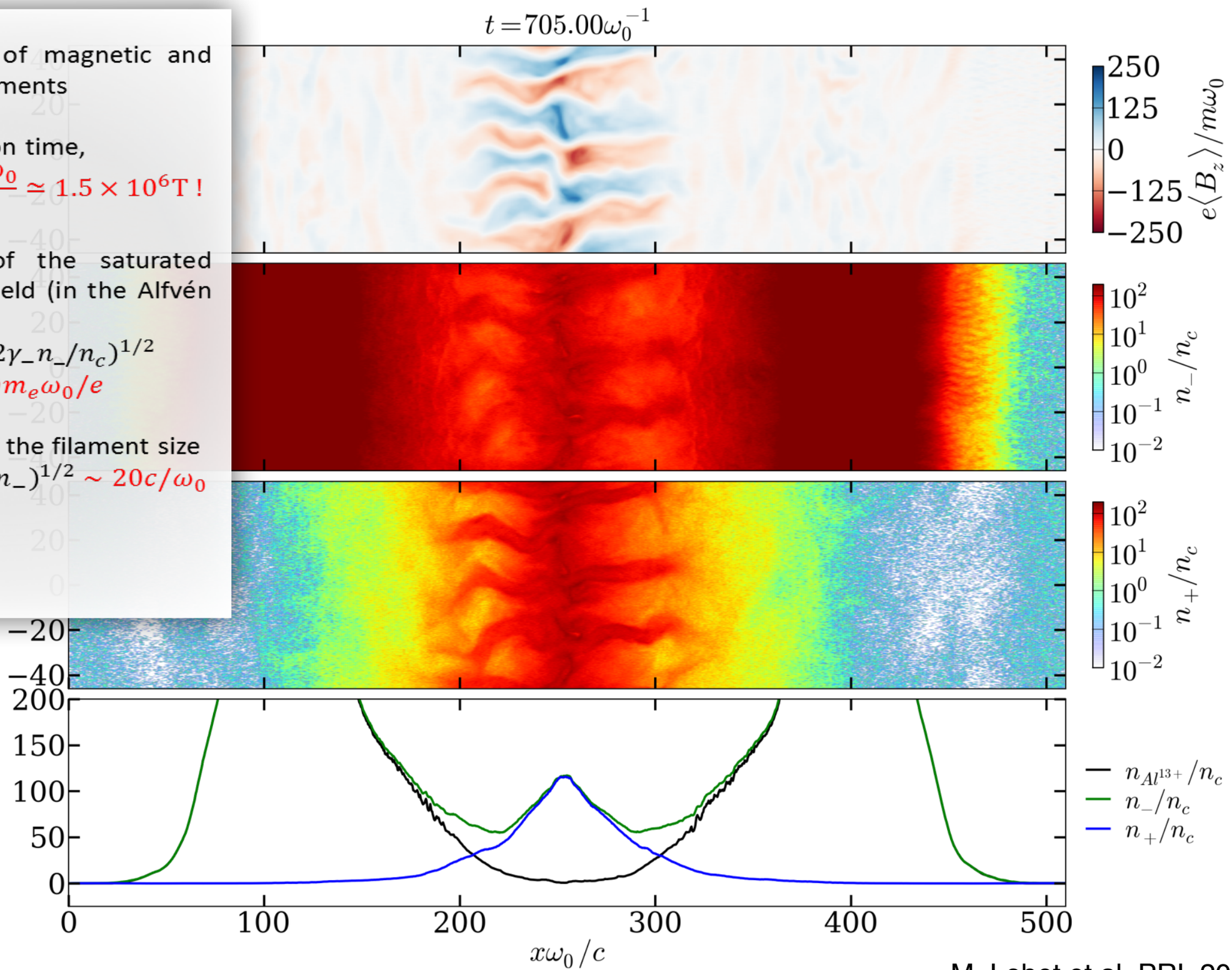

M. Lobet et al. PRL 2015

Neglecting radiation losses significantly lowers the compression ratio

With the radiation losses

- Accumulation of matter in the overlap region up to a density peak $n_{peak} \sim 128 n_c \sim 2.85 n_{\pm}$.
- The measured compression ratio ~ 3 approaches the expected value in a strong 2-D relativistic shock.

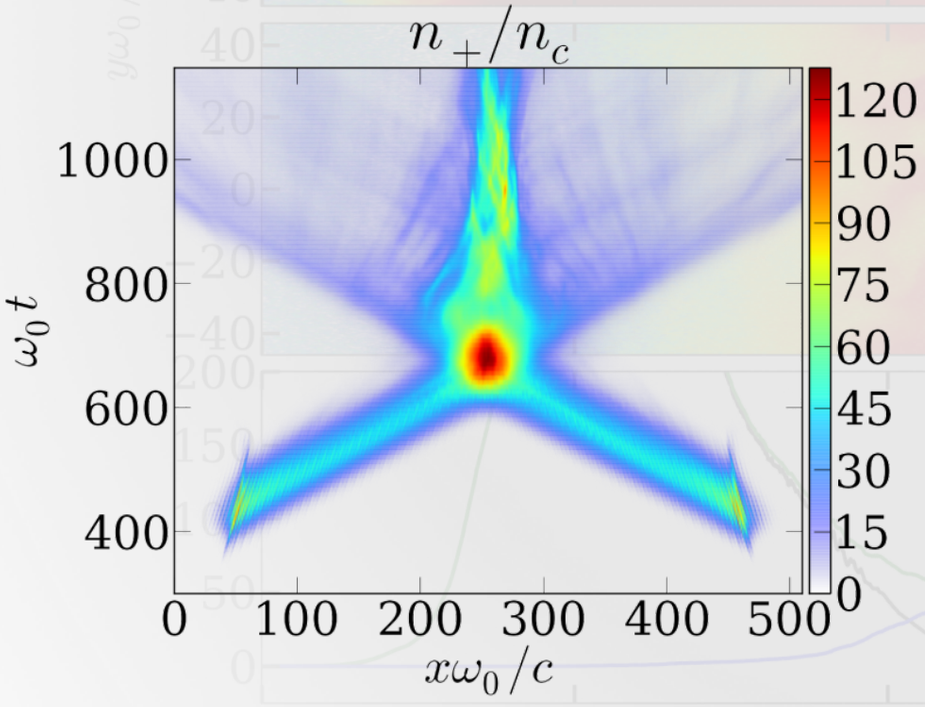

Compression ratio ~ 2.85

Without the radiation losses

- The highest-energy particles undergo weaker deflections through the turbulent region.
- This weaker scattering decreases the compression ratio down to ~ 2.4 without radiation.
- The compressed structure is not confined at larger times, in contrast to the radiative case.

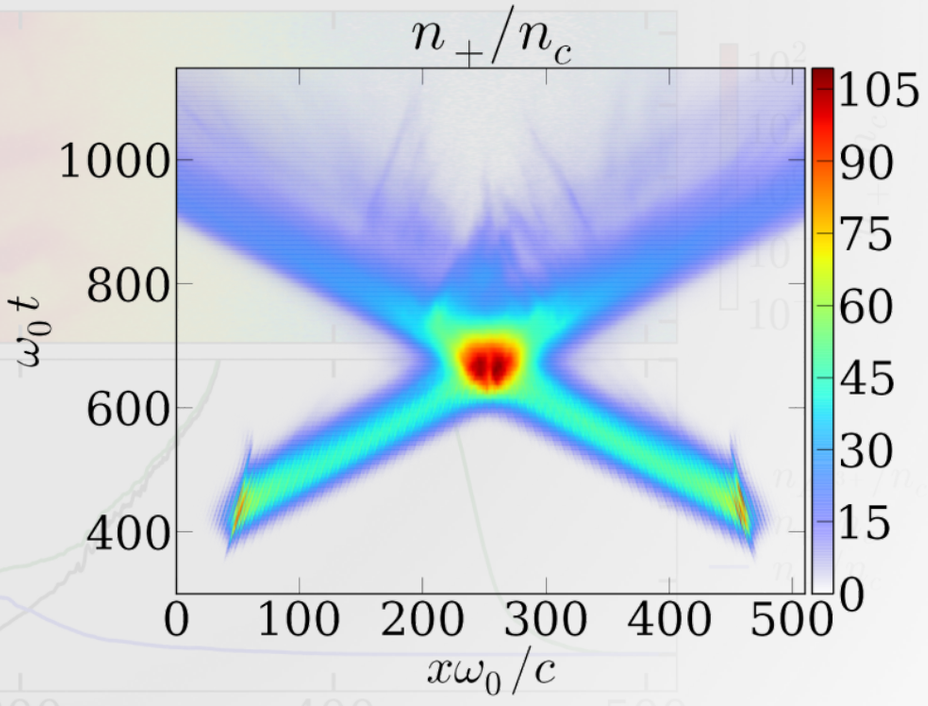

Compression ratio ~ 2.4

M. Lobet et al. PRL 2015

Outline

- High power laser systems and applications
- Collisionless shocks for laser particle acceleration
- Importance of collisionless shocks in astrophysics
- Experimental and numerical studies of collisionless shocks of interest for astrophysics
- Collision of plasmas in an external magnetic field as a platform to study magnetized collisionless shocks
- Collisionless shocks in electron-positron plasmas using extreme-light laser pulses
- **Conclusions and perspectives**

Conclusions and perspectives

- Steady progress in the development of high power laser systems and their applications
- Collisionless shocks are promising accelerating mechanisms in high intensity laser-plasma interaction
- Laboratory astrophysics experiments on MJ-scale facilities are still in their infancy but with progresses in diagnostics and simulations they should allow to test astrophysical models of collisionless shocks
- With the construction of UHI laser facilities it should be possible to achieve pair plasma collisions in the laboratory.